TUM School of Engineering and Design
Technical University of Munich

Sustainable deep geothermal reservoir management

Annette Maria Elisabeth Dietmaier

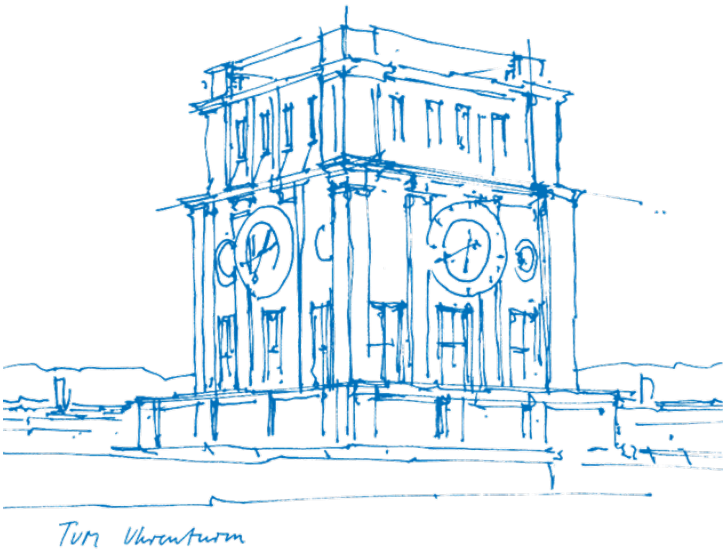

Sustainable deep geothermal reservoir management

Annette Maria Elisabeth Dietmaier

TUM School of Engineering and Design
Technische Universität München

Sustainable deep geothermal reservoir management

Annette Maria Elisabeth Dietmaier

Vollständiger Abdruck der von der TUM School of Engineering and Design der Technischen Universität München zur Erlangung des akademischen Grades einer

Doktorin der Naturwissenschaften (Dr. rer. nat.)

genehmigten Dissertation.

Vorsitz:
Prof. Dr. Roberto Cudmani

Prüfer der Dissertation:
1. Prof. Dr. Thomas Baumann
2. Prof. Dr. Thomas Hamacher

Die Dissertation wurde am 03.06.2025 bei der Technischen Universität München eingereicht und durch die TUM School of Engineering and Design am 30.07.2025 angenommen.

To Oscar, who never read a single page but made every one possible.

Abstract

Climate change is one of the most pressing challenges of our time, reshaping ecosystems, water availability, and energy systems worldwide. Deep groundwater, stored in aquifers hundreds to thousands of meters below the surface, plays a dual role in addressing these challenges. On the one hand, it serves as a valuable energy resource in geothermal applications, providing heat for district heating and power generation. On the other hand, deep aquifers act as a last-resort water source, shielded from anthropogenic contamination by overlying geological layers. Despite their importance, deep groundwater systems remain poorly understood, largely due to limited data availability, resulting in inadequate regulatory protection. Existing groundwater regulations, such as the EU Water Framework Directive (WFD), focus on shallow aquifers and neglect the unique characteristics of deep geothermal reservoirs. Further, unlike surface water and shallow groundwater bodies, deep thermal aquifers recharge and undergo chemical alterations on timescales of centuries to millennia, meaning they are not renewable in human time frames. Without a more adapted and data-driven approach, there is a risk of overexploiting these resources, leading to irreversible damage to both geothermal plants and the aquifers themselves. Hydrochemical indicators of groundwater allow insights into the rock formation through which the water has traveled and with which it has interacted, as the surrounding rock matrix determines the dissolution and precipitation of certain minerals, creating a hydrochemical fingerprint of each deep groundwater well. Thus, hydrochemistry was used in this thesis as a tool to better understand the flow and mixing patterns of the deep groundwater in the Northern Alpine Foreland Basin and to develop more sustainable management practices for deep-groundwater aquifers.

A new workflow was introduced to systematically assess hydrochemical variations using two clustering algorithms (DIANA and k-means). The data set included between 5 and 42 hydrochemical analyses per well, with annual sampling intervals covering up to 30 years. By using hydrochemical signatures as indicators of flow path changes, two operational states were defined: the Natural Range Corridor (NC), which represents a well-specific natural variation, and the Action Corridor (AC), which signals potentially unsustainable development. If a well's hydrochemistry enters the AC, it should prompt a detailed reassessment of its operation. To demonstrate the method's effectiveness, the workflow was applied to two wells with differing geological conditions. The approach successfully identified distinct fluctuation events, proving its potential as an early warning system. By detecting hydrochemical variations before they violate regulatory thresholds, this workflow provides a robust, reproducible, and data-driven method to evaluate the sustainability of deep groundwater exploitation. This method offers a practical tool to support both well operators and regulatory bodies by providing a more reliable assessment than current regulatory thresholds, which often apply arbitrary percentage limits without considering site-specific geochemical dynamics.

The first study was based on yearly data because deep geothermal aquifers suffer from a severe lack of high-quality, high-resolution data. This is due to inaccessibility and high sampling costs. In Lower Bavaria

and Upper Austria, the standard monitoring frequency is determined by national regulations, which demand one sample a year. While previous studies suggested that robust groundwater assessments require sampling every 1–3 months, these findings were based on shallow aquifers, leaving their applicability to deep systems uncertain. In order to evaluate whether annual sampling adequately captures sub-yearly hydrochemical fluctuations in deep aquifers, the second study compared yearly data with quasi-continuous hydrochemical measurements from two wells in southeastern Germany, assessing differences in mean values, trend detection, and seasonality. The ability of annual data to support reliable forecasting using the ARIMA algorithm was examined, and the potential of virtual sensors to enhance limited data sets was explored. Results showed that the examined deep aquifer exhibits seasonal hydrochemical variations, which were not captured by annual sampling. Since yearly measurements were taken at similar production states, they failed to reflect the full range of hydrochemical dynamics. Forecasting based on annual data did not represent the variability observed in continuous measurements, and limited data availability prevented strong parameter correlations beyond the obvious relationships between drawdown and extraction volume ($R = 0.93$), and drawdown and electric conductivity (EC) ($R = 0.99$). None of the calculated hydrochemical ratios showed any strong correlations with the physical parameters ($R > 0.6$) but only with their own constituents. Consequently, annual sampling provided only a partial picture of well dynamics, potentially leading to regulatory issues or operational challenges such as scaling and gas release. While not a substitute for detailed analyses, virtual sensors, when trained with larger data sets, could support early detection of hydrochemical changes and diminish the need for high-frequency, cost-intensive sampling campaigns. The results highlight a severe lack of hydrochemical data on deep groundwater aquifers, particularly concerning seasonal variations, and suggest that increasing the minimum sampling frequency from once per year to at least three times per year would greatly improve monitoring accuracy.

The third study in this thesis assessed the development of flow paths upon reinjection. Upper Jurassic waters exhibit a carbonate signature, with calcium and magnesium often replaced by sodium due to ion exchange along infiltration pathways. Upon cooling, these waters become undersaturated, leading to dissolution around reinjection wells. These reactions, which take place within days to weeks, constitute an exception to the slow recharge and reheating dynamics in deep aquifers. While dissolution kinetics and volume changes have been studied, microscopic alterations to flow paths have remained less explored. To do this, a limestone sample was exposed to elevated CO_2 partial pressure (5.9 bar) in an autoclave, with artificial structures introduced to induce localized dissolution effects. The post-treatment analysis consisted of optical microscopy, 3D micro-scanning, and confocal laser scanning microscopy (CLSM). Each imaging method had specific strengths and limitations. CLSM provided high-resolution (xy-resolution: $0.1 \times 0.1\ \mu m^2$) surface roughness assessments but was unable to capture overhangs. Optical microscopy was cost-effective and user-friendly, effectively visualizing preferential dissolution pathways but lacking precise roughness quantification. Despite its lower spatial resolution, 3D micro-scanning uniquely resolved overhangs. Dissolution resulted in significant surface roughening, micrometer-scale moldic pore formation, and the widening of artificial structures. 3D micro-scanning quantified these changes, while CLSM revealed fine-scale roughness details. Increased fracture surface roughness and widened flow paths enhance water transport and dissolution, potentially accelerating thermal breakthroughs at geother-

mal plants. These findings contribute to a better understanding of reservoir behavior on a pore scale, aiding in the sustainable management and efficient extraction and reinjection of geothermal energy.

The results produced by this thesis emphasize that deep geothermal groundwater management requires a paradigm shift. Given the high financial costs of deep groundwater exploration and monitoring, operators and policymakers must invest in more comprehensive data collection efforts. This includes a higher sampling frequency and integrated hydrogeochemical models to predict long-term sustainability. Without these measures, geothermal operations risk both resource depletion and regulatory non-compliance, ultimately threatening the viability of deep geothermal energy as a sustainable solution to provide energy and endangering the certification of balneological wells.

Zusammenfassung

Der Klimawandel ist eine der drängendsten Herausforderungen unserer Zeit und verändert Ökosysteme, Wasserverfügbarkeit und Energiesysteme weltweit. Tiefes Grundwasser, das in Aquiferen in Hunderten bis Tausenden Metern Tiefe gespeichert ist, spielt bei der Bewältigung dieser Herausforderungen eine doppelte Rolle. Einerseits dient es als Energiequelle für Fernwärmenetze und Stromerzeugung; andererseits stellt es eine Wasserreserve dar, die durch dichte geologische Schichten vor Kontamination geschützt ist. Trotz dieser Bedeutung sind die gesetzlichen Schutzmaßnahmen für Tiefengrundwassersysteme bislang unzureichend, was vor allem auf eine lückenhafte Datenbasis und damit einhergehend auf ein begrenztes Systemverständnis zurückzuführen ist. Bestehende Vorschriften wie die Wasserrahmenrichtlinie (WRRL) der EU wurden für oberflächennahe Grundwasserkörper konzipiert und berücksichtigen nicht die besonderen Eigenschaften tiefer Aquifere. Im Gegensatz zu oberflächennahen Grundwassersystemen verändern sich tiefe Grundwasserkörper auf Zeitskalen von Jahrhunderten bis Jahrtausenden und sind somit nicht innerhalb menschlicher Zeitrahmen erneuerbar. Ohne eine gezieltere, datenbasierte Herangehensweise besteht die Gefahr der Übernutzung, was zu irreversiblen Schäden sowohl an Geothermieanlagen und Heilquellen als auch an den Aquiferen selbst führen kann. Hydrochemische Indikatoren des Grundwassers ermöglichen Einblicke in Fließpfade und die Gesteinsformationen, durch die das Wasser geflossen ist und mit denen es interagiert hat, da die umgebende Gesteinsmatrix die Auflösung und Ausfällung bestimmter Mineralien bestimmt; so weist jede tiefe Grundwasserquelle einen eindeutigen hydrochemischen Fingerabdruck auf. Daher wurde die Hydrochemie in dieser Arbeit als Instrument verwendet, um die Fließ- und Mischmuster des tiefen Grundwassers im niederbayerischen/oberösterreichischen Molassebecken besser zu verstehen und nachhaltigere Bewirtschaftungspraktiken für tiefe Grundwasserleiter zu entwickeln.

Zunächst wird ein neuer Workflow vorgestellt, der mithilfe von zwei Clustering-Algorithmen (DIANA und k-means) hydrochemische Veränderungen systematisch bewertet. Die Datengrundlage umfasste zwischen 5 und 42 jährlich entnommene hydrochemische Analysen pro Quelle, welche sich auf einen Zeitraum von bis zu 30 Jahren verteilten. Durch die Verwendung hydrochemischer Signaturen als Indikatoren für Fließwegänderungen konnten zwei Betriebszustände identifiziert werden: der natürliche Korridor (NC), der die quellenspezifische natürliche hydrochemische Schwankungsbreite repräsentiert, und der Notfallkorridor (AC), der auf eine möglicherweise nicht nachhaltige Entwicklung hinweist. Wird der AC überschritten, löst dies eine detaillierte Überprüfung des Brunnenbetriebs aus. Zur Validierung des Ansatzes wurde der Workflow auf zwei Quellen mit unterschiedlichen geologischen Bedingungen angewendet. Er identifizierte erfolgreich ungewöhnliche Schwankungsereignisse und zeigte sein Potenzial als Frühwarnsystem. Durch die frühzeitige Erkennung hydrochemischer Veränderungen bevor regulatorische Grenzwerte verletzt werden, ermöglicht dieser Workflow eine robuste, reproduzierbare und datenbasierte Bewertung davon, wie

nachhaltig eine Quelle betrieben wird. Zudem bietet das Verfahren eine verlässlichere Grundlage für Betreiber und Behörden, da es über die derzeitigen willkürlichen Grenzwerte hinausgeht und standortspezifische geochemische Dynamiken berücksichtigt.

Selbst wenn nachhaltige Betriebsbedingungen definiert sind, besteht bei tiefen geothermischen Aquiferen ein erhebliches Defizit an brauchbaren Daten. In Niederbayern und Oberösterreich sehen nationale Bestimmungen momentan eine Probenahme pro Jahr vor. Die Ergebnisse früherer Studien legen nahe, dass eine robuste Grundwasserbewertung Probenintervalle von 1 – 3 Monaten erfordert; diese Empfehlungen basieren allerdings auf oberflächennahen Aquiferen, sodass ihre Übertragbarkeit auf tiefe Systeme unklar ist. Um zu beurteilen, ob jährliche Probenahmen saisonale hydrochemische Schwankungen in tiefen Aquiferen ausreichend abbilden, wurden Jahresdaten mit quasi-kontinuierlichen hydrochemischen Messungen von zwei Bohrungen in Südostdeutschland verglichen. Dabei wurden Unterschiede in Mittelwerten, Trendanalysen und Saisonalität untersucht. Zudem wurde die Fähigkeit jährlicher Daten zur zuverlässigen Vorhersage mittels des ARIMA-Algorithmus bewertet und das Potenzial virtueller Sensoren zur Ergänzung begrenzter Datensätze geprüft. Die Ergebnisse zeigten, dass tiefe Aquifere saisonale hydrochemische Schwankungen aufweisen, die durch jährliche Probenahmen nicht erfasst werden. Da diese Messungen meist bei ähnlichen Betriebszuständen erfolgen, spiegeln sie nicht die gesamte Bandbreite der hydrochemischen Dynamik wider. Prognosen, die auf Basis jährlicher Daten berechnet wurden, deckten die Variabilität kontinuierlicher Messungen nicht ab; aufgrund der begrenzten Datenverfügbarkeit konnten nur beschränkt statistisch signifikante Korrelationen zwischen einzelnen Parametern festgestellt werden, z.B. bei den offensichtlichen Beziehungen zwischen Absenkung und Entnahmemenge ($R = 0.93$) sowie Absenkung und elektrischer Leitfähigkeit ($R = 0.99$). Die berechneten Ionenverhältnisse zeigten starke Korrelationen mit den eigenen Bestandteilen, jedoch nicht mit anderen physikalischen Parametern ($R > 0{,}6$). Somit liefern jährliche Probenahmen nur ein unvollständiges Bild der Brunnenentwicklung, was regulatorische Probleme, aber auch Herausforderungen im Brunnenbetrieb wie Scaling oder Entgasungen verursachen kann. Auf Basis der saisonalen Schwankungen ergab sich eine Mindestprobenahmefrequenz von drei Proben pro Jahr. Während virtuelle Sensoren keine detaillierten Analysen ersetzen, könnten sie mit ausreichend Trainingsdaten eine frühzeitige Erkennung hydrochemischer Veränderungen ermöglichen und den Bedarf an kostenintensiven Komplettmessungen reduzieren. Die Ergebnisse unterstreichen den gravierenden Mangel an hydrochemischen Daten, insbesondere zur saisonalen Variabilität, und legen nahe, dass eine Erhöhung der Probenahmefrequenz von einmal jährlich auf mindestens dreimal jährlich die Überwachungsgenauigkeit erheblich verbessern würde.

Der dritte Teil dieser Arbeit untersuchte die Entwicklung von Fließwegen an der Reinjektionsstelle. Das Tiefengrundwasser des Oberjuras zeigt eine karbonatische Signatur, wobei Calcium und Magnesium entlang der Infiltrationspfade oft durch Natrium ersetzt werden. Durch das Abkühlen im Wärmetauscher entsteht in diesen Wässern eine Untersättigung gegenüber des Aquifergesteins, was zu Auflösungserscheinungen des Gesteins in der Nähe des Reinjektionsbrunnens führt. Diese Reaktionen stellen eine Ausnahme der sonst langsamen Reaktionen und Dynamiken in tiefen Aquiferen dar. Während die Kinetiken der Gesteinslösung und volumetrische Veränderungen bereits untersucht sind, bleiben mikroskopische Veränderungen der Fließwege bislang wenig erforscht. Zur Untersuchung dieser Prozesse wurde ein Kalksteinwürfel in einem Autoklaven erhöhten CO_2-Partialdrücken (5.9 bar) ausgesetzt. Mit einem Dremel wur-

den dem Würfel künstliche Störungen beigefügt, um die Lösungseffekte zu lokalisieren. Die Proben wurden anschließend mit optischer Mikroskopie, 3D-Mikroscanning und konfokaler Laserscanning-Mikroskopie (CLSM) analysiert. Jede Bildgebungsmethode wies spezifische Stärken und Einschränkungen auf. CLSM lieferte hochauflösende (0.1 x 0.1 µm²) Oberflächenrauhigkeitsanalysen, konnte jedoch Flächen unter Überhängen nicht erfassen. Die optische Mikroskopie war kostengünstig und benutzerfreundlich und erwies sich als effektiv bei der Visualisierung bevorzugter Lösungswege, jedoch fehlte ihr eine präzise Rauigkeitsquantifizierung. 3D-Mikroscanning hatte zwar eine vergleichsweise geringe räumliche Auflösung, dafür war es in der Lage, Überhänge abzubilden. Die Gesteinslösung führte zu einer signifikanten Oberflächenverrauung, der Bildung mikrometergroßer moldischer Poren und der Erweiterung der künstlichen Störungen. 3D-Mikroscanning quantifizierte diese Veränderungen, während CLSM feine Rauigkeitsdetails sichtbar machte. Eine erhöhte Rauhigkeit in den Störungen und erweiterte Fließwege begünstigen den Wassertransport und die weitere Auflösung, was potenziell thermische Durchbrüche in geothermischen Anlagen beschleunigen könnte.

Insgesamt zeigt die vorliegende Thesis, dass das Management tiefer geothermischer Grundwasserleiter einen Paradigmenwechsel erfordert. Angesichts der hohen finanziellen Kosten für Exploration und Überwachung müssen Betreiber und politische Entscheidungsträger verstärkt in eine umfassendere Datenerhebung investieren. Dazu gehören häufigere Probenahmen und integrierte hydrogeochemische Modelle zur Bewertung und Vorhersage langfristiger Nachhaltigkeit. Ohne diese Maßnahmen drohen nicht nur eine Übernutzung der Ressource, sondern auch regulatorische Verstöße, was die langfristige Verwendung geothermischer Energie oder die Zertifizierung medizinischer Heilquellen gefährden könnte.

Structure of this Thesis

The structure of this thesis follows the path of geothermal water up to, through, and out of a geothermal plant (Fig. 1), starting at the inflow pathways up until the production well, where its hydrochemical properties are used to assess its origins and changes in the hydrochemical composition. This serves as a proxy for determining the grade of sustainability at which a given well is being operated (1st publication, chapter 4). The second publication (chapter 5) assesses the correlation between yearly and sub-yearly hydrochemical samples taken at the well-head, while the third publication (chapter 6) explores the effects of reinjecting cooled-off water back into the aquifer by comparing three types of microscopy to assess dissolution effects in the rock matrix.

Publications

Scientific, peer-reviewed articles published in the context of this thesis are presented here. Detailed information on author contributions is given in the respective chapters listed above.

1. Dietmaier, A., & Baumann, T. (2023). Assessing sustainable development of deep aquifers. Water Resources Management, 37(10), 3857-3874. DOI: 10.1007/s11269-023-03529-6.

2. Dietmaier, A., & Baumann, T. (2023). Forecasting changes of the flow regime at deep geothermal wells based on high-resolution sensor data and low-resolution chemical analyses. Advances in Geosciences, 58, 189-197. DOI: 10.5194/adgeo-58-189-2023.

3. Dietmaier, A., Mattheis, J., Weller, D., Stober, I., Drews, M, and Baumann, T. (2025). Visualization and semi-quantitative analysis of dissolution processes at artificial structures in carbonate rocks using optical, 3d micro-scanning and confocal laser scanning microscopy. Geothermal Energy, 13(1):32, 2025. DOI: 10.1186/s40517-025-00355-4.

Funding

The first publication was funded by the Bavarian State Ministry of Science, Research and Art in the Framework of the Geothermal Alliance Bavaria and the Bavarian Environmental Protection Agency (LfU).

The second and third publications were funded by the Bavarian State Ministry of Science, Research and Art in the Framework of the Geothermal Alliance Bavaria.

All publications contributed to the second funding phase of the Geothermal Alliance of Bavaria (GAB 2.0), more precisely, work package “4: long-term”.

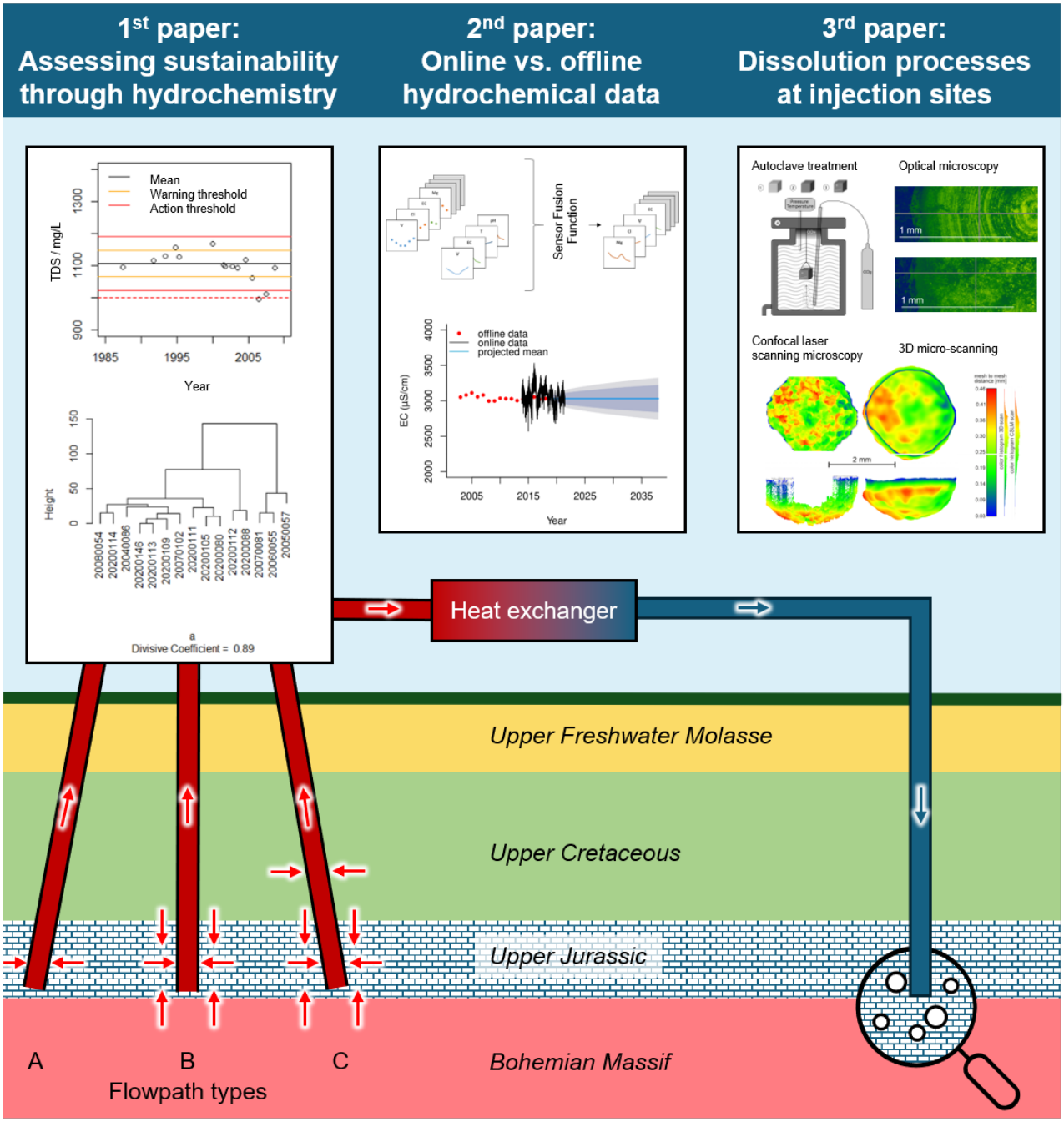

Figure 1 Graphical abstract of this thesis and the three presented studies.

Acknowledgements

I would like to express my gratitude to Prof. Baumann for his guidance, support, unwavering optimism, and feedback. By adopting me as his PhD student in the middle of a pandemic, he ensured my dream of achieving a PhD could see the light of day eventually. His expertise, encouragement, and dedication have been instrumental in shaping this dissertation and my personal and academic growth. Personal note: I cannot thank you enough for introducing me to the fabulous world of Neil Gaiman, Aziraphale, Crowley, et al.

Further, I want to thank Ingrid Stober for her mentorship, kind words and encouragement to keep going when the going got tough.

I am further very grateful for the positive and constructive collaboration on my third publication with Prof. Dr. Michael Drews, Justin Mattheis, and Daniel Weller.

My sincerest thanks also go to the Geothermal Alliance Bavaria (GAB) and the Bavarian Ministry of Science and the Arts, whose funding made this study possible, along with the Bavarian Environmental Agency (LfU), which funded, guided, and supported my first publication. The TUM Graduate School supported my research stay at Professor Greg McDermid's remote sensing lab at the University of Calgary in Canada in the summer of 2023. Thank you, Greg, for having me again for another summer of adventures in your lab and your field sites. You are a personal and academic role model and I hope to someday work with you again.

At the TUM Chair of Hydrogeology, I would like to thank my colleagues, Mo, Marlis, Renata, Felix, Lea, Christine, Bob, and all the others for the lovely lunch breaks, feedback, and encouragement. Thank you to Jarka Obel and Anja Wunderlich for helping me out with lab-related problems. I am further deeply grateful to Lilly Zacherl for going through the trials and tribulations of pursuing a PhD with me. The four years at TUM and the almost-apocalypse wouldn't have been the same without you or our daily lunch walks with Oscar.

To my parents and my sister, thank you for your support and patience. Your guidance (and occasional tough love) kept me going, and I'm excited to finally join the family PhD club.

Though not blood-related, I am also thankful to all my friends who have endured four years of complaints as well as raves about the PhD life. Christiane, Michi, Dagmar, Maria, Hannah, Manuel, Kersten, Kelly, I could not have done this without any of you. Thank you, Lizzy, for beta-reading this dissertation.

Finally, I want to thank Con O'Neill without whom I might have given up. Thank you for telling me to finish my f*cking PhD.

Contents

Acronyms

AI	artificial intelligence. 96
ARIMA	autoregressive integrated moving average. 91
CFC	chlorofluorocarbons. 22
CLSM	confocal laser scanning microscopy. 57, 58, 86, 92–94
DIANA	divisive analysis clustering. xxvii, 87
DQS	Definitions and Quality Standards for the Nomination of Health Resorts, Resort Towns and Curative Sources. 21, 22, 88, 94
EC	electric conductivity. 14, 15, 23, 45, 85, 88, 89, 91
EEG	Renewable Energy Sources Act (Erneuerbare-Energien-Gesetz). 4, 16
EU	European Union. 1, 3, 21
GHG	greenhouse gas. 1, 3, 5, 16, 17
IPCC	Intergovernmental Panel on Climate Change. 1
LfU	Bavarian Environment Agency (Bayerisches Landesamt für Umwelt). xxvi, 11, 22, 86, 91, 94, 95
LNH	Lanshuter-Neuöttinger-Hoch. 7, 8
MCT	micro computed tomography. 19, 93
NAFB	Northern Alpine Foreland Basin. xxvii, 5–7, 87, 89–91
NECP	National Energy and Climate Plan. 3, 16
NMRI	nuclear magnetic resonance imaging. 19, 93

PAH polycyclic aromatic hydrocarbons. 14, 15
PFAS per- and polyfluoroalkyl substances. 14, 15
PFC perfluorinated compounds. 22

RCP representative concentration pathway. 1

SDG Sustainable Development Goal. 4
SI saturation index. 18, 23, 24
SVHC semi-volatile halogenated hydrocarbons. 14

TDS total dissolved salts. 2, 7, 8, 12, 13, 23, 88
THCM thermo-hydro-chemo-mechanial. 100

UJA Upper Jurassic Aquifer. 5–8, 12, 14, 19

VOC volatile organic compounds. 14
VS virtual sensors. 15, 89–92, 96

WFD Water Framework Directive. 14, 21, 25, 94, 100
WRRL Wasserrahmenrichtlinie. xiii

XCT X-ray computed tomography. 93

List of Figures

List of Tables

1 Introduction: Climate Change Meets Energy Crisis – A Perfect Storm and its Impacts on Groundwater

1.1 Climate Change and its Impacts on Groundwater

In the early to mid-2020s, Europe faces the intertwined challenges of two crises: climate change and political instabilities affecting energy resources. Just like the rest of the world, the European Union (EU) can no longer afford to ignore the effects of climate change on the environment, weather, and anthroposphere: people are dying, rivers are drying out, forests are going up in flames, and storms and floods are destroying whole towns. “Human-induced climate change, including more frequent and intense extreme events, has caused widespread adverse impacts and related losses and damages to nature and people, beyond natural climate variability” [53]: the sixth Assessment Report published by the Intergovernmental Panel on Climate Change (IPCC) stresses with immense urgency the all-encompassing dangers our planet will face due to climate change. Planet Earth has received its nickname “the blue planet” for a reason, that is, our water allows for life on Earth, unlike any other planet in our solar system. While climate change affects our entire planet, its impacts most heavily affect the hydrological cycle [93].

The IPCC differentiates between four representative concentration pathways (RCPs), which describe scenarios driven by varying degrees of **atmospheric warming**. The increase in atmospheric and surface temperatures has far-reaching consequences. Generally, climate change has led to changes in the quantity, frequency, and timing of precipitation [30]. In the past decade, weather extremes in the EU have become more frequent and intense [53]. In the Mediterranean, greenhouse gas (GHG) forcing has led to drier summers, whereas in the relatively humid European climates, heavy precipitation events have increased in frequency and intensity [53]. While total annual precipitation has increased, it now falls in the form of sporadic and unpredictable extreme rainfall events, which allows for a parallel increase in droughts and hot spells. In the case of heavy rainfall following a prolonged dry period, only a small fraction of the water is able to infiltrate into the dried-up soil and recharge shallow aquifers. Most of it collects in surface run-off, gathers in the nearest stream, and is whisked away within hours before it can support local or regional aquatic or groundwater-dependent ecosystems (Fig. 2.1). Sealed surfaces, such as urban settlements, contribute to the impairment of aquifer recharge.

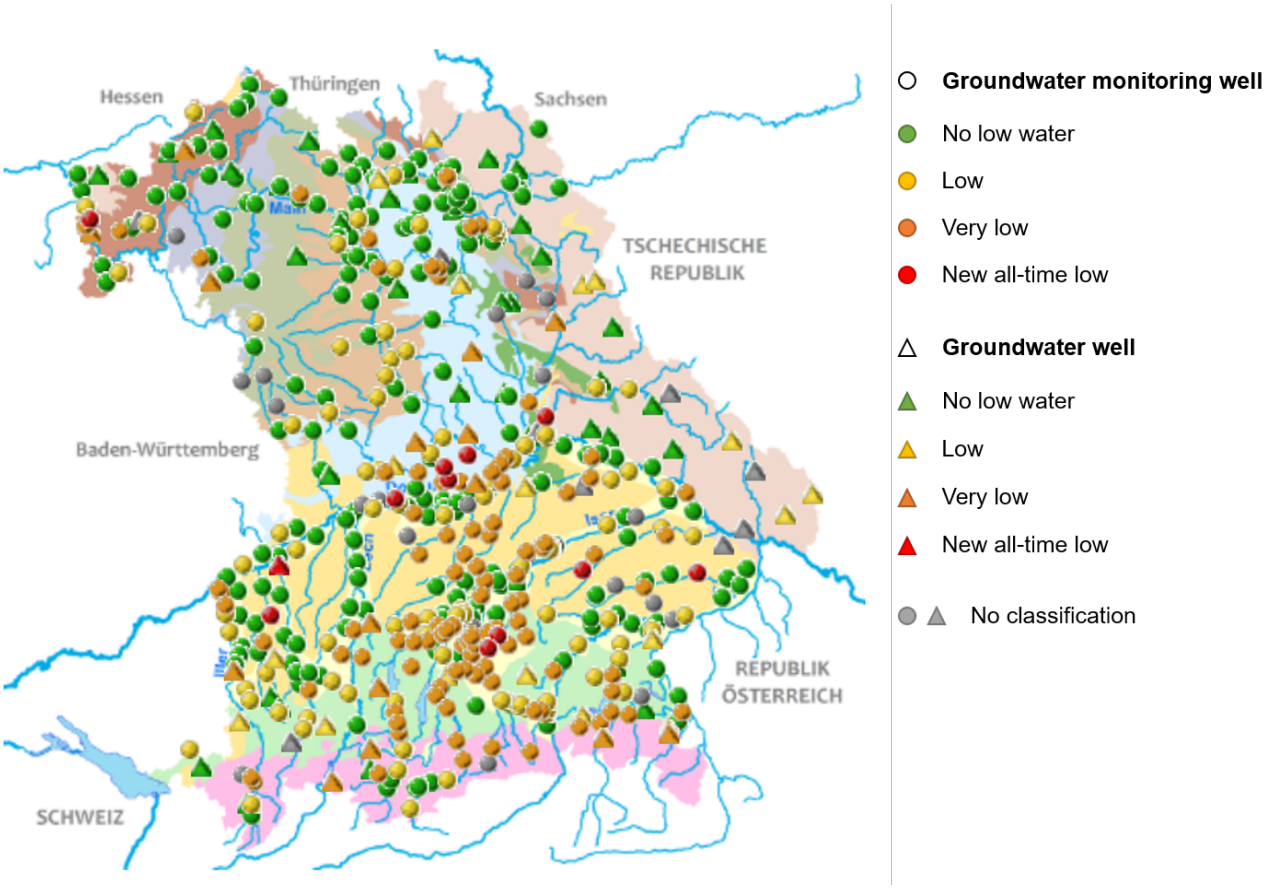

Figure 1.1 Groundwater levels in Bavaria on October 25, 2023. More than half of the wells display low, very low, or new all-time low values at a time of year that is historically characterized by efficient aquifer recharge [74].

All these dynamics culminate in a noticeable decrease in water and food security, imminent dangers that have been observed in central Europe for at least a decade [53]. For example, in October 2023, over half of all Bavarian shallow groundwater wells (groundwater levels between 0.5 and 97 m below ground level) displayed various grades of low water levels: out of 423 wells, 105 showed low, and 108 showed very low water levels. 11 wells measured new all-time low values (Fig. 1.1) [74]. These numbers are especially grievous considering that the middle of autumn has traditionally been characterized by continuous, gentle rainfall, perfect conditions for efficient groundwater **aquifer recharge**. This was not the case in 2023, and an exceptionally dry autumn has led to new shallow groundwater lows in a time of year when aquifers typically recharge.

Rising atmospheric and surface temperatures influence not only the quantity, but also the **quality of shallow groundwater** and surface water bodies. Extreme rainfall events, droughts, and floods have been observed to lead to the qualitative degradation of freshwater systems and to outbreaks of water-related diseases [53]. For example, it is hypothesized that aquifer recharge variability can induce changes in the pressure field of an aquifer and thereby lead to changes in the aquifer's flow paths and thus its hydrochemical composition [6, 29]. Meanwhile, the timing of aquifer recharge may further determine the concentration of total dissolved salts (TDS) and contaminants in shallow groundwater and surface water bodies: aquifers recharged after an extended dry period often show higher TDS values, whereas gentle and longer-term

recharge (such as recharge during the spring snow and ice melt) tends to result in a dilution of the water [30].

1.2 The European and German Energy Transition

Considering the threats induced by climate change, the EU is in dire need of alternative, carbon-neutral energy resources. In 2020, the European Commission approved an ambitious and comprehensive set of policy initiatives called the European Green Deal, which aims to address environmental, economic, and social challenges in order to make Europe climate-neutral by 2050. Having been called “Europe’s man-on-the-moon moment” by Commission President Ursula von der Leyen after its ratification as the European Climate Law in April 2021, it is meant to lead the third industrial revolution, to clean the European energy system, to work with nature, to protect our planet and health, and to boost global climate action [32]. By ratifying the first European Climate Law, all European member states commit to turning the EU into the first climate-neutral continent by 2050.

Germany has long assumed a front-runner role in the global fight against climate change, expressed, i.e., in the ambitious national “Energiewende” or energy transition plan. The German Climate Action Act, approved in late 2019, is a framework of national legislation outlining legally binding targets and policies for Germany to meet its climate goals [16]: reducing GHG emissions by 55 % by the year 2030 and to reach climate neutrality by 2050 [16]. In 2021, the Federal Constitutional Court of Germany amended these goals, now aiming to reduce GHG emissions by 65 % by 2030, and to reach climate neutrality by 2045 rather than 2050. After 2045, a net negative carbon emission strategy is desired (Fig. 1.2) [16]. The German National Energy and Climate Plan (NECP) outlines the political goals of reaching the national climate targets, while maintaining competitiveness and reliability of supply, based on three strategic aims:

- Increase the share of renewable energies in total energy consumption
- Reduce primary energy consumption
- Increase overall energy efficiency.

These aims go hand in hand with a list of central goals, which include, e.g., climate targets, renewable energy targets (share of renewable energies in the gross final consumption of 30 % by 2030 in Germany), and energy security targets (coverage of Germany’s energy demand at all times, and resilience to supply crises). Concerning the resilience to supply crises, the ongoing war in Ukraine has exposed both the continued reliance of Germany on fossil fuels for energy and the importance of finding alternative resources to Russian natural gas. In the winter of 2022/23, when geopolitical tensions between Germany and Russia led to concerning disruptions in gas supplies from Russia and thus to gas shortages in Germany, the vulnerability associated with such heavy reliance on a single source became more evident than ever before. The motivation behind finding alternative energy resources to fossil fuels is thus twofold and includes a strong focus on climate action combined with greater independence from imported oil and gas.

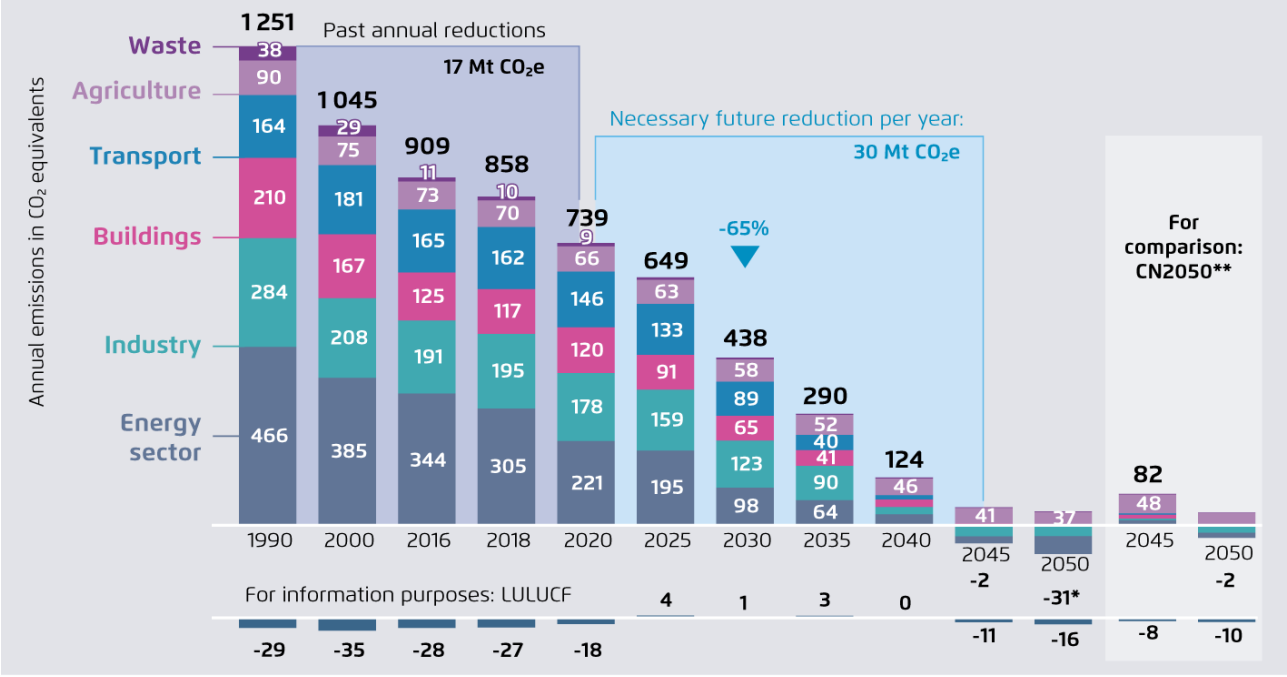

Figure 1.2 Historical, current, and projected carbon emissions in Germany broken down by sector on a projected pathway to reach the goals formulated by the Climate Action Act of 2021 [1].

1.3 Utilization and Potential of Geothermal Resources in Bavaria and Beyond

1.3.1 Theoretical Potential of Geothermal Waters to Support Sustainable Development

Given the urgent need for alternative energy sources due to climate change, geopolitical instability, and legislative mandates, potential solutions must be explored. Among hydro, wind, solar power, and biomass energy, the German Renewable Energy Sources Act (Erneuerbare-Energien-Gesetz) (EEG) [15] lists geothermal power as one of the five possibilities to help minimize adverse climate change effects. Geothermal waters offer heating, cooling, and the production of electricity, fulfilling the demands of an alternative resource to fossil fuels and playing a key role in building a more sustainable future. Additionally, some deep geothermal waters are of adequate quality to be used for human consumption and balneological treatments. The following list shows how geothermal aquifers could potentially support a number of the United Nations Sustainable Development Goals (SDGs) [96]:

- **SDG 3: Good health and well-being.** Geothermal waters can be used for medical spa purposes with a local specialization on specific ailments to be treated. This focus depends on the hydrochemical composition, including trace ions and total mineralization of the waters and their temperatures.

- **SDG 6: Clean water and sanitation.** In contrast to shallow aquifers, deep groundwater is shielded from above-ground contamination, making it a more reliable source of clean water. However, its suitability for drinking purposes depends on its hydrochemical composition and necessary treatment.

- **SDG 7: Affordable and clean energy.** Geothermal energy can be utilized for cooling, heating, and electrical power generation purposes with a minimal GHG footprint. Unlike solar and wind energy, which depend on fluctuating weather conditions, geothermal energy provides a constant and reliable power source by tapping into the Earth's internal heat.

- **SDG 11: Sustainable cities and communities.** By offering a decentralized supply of heating and electrical power, geothermal energy alleviates the strain on centralized energy grids, reduces air pollution, and offers efficient heating and cooling for buildings through heat pumps or district heating networks.

- **SDG 13: Climate action.** Geothermal power extraction has a minimal GHG footprint, especially when managed properly. Unlike fossil fuel-based energy, it does not rely on combustion, making it a cleaner alternative.

- **SDG 15: Life on land.** Geothermal power generation occupies less land than alternatives, e.g., solar power, and thus helps reduce the land-use footprint associated with electricity generation. This is especially relevant in crowded areas with potential land-use conflicts.

1.3.2 Geothermal Resources in Bavaria and Austria

Even though the general focus in utilizing geothermal waters is often put on heating and power generation, in Bavaria and Austria, balneology is the oldest documented use of geothermal waters. Healing wells still play a significant role in Germany's medical spa industry today, with Bavaria being home to 38 medical spas [39]. Only in the last few decades has the exploitation of geothermal energy for heating and electricity production become another major use of this resource [40].

The Study Area

The studies presented in chapter 3 are based on the analysis of data gathered at nine wells in the NAFB. Figure 1.4 illustrates the locations of eight of these nine wells inside the German groundwater aquifer DEGK1110 and the Austrian aquifer GK100158. The ninth well, Bad Abbach Kaisertherme, lies just west of the northwestern DEGK1110 boundary.

According to unpublished inspection reports available to the Chair of Hydrogeology at TUM, the nine studied wells vary in age, with some having been in operation for approximately a century, while others were established in the 1990s. All wells produce geothermal waters from the deep Upper Jurassic Aquifer (UJA) (subsubsection 1.3.2); however, the types of use differ, with four wells being used exclusively for balneology and three wells for district heating. One well additionally produces electrical power alongside district heating.

Table 1.1 Names, years of establishment, and types of use for the nine wells located in the study area on which the analyses of this thesis are based. Types of use include: B - Balneology; G - Geothermal power/heat production; F - District heating; E - Electrical power generation.

Well name	Well ID	Groundwater aquifer	Certified in	Usage(s)
Bad Abbach Kaisertherme	BAK	DEGK1110	1999	B
Bad Birnbach T3	BB3	DEGK1110	1973	B
Bad Füssing Therme 1	BF1	DEGK1110	1937	B
Simbach-Braunau TH-2	SB2	DEGK1110/GK100158	1999	G (F)
Straubing TH-1	STR	DEGK1110	1990	B, G
Altheim TH-1	ALT	GK100158	1989	G (F, E)
Bad Schallerbach TH-1	BS1	GK100158	1918	B
Haag TH-1	HAA	GK100158	1991	G (F)
St. Martin TH-1	STM	GK100158	1998	G (F)

Geological Conditions in the Northern Alpine Foreland Basin

The NAFB possesses a combination of geological properties that make it home to the highest number of geothermal plants in Germany [11]. The formation of the NAFB, a sedimentary basin in southern Germany and north-western Austria (Fig. 1.4), dates back to the Late Jurassic and was shaped by a constant alternation of marine and continental sedimentation processes. Approximately 150 million years ago, a global rise in sea level flooded what is now central Europe, mainly today's southern Germany and parts of Austria, forming an epicontinental sea north of the Tethys Ocean [51]. The marine environment that developed under the waters of the Tethys Sea facilitated the formation of two main groups of hydrologically relevant sediments: compacted carbonates formed under the pressure of the deep sea, centrally within the marine basin, while reef conditions in the shallower regions of the sea produced dolomites and limestone.

These two formations led to aquifers with distinct porosity characteristics: low matrix porosity in compacted carbonates and high matrix porosity in reef limestones [8]. The overlying layer shows evidence of significant karstification, which suggests a decrease in sea levels at the end of the Jurassic, whereby the upper carbonate sediments were exposed to the erosion of the warm and humid climates of the Cretaceous and the early Tertiary [76]. As a result, early alpine orogenesis in the Tertiary led to the deposition of eroded terrestrial material in the NAFB and gradually moved the basin northward [76]. Today, the karstified UJA, regionally referred to as the "Malm" formation, represents the most productive geothermal and balneological aquifer within the NAFB and even within Europe thanks to its high matrix porosity [8, 9, 44].

Geographically, the NAFB extends from the Franconian Jura in the north to the edge of the Bavarian Alps in the south and from the German state Baden-Württemberg in the west to Upper Austria in the east [68, 11]. The UJA dips toward the south and reaches depths of 5,000 m in the central basin around Munich [8, 67, 11], and even 6,000 m at its southern margin [78]. Its maximum vertical thickness is approximately 600 m [78]. Its vast expanse of porous rock formations and underground reservoirs boasts a substantial potential for geothermal heat and power production, as well as highly-mineralized healing waters for med-

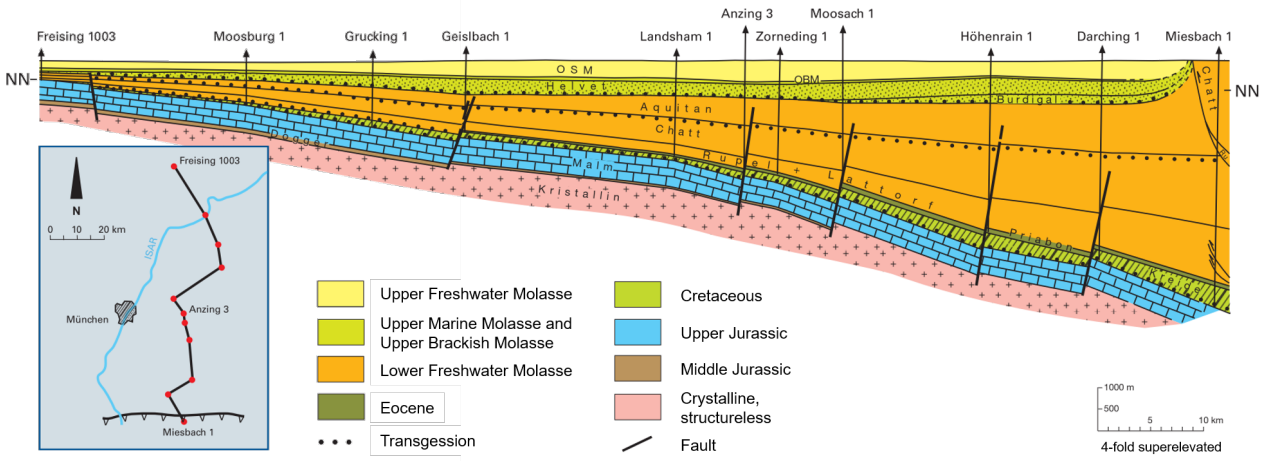

Figure 1.3 Profile of the Upper Jurassic Aquifer in the Northern Alpine Foreland Basin, adapted from the Bavarian Geothermal Atlas [11] (colour-corrected for improved readability).

ical spas, producing waters with temperatures of up to 160 °C at typical production rates of 30 - 150 L/s [68, 11].

Spatial Variability of Groundwater Chemistry in the Study Area

Most of the high porosity carbonates in the UJA are generally characterized by freshwater, with total TDS values increasing with the depth of the aquifer, leading to occasional saltwater occurrences in the very south of the NAFB (e.g., Opfenbach well with 25 g/L NaCl at 3700 m below ground level) [43]. While the UJA waters are relatively homogeneous, they can be divided into three geographical regions based on the composition of their main ions.

In the **northern margins** of the NAFB, waters of the type Calcium-(Magnesium)-Bicarbonate are observed [78]. Given that the UJA's recharge areas are located here along the river Danube [67], these meteoric waters are relatively young and show low TDS values of around 500 mg/L [12]. Their high magnesium levels stem from larger shares of Dolomite in the aquifer rock matrix [78]. There is a noticeable variability in the northern waters' calcium-magnesium-ratio, which might be caused by different mineralogical conditions in the aquifer [77].

The waters in the **central basin**, located south of the northern margins along the Danube and west of the Lanshuter-Neuöttinger-Hoch (LNH) between Munich and Regensburg, have TDS values of around 600 mg/L in the north; going south, sodium and chloride concentrations increase to 120 - 150 mg/L, and TDS values increase to 660 mg/L [12]. In the central basin, the waters typically belong to the Sodium-(Calcium)-Bicarbonate type [78]. Responding to the increase in sodium and chloride, Sodium-Calcium-Magnesium-Bicarbonate waters dominate in the northern part of the central basin. In contrast, Sodium-Calcium-Bicarbonate-Chloride is the more prevalent type in the southern parts of the central basin [12]. This change in hydrochemistry compared to the formation area further north is due to an influx of ion exchange waters from the layers above and below the main aquifer. This explains the large sodium surplus relative to the chloride concentration since the UJA waters contain relatively little sodium [78]. In contrast, sulfate concentrations decrease going south due to thermochemical sulfate reduction and methanogenesis

starting at 100 °C [12]. The resulting H_2S and methane can be detected in all UJA waters in the central NAFB [11, 12].

The **eastern basin** is located east of the LNH and exhibits high TDS values compared to the central and northern basins of around 1100 - 1500 mg/L [12], as well as high concentrations of trace elements (e.g., fluoride and iodide concentrations of 7 - 10 mg/L and 460 -500 µg/L, respectively) [78]. These eastern waters are characterized as the Sodium-Bicarbonate-Chloride type, separated distinctly from the rest of the basin by the LNH [12]. They have evolved from ion exchange waters, resulting in very low ratios of alkaline earths to alkali (0.01 - 0.06) [12]. Their hydrochemical signatures resemble those of the waters found in the overlying Cretaceous and Tertiary layers, which hints at hydraulic contact between the aquifers and almost complete seclusion from the western and northern rest of the UJA [78, 11]. Their high TDS values might also be linked to a contribution of salinary pore waters or an influx of highly mineralized deep groundwater from the crystalline basement of the Bohemian Massif [59]. Regarding specifically their high bicarbonate concentrations of around 500 - 700 mg/L, a reasonable explanation is infiltrating waters from oil fields [78]. Showing no signs of ^{3}H or ^{14}C, the waters found in Lower Bavaria and Upper Austria are assumed to be quite old [98].

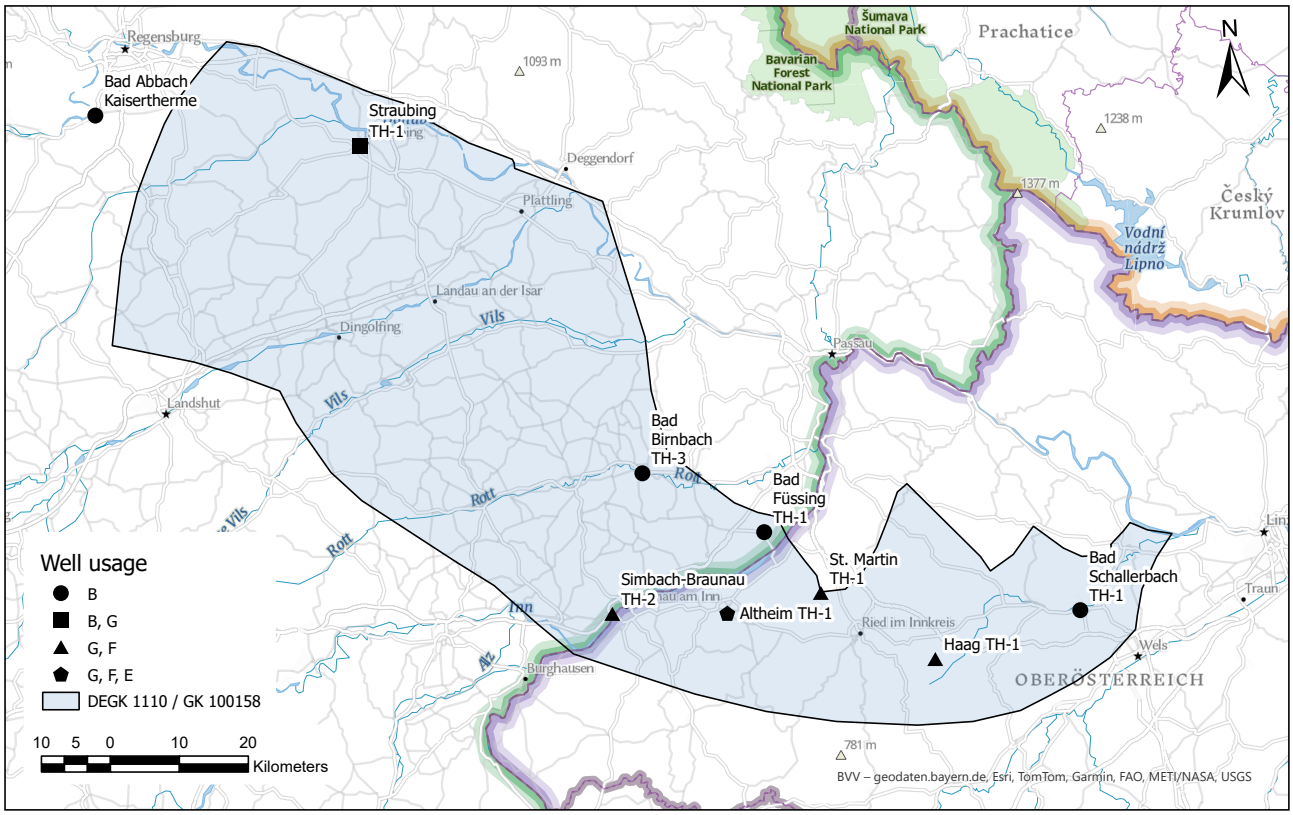

Figure 1.4 The study area, which covers a large part of the Molasse basin in Bavaria and Austria. The blue shaded area delineates the aquifer DEGK1110 (Bavaria) and GK100158 (Austria).

1.3.3 Utilization and Development of Bavarian Geothermal Resources

The high porosity and deep location of the UJA make for ideal conditions for deep geothermal energy production and balneological (medical) spas. In Bavaria, there is currently a total of 24 deep geothermal

power plants. 14 more installations are in the planning stage, and 4 more wells are being built [17]. In addition, Bavaria is home to 39 balneological wells and spas, of which 25 are officially recognized and certified as medical baths [17].

In Bavaria, **deep hydrothermal energy production** considers wells which exploit aquifers > 400 m and up to 7000 m below ground level [11]. This application uses heat stored in hot water reservoirs with temperatures of at least 40 °C but often > 100 °C [2]. Low enthalpy geothermal plants can be profitable when high production volumes balance out the relatively low temperatures [11]. Typically, these warm waters are harnessed through geothermal doublets (Fig. 7.1), geothermal plants consisting of a production well and a reinjection well. The waters are moved to the surface via an underwater pump in the production well. If the water temperatures are high enough (> 70 °C at production volumes of 28 - 50 L/s), the thermal energy can be utilized directly through a heat exchanger, which transfers the energy into a heating network; otherwise, the system might require heat pumps (40 - 70 °C and approx. 40 L/s). Wells producing large amounts of water at > 80 °C can be used for electrical power generation [11]. After the heat has been extracted from the waters, the cooled-off fluid is reinjected into the aquifer through the reinjection well to be reheated and to support a quantitative balance of the aquifer (Fig. 7.1). To maintain the plant's longevity, it is critical to space the production well and the reinjection site far enough apart from one another to avoid a thermal or hydraulic short circuit. The minimal distance depends on the reinjection temperature and volumes, as well as the hydraulic and thermic conditions in the aquifer [85].

While geothermal power plants and their profitability depend on production volume and temperature potentials, **balneological** wells are additionally limited to locations with specific hydrochemical signatures. Depending on these conditions, geothermal waters can cover a bath's heating and energy expenditures, and offer medical spa treatments using the water's hydrochemical composition and its accompanying gases. While being restricted by the waters' mineralization, balneologically used wells can cope with much lower temperatures and production volumes (> 20 °C and > 2 - 3 L/s, respectively) [11]. Balneological installations generally do not require reinjection wells. For one, this is due to their small production volumes being much lower than those of geothermal doublets. On the other hand, waters that have been used in a public swimming pool or for medical treatments cannot be reintroduced to the aquifer due to a high chance of contaminating the pristine reservoir waters. Instead, the used and cooled-off waters are discarded through the public sewage system, resulting in a net discharge from the aquifer because the produced water volumes are not replaced in the reservoir (Fig. 7.1). An exception to this is Bad Füssing, where the same aquifer is utilized for both balneological applications and heating purposes. The waters for each use are kept in separate piping systems, allowing the heating water to be reinjected after use, as it never comes into contact with potential human contamination sources.

2 State of the Art: Can Geothermal Resources Save the Sinking Ship?

2.1 Unique Features of Deep Groundwater Systems

2.1.1 Slow Generation and Compartmentalization

Ironically, the defining feature of deep groundwater, being its **depth below surface**, varies greatly in existing literature and ranges between > 150 m [57] and > 600 m [3]. Regardless of their minimum depth, Fig. 2.1 shows that deep groundwater aquifers are separated from shallow groundwater, which can occur at depths of just a few centimeters to meters below ground. These secluded deep aquifers hold the largest fraction of water found in groundwater aquifers, making up 80 % of all groundwater, and show the least connection to the rest of the terrestrial water cycle [37, 36]. Thus, one might argue that this separation is a more defining feature of deep groundwater aquifers than their minimum depths. Accordingly, a guideline published by the LfU in 2023 describes these groundwater bodies as **slowly-generating aquifers** instead of deep groundwater [40]. In their definition, the slow (re-)generation is caused by a segregation due to an extensive, thick, and impermeable layer above the aquifer, a decrease in permeability at depth due to a significant change within the groundwater storey, or a large thickness of the groundwater storey [40]. Thus, deep groundwater might no longer (only) be described based on its depth, but also its slow (re-)generation and, therefore, its typically old age.

Groundwater age is a function of distance from the recharge area, indicating the time since the water entered the groundwater system [35]. Residence time indicates the average turnover time, representing the ratio of the volume of water in a groundwater system to the system's volumetric recharge or discharge rate [35]. Only thin layers of soil and sometimes rock shield shallow aquifers from surface water infiltration after a precipitation event, which means that shallow aquifers react to precipitation events in the form of baseflow in time frames of minutes to days, depending on watershed size, surface and soil properties, and the precipitation event [105]. Consequently, most of the groundwater found in the upper 100 m of the Earth's crust is only a few days to decades old and is therefore considered modern groundwater [55]. In contrast, deep aquifers are separated from vertical surface water infiltration by sometimes thousands of meters of soil, rock, and impermeable strata, preventing short-term aquifer recharge. Some deep water occurrences have been dated to millions and even billions of years old [97, 19]. These waters can be found trapped as inclusions in minerals formed in the earliest crustal history. For example, an old fracture system in South Africa, 2.8 km below the surface, was found to host fluids isolated from the photosphere tens of millions of years ago [62]. Similar fluids were found in deep fractures in a mine in Timmins, Canada, located in the Canadian Precambrian Shield. Xenon isotope changes were used to calculate a minimum

mean residence time for these fluids of about 1.5 billion years [50]. Central European deep groundwater, such as the UJA in Bavaria and Austria, is significantly younger; however, it exceeds the limit of what is considered modern groundwater (some 50 years). Using radiocarbon dating with dissolved inorganic carbon and dissolved organic carbon, [48] assessed the age of seven UJA wells, determining an age range of young and old components of between 4,200 and 25,000 years. Multiple studies confirm the existence of fossil groundwater (i.e., groundwater recharged by pre-Holocene precipitation more than 12,000 years ago) in the UJA [55]. A study at three wells in the central basin using ^{81}Kr even determined water ages between 60,000 and 135,000 years [47], and one of the latest studies on the topic of groundwater age, using a combination of $^{14}C_{DOC}$ and ^{81}Kr dating, found a likely confluence of a younger and an older component, dating to 9,800 - 18,700 years, and 300,000 years, respectively [103].

The exceptionally old age of some deep groundwater occurrences hints at a **compartmentalization** of deep aquifers in addition to the stratification of groundwater bodies caused by differences in their densities [36] (Fig. 2.1). However, waters at depths of up to 5 km below surface level have shown stable isotope signatures indicating, like most groundwater bodies, meteoric origin, thereby pointing to at least some connection to the terrestrial water cycle; be that in the past or the present [69, 38]. The idea of compartmentalization is supported by new evidence produced in a study that used a chloride mass balance approach to quantify the contribution of deep groundwater to streamflow [36]. The results show that groundwater found below 500 m underground, while representing 40 % of global freshwater resources and 80 % of global groundwater [37], contributes less than 0.1 % to streamflow, and is therefore practically cut off of the rest of the hydrological cycle (Fig. [36]) 2.1.

In the context of climate change and this dissertation, its isolation from the rest of the water cycle means that, while it barely contributes to streamflow, deep groundwater is also minimally, if at all, affected by surface-level changes in meteorological conditions. Therefore, it constitutes a unique resource of immense amounts of water that are not currently deteriorating due to climate change or anthropogenic contamination and deserve special protection. This would ensure that these waters are spared for a future period in which most, if not all, other freshwater resources are no longer available for human, industrial, or agricultural consumption.

2.1.2 Hydrochemical Quality

Due to the long residence times of water in these aquifers, the quality of deep groundwater and its related drivers and indicators differ from those applicable to shallow groundwater aquifers. Depending on the land use and land cover, population density, and geological and geomorphological conditions, groundwater contaminants in shallow aquifers in Germany include nitrate pollution from agricultural activities and the use of fertilizers, and from urban environments, [75], which go hand in hand with the influx of pesticides and their metabolites [5]. Further, a whole list of pharmaceuticals, estrogenically active compounds, and various kinds of pathogens have been identified in both groundwater and surface water due to incomplete elimination in wastewater treatment plants [82, 86, 63, 80]

In contrast, deep groundwater quality is tied to different contamination risks than anthropogenic contaminants [57]. **TDS** is a common indicator used for assessing deep groundwater quality. Typically, TDS

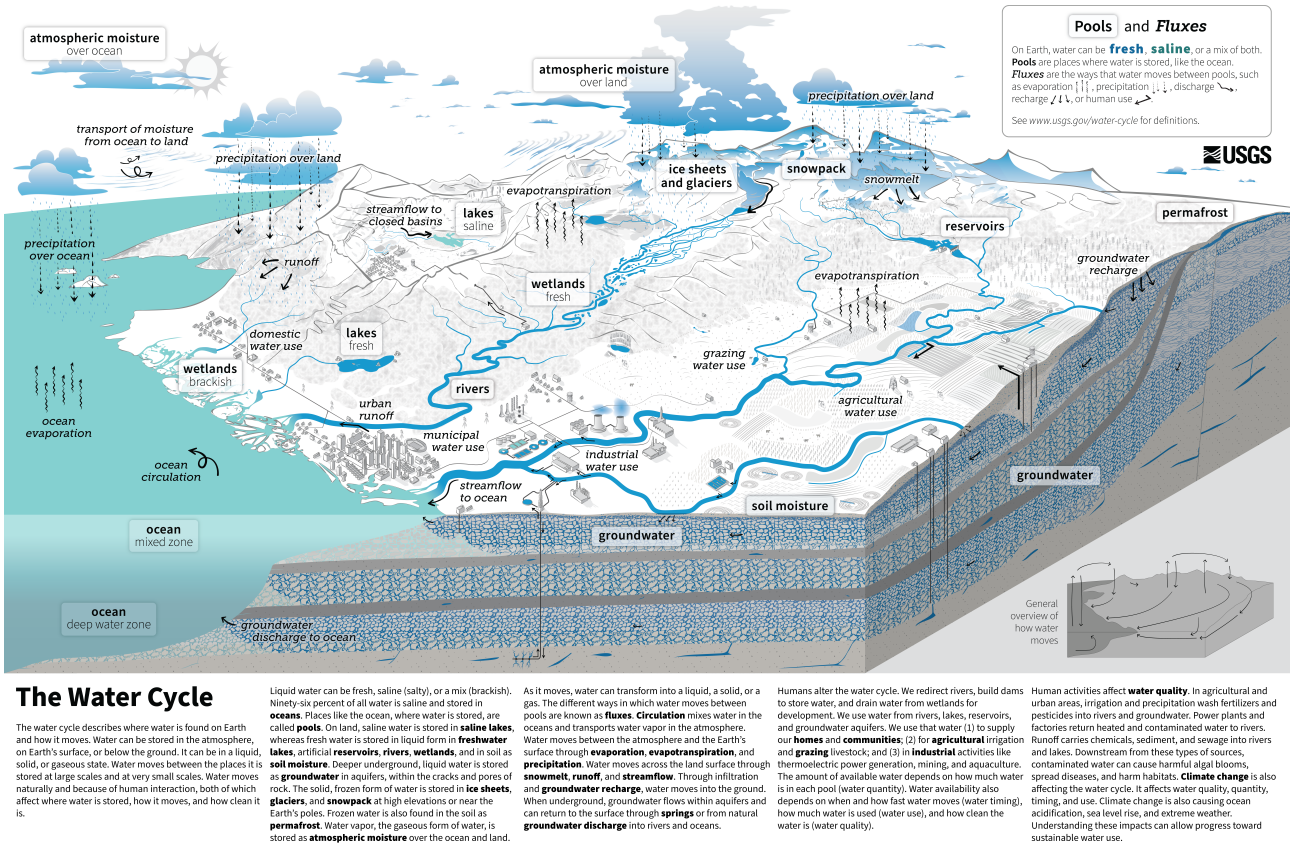

Figure 2.1 A new schematic of the hydrological cycle with an adequate representation of deep groundwater, highlighting the vast expanse of deep aquifers, as well as the significant compartmentalization of the individual bodies of groundwater [21].

values increase with depth due to the long residence times of deep groundwater and prolonged water-rock interactions along the flow path. However, instead of finding a linear correlation between depth and TDS values, a study in California observed the most significant differences between these parameters at a depth of 1,000 m below surface across 17 groundwater basins [58], with TDS values > 10,000 mg/L most commonly found in wells with a depth > 1,000 m [58]. Deep groundwater receives its reputation of insufficient quality for human consumption or irrigation purposes from these high TDS values [57]. However, groundwater with TDS values < 3000 mg/L is still considered fresh water, and waters with TDS values < 10,000 mg/L are usable for many application purposes, especially as treatment options are improving and desalination becomes more accessible [57]. Thus, the close connection between drinkability and TDS values makes TDS a critical parameter in determining deep groundwater quality.

Despite their great depths below the surface, deep groundwater aquifers can still be influenced by contaminating substances, e.g., fossil **oil and gas** fields, either by direct adjacency or intrusion of oil field waters or by disruptive oil and gas exploitation activities [58]. For example, a study from the Athabasca Oil Sands Region in Alberta, Canada, one of the largest proven reserves of crude oil, examined spring water from the underlying deep aquifer, which was hypothesized to be influenced by the presence of oil field waters in the region. The assessed waters, which are composed of up to 75 % of Laurentide glacial meltwater and were affected by the dissolution of Devonian evaporite and carbonate deposits, showed TDS

values of up to > 50,000 mg/L [45]. Bitumen contains heavy metals of which arsenic, iron, molybdenum, nickel, selenium, and zinc were found in spring water in this study area, partially exceeding water quality guidelines for the protection of aquatic life, alongside seven polycyclic aromatic hydrocarbons (PAH) with concentrations of up to > 270 mg/L [45].

Based on the high gas loading, hydrochemical characteristics, and high concentrations of hydrocarbons, parts of the southwestern UJA seem to be in contact with oil field waters, too [68]. One UJA well in Pullach even produces oil along with the geothermal water, indicating the presence of an oil phase along preferential flow pathways and/or as a larger reservoir [9]. Close contact with oil fields is often indicated by high mineralization values, with oil field waters from overlying strata displaying Na-Cl-concentrations similar to seawater values and oil field waters from underlying strata displaying much higher mineralization values [67]. These oil field waters are characterized by high bicarbonate values, hinting at oil field water influences, especially in the eastern basin of the UJA [67].

In addition to oil field waters, deep groundwater aquifers can be affected by the intrusion of **salinary waters**. While this is also possible in shallow aquifers located in the vicinity of coastlines where ocean water infiltrates into connected groundwater bodies, land-locked deep aquifers interact with salinary water either through reinjection of disposal water from the oil and gas industry [56], or, as is the case in this thesis' study area, through intrusion of salinary pore water from overlying strata [77]. In the UJA, these waters stem mostly from salinary Purbeck sediments and lead to elevated sodium and chloride concentrations [67].

2.1.3 Challenges of Data Availability

While subsections 2.1.1 and 2.1.2 discussed the inherent properties of deep groundwater and the differences between deep aquifers and shallow aquifers, it would be amiss not to mention a meta property affecting deep aquifers much more than shallow aquifers: poor data availability. In Bavaria, a total of 1,861 state-funded groundwater wells monitor shallow aquifers [10], of which 599 are equipped to monitor the goals of the 3rd river basin management plan determined by the Water Framework Directive (WFD), e.g., basic chemistry (ion composition), metals, non-relevant metabolites, PAH, per- and polyfluoroalkyl substances (PFAS), pesticides and relevant metabolites, semi-volatile halogenated hydrocarbons (SVHC), and volatile organic compounds (VOC). In addition, there are > 12,000 private monitoring sites adding to a vast amount of data concerning shallow groundwater [10]. In contrast, data on deep aquifers are sparse, both in temporal and spatial resolution, due to a lack of accessibility, technical feasibility, and monetary profit [46]. According to [42], in March 2025, there were 69 deep groundwater wells in Bavaria used for balneological, geothermal, and electricity generation purposes. Readily available parameters include primary and secondary use, temperature, flow rate, depth, and annual energy production values [42].

Figure 2.2 shows the years for which data were available in the extensive database at the Chair of Hydrogeology at TUM in November 2023 and illustrates the **low temporal resolution**. The data points include a full hydrochemical assessment of mineralization and parameters such as temperature, production volume, pH, and electric conductivity (EC), collected once a year to monitor water quality in spas and scaling and corrosion potential in geothermal plants. It is apparent that in the best-case scenario, for these

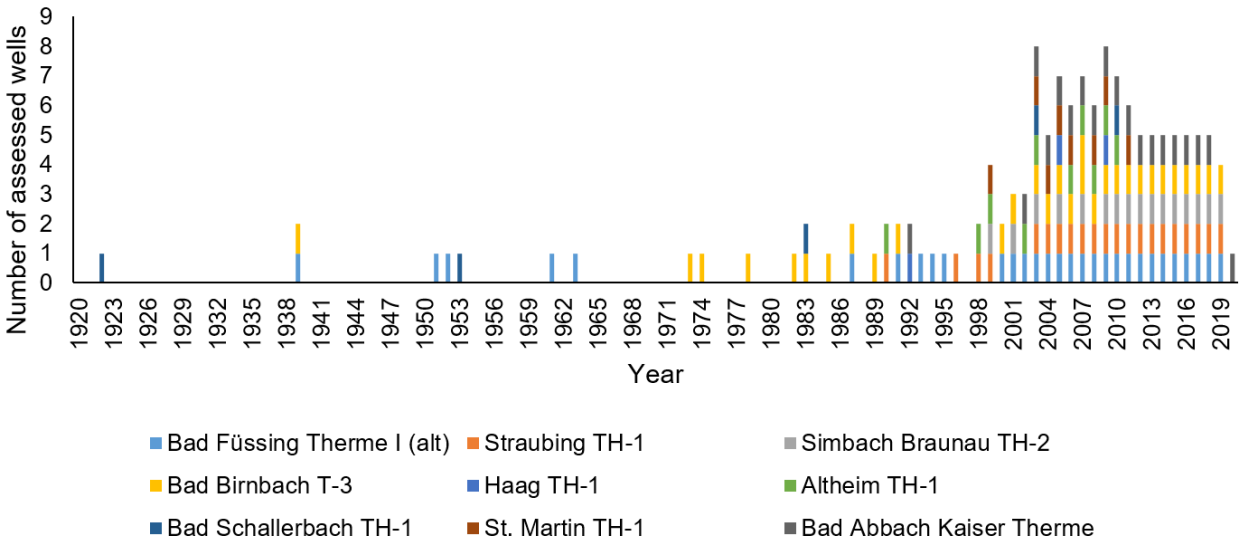

Figure 2.2 Years in which yearly data points on the hydrochemical composition are available at the nine deep groundwater wells examined in this dissertation, color-coded by the individual well sites [23].

wells, such data are available on a yearly basis, though long gaps are noticeable for most of the wells. A more or less coherent data basis is only available for the time after the early 2000s. Hydrochemical data are only accessible through well operators, making efficient data assimilation difficult; however, even with unrestricted access, scientists would still be limited to yearly analyses.

One idea to tackle this challenge is to apply **virtual sensors (VS)** to deep groundwater data. VS constitute a software layer that provides indirect measurements of process parameters based on aggregated and synthesized data originally gathered by physical (or other virtual) sensors [65]. Through known correlations between the signals of physical sensors, they synthesize information in complex functions and produce new data that, in some cases, would otherwise not be measurable via physical sensors at all (Fig. 2.3). This concept is linked to sensor networks, a linking of sensors at the physical hardware level, and sensor fusion, whereby information is merged on an information level [65]. By fusing parameters that are currently affordably observable at a high resolution (e.g., temperature, EC, pH, production rate, pressure, as well as meteorological data and heating demand) with parameters that are too expensive to be analyzed more than once or a few times a year (e.g., ionic composition and contaminants such as PAHs or PFAS, etc.), VS could help improve temporal resolution. A successful application of VS would be a great achievement for the deep geothermal research community and for the operators of these wells since VS are cost-effective (both in the acquisition and in upkeep) [91], they can be deployed in environments too hostile, e.g., highly corrosive or inaccessible towards physical sensors, they can be updated by simply adjusting the algorithm, and they are not affected by naturally occurring sensor drifts which affect physical sensors [65].

The **low spatial resolution** is the result of high drilling costs and technical difficulties associated with drilling wells extending into depths of thousands of meters [55, 46]. Thus, many studies of deep aquifers rely on data gathered at deep wells from the oil and gas industries, where monetary investment is done on larger scales [58, 46]. This study bases its analysis on data from nine wells, which have to suffice to cover

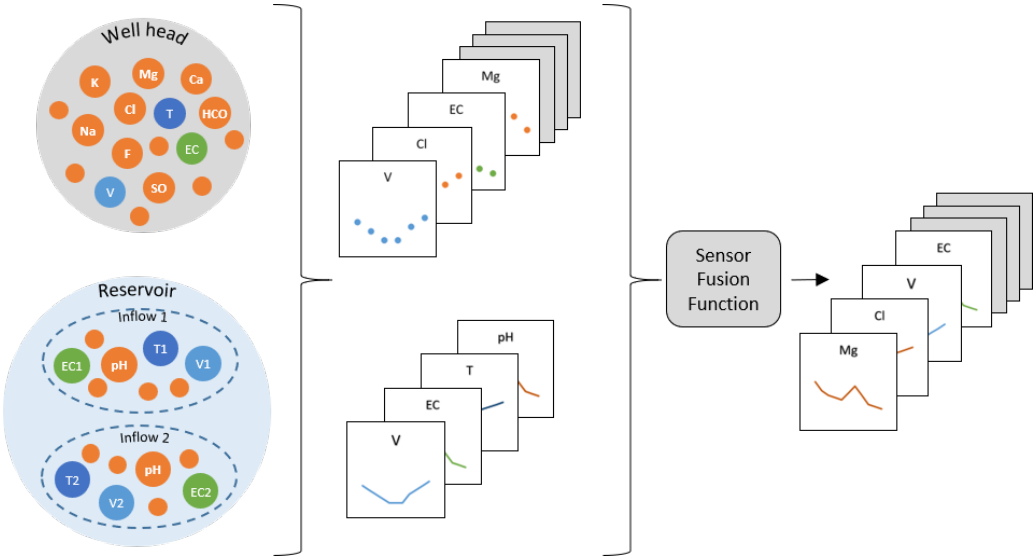

Figure 2.3 Potential application of virtual sensors in the context of deep aquifers. Two data types are collected, describing conditions at the wellhead and reservoir, resulting in two data sets with high and low temporal resolution, respectively. After being processed by a sensor fusion function, high-resolution information on all parameters becomes available.

an area spanning parts of two Bavarian administrative districts (Upper Palatinate and Lower Bavaria) and one Austrian state (Upper Austria), which stands in no relation to the spatial density of monitoring wells for shallow groundwater.

2.2 Renewable Resources vs. Sustainable Exploitation

As outlined in section 1.2, geothermal energy is identified as a potential contributor to the German energy transition in both the NECP [34] and the EEG [15]. At the same time, in the broader context of sustainability, it is worth questioning whether geothermal waters truly qualify as a renewable resource or whether their utilization should instead be regarded as a form of heat mining. To address one of this thesis' central questions, that is, regarding the classification of hydrothermal systems as renewable, it is essential to closely examine the concepts of *renewable energy* and *sustainable use*.

The term "renewable" in and of itself means capable of being renewed. The Oxford English Dictionary further defines **renewable resources** as not depleted when used. In a broader sense, this understanding can be extrapolated to include all forms of energy from natural resources, which are replenished at a higher rate than they are consumed [95]. Sunlight, wind, hydropower, and ocean (wave) power are prominent examples of resources constantly being replenished [95] (some more obviously than others) by incoming solar radiation. Consequently, while technically of natural origin, oil and gas are excluded in this definition since they are not replenished faster than being exploited; they took hundreds of millions of years to form [95] while humanity is doing its best to use them up in merely a few centuries. Strictly speaking, this could also classify geothermal power production as a non-renewable energy resource, as the slow reheating process takes much longer than the exploitation time frame. Although the definition of renewable resources does not concern the amount of GHG emissions associated with them, generating renewable

energy typically emits very low volumes of GHGs compared to burning oil and gas: per kWh_e, on-shore wind power produces 12 gCO_2-eq, hydro power produces 4 gCO_2-eq, and geothermal power produces 45 gCO_2-eq [72].

Discussions on renewable energies often include the term **sustainability**, which considers the broader concept of using resources in a balanced and responsible fashion. A word commonly used with little afterthought in today's everyday conversations, it was officially defined in 1987 by the United Nations Brundtland Commission. According to this commission, it defines the ability to "meet the needs of the present without compromising the ability of future generations to meet their own needs" [94]. In that sense, sustainability applies to various aspects of life, not just resources, with the goal being to create long-lasting systems and practices that don't deplete resources, harm the environment, or exploit communities [94]. This is a critical differentiation: in this thesis' context, and in the context of geothermal energy utilization, the exploitation of finite resources can still be done responsibly and thus considered sustainable.

2.3 The Sustainability of Geothermal Exploitation

2.3.1 Geothermal Power Plants with Reinjection

When considering the sustainability of geothermal energy and heat production, an essential factor is the life expectancy of a geothermal well. Typically, deep geothermal power plants can be maintained profitably for 20 - 30 years, with the oldest European geothermal doublet running successfully since 1969 and without indicating a decrease in production temperatures in the Paris Basin [11]. In general, the life expectancy of a geothermal plant depends on two major factors: its thermal breakthrough time and the structural and technical integrity of the well site's hardware, such as pumps, piping, and heat exchangers.

As discussed in subsection 1.3.3, the geothermal doublets in this study produce hot water through deep production wells, run it through a heat exchanger, and reinject the cooled-off fluid back into the aquifer, where it can be reheated by the surrounding hot aquifer rock matrix. Depending on the distance to the production well site and production volumes, this cool front will eventually reach the warmer production well, an event called **thermal breakthrough** [11]. Correspondingly, the time the cold front takes to reach the production site is named thermal breakthrough time. The thermal operating life does not necessarily end immediately upon thermal breakthrough. If the mixed waters consisting of reinjected cold waters and hot production waters exceed the minimal temperature value over which well operation is still profitable, the well's life expectancy can lie well beyond its thermal breakthrough time [11].

It is important to note that the thermal breakthrough happens in a chemically dynamic setting, as chemical interactions between the aquifer rock matrix and the reinjected waters can affect the transmissivity and, thus, the flow rates in the rock matrix, as was shown for granite and sandstone aquifers by [83, 84], and for carbonate aquifers by [106, 66]. In the latter case, these interactions are driven by the **carbonic acid system** [104] shown in Figure 2.4.

Initially in chemical equilibrium before being extracted from the aquifer, the hot water contains gases, including CO_2. As the fluid is cooled off in preparation for reinjection, the decrease in temperature causes a shift in the hydrochemical equilibrium of the produced waters. Henry's law states that the solubility of

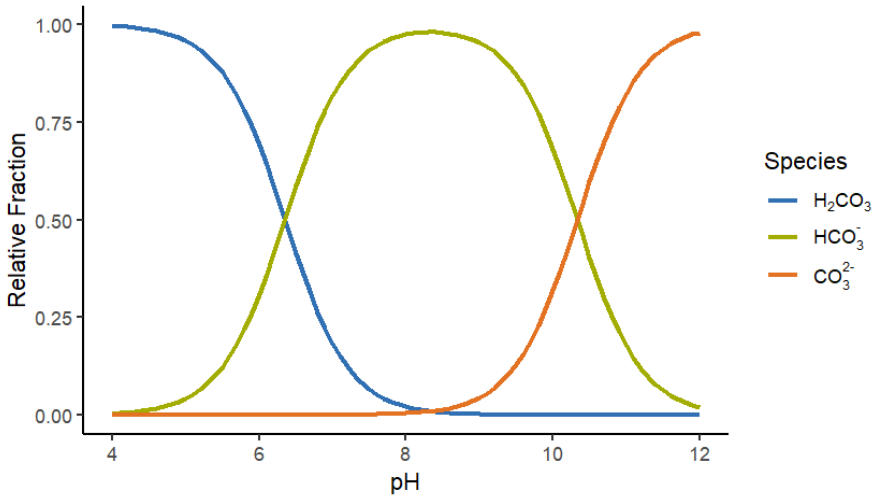

Figure 2.4 The lime-carbonic acid-equilibrium: the proportion of H_2CO_3, HCO_3, and CO_3^{2-} in a water sample as a function of pH.

a gas in a liquid is directly proportional to the partial pressure of the gas above the liquid and inversely proportional to the temperature of the liquid [49]. As the water cools down, CO_2 from the gas phase dissolves into the water, resulting in carbonic acid (H_2CO_3), lowering the saturation index (SI) of calcite over time (from production to injection):

$$\mathrm{CO_2(aq) + H_2O \rightleftharpoons H_2CO_3} \tag{2.1}$$

At a pH < 6.5, the CO_2 in the water is primarily present as aqueous CO_2. The resulting carbonic acid (Fig. 2.4) can dissociate, forming bicarbonates and carbonates (Equations 2.2 and 2.3):

$$\mathrm{H_2CO_3 \rightleftharpoons H^+ + HCO_3^-} \tag{2.2}$$

$$\mathrm{HCO_3^- \rightleftharpoons H^+ + CO_3^{2-}} \tag{2.3}$$

When this water comes into contact with carbonate rock, it causes the calcium carbonates to dissolve (Equation 2.4):

$$\mathrm{CaCO_3 + CO_2 + H_2O \rightleftharpoons Ca^{2+} + 2\,HCO_3^-} \tag{2.4}$$

The dissolving effects of Equation 2.4 directly impact thermal breakthrough time: by cooling the water, the saturation index of calcium drops, facilitating dissolution processes in the aquifer in the vicinity of the reinjection well, and, if dissolution took place before, precipitation effects where the water is able to heat up again. This can lead to pore enlargement and changes in pore geometry and pore surface roughness close to the well, affecting the flow paths and traveling speed of the reinjected cool waters: fracture morphology, especially local apertures and wall roughness, has been found to be the most significant factor determining flow patterns [28].

Increased fracture surface roughness slows down water flow and increases localized turbulence in the water [28, 70]. This can cause capillary trapping [70]: in extreme cases, as with concave pores and

high pore wall roughness, the water at the innermost end of a dead-end cavity can be trapped until it becomes completely saturated, leading to concentration-limited diffusion until the saturated water diffuses out of the cavity [99, 28, 70]. In contrast, smoother fractures let the water flow freely and quickly without or with less eddie formation. In a pore space characterized by straight or convex pore walls and low surface roughness, the residence time of the water is, thus, relatively low, and new, still-undersaturated water can reach exposed fracture surfaces more easily. Therefore, any slightly saturated fluid is replaced quickly, creating rate-limited dissolution conditions. Since fracture surface roughness plays a critical role in mineral precipitation, [88] conducted flow-through experiments on calcite material. They observed enhanced gypsum precipitation on rougher fracture surfaces: pores with rough surfaces clogged much faster than smooth (polished) fractures. They concluded that the most critical factors influencing reaction rates (relative dominance of precipitation and dissolution) and, thus, hydraulic conductivity of fractures, are fracture wall roughness, the chemical composition of the fluid, and residence time [88]. Additionally, [28] found fracture morphology, especially local apertures and wall roughness, to be key parameters determining flow patterns. Further factors playing into the effects pore surface roughness has on site- and reservoir-specific parameters include interfacial tension, contact angle, and viscosity ratios [70].

Various methods have been applied in the field of characterizing pore space development. Micro computed tomography (MCT) has been used extensively, especially in petroleum geology, for assessing dynamic changes in rock matrix structure [108], and excels as a non-destructive method of characterizing pore networks, the internal structure of and fluid-flow dynamics in rock samples with an optimized resolution of less than 1 µm [79, 108]. These advantages are achieved by using an X-ray source and a detector, which produce a series of 2D radiographic images taken around a single axis of rotation. X-ray imagery uses the stark molecular contrast between solid and gaseous phases (rock matrix and pore spaces, respectively) [108], and works best with homogeneous materials like Berea sandstone [18]. Combining these images results in the examined object's 3D reconstruction (3D tomogram). X-ray imagery has been proven especially useful for the 3D characterization of natural porous media and fluid distributions within these natural porous media [102]. Another method is nuclear magnetic resonance imaging (NMRI). Similarly to MCT, it allows insights into the internal structure of a core plug; however, it focuses on the contrast between solid and liquid phases (rock matrix and fluid-filled pore spaces, respectively) [28, 71] and produces images with resolutions of $< 1\,\mathrm{mm}^3$ in all three directions [28, 27], which is a coarser resolution than that produced by MCT. NMRI has been applied, e.g., in the fields of monitoring capillary adsorption, structure and flow mapping, and porosity and saturation mapping [71].

Looking at the longevity of a well through the lens of renewable resources, the time it takes for the cooled-off waters to reheat in relation to the period of successful aquifer exploitation must also be considered, as renewable resources are characterized by a shorter, in this case **thermal, replenishment** of the resource than its exploitation period (section 2.2). In the case of geothermal doublets, the restoration of the initial temperature conditions takes much longer than their typical life expectancy [11]. One study showed that the reheating time could exceed the exploitation time 100-fold if the heat restoration is purely driven by conductive heating [101]. It was followed up by an assessment of the operation of a hydrothermal doublet in the UJA using a 3D system model to determine the natural reheating of the reinjected cooled-off waters [100]. The researchers in this study assumed an initial production temperature of 100 °C, an operation time

of 50 years, production volumes of 50 L/s, and reinjection temperatures of 55 °C. Based on site-specific geometrical, hydraulic, and thermal conditions, most importantly transmissivity, the model calculated the dispersion of the reinjected fluid and determined natural reheating times of 1,000 and 2,000 years, after which the reinjected waters reach temperatures of 91 °C and 97 °C, respectively. After 8,000 years, the temperature field is regenerated to a value close to the initial production temperature of 99.3 °C [100]. While the study dates back to 2005 and does not entirely reflect the current state of research, particularly in that it omits dissolution processes, it remains one of the few investigations into thermal recharge. As such, it still provides insight into the long-term dynamics of reservoir reheating.

2.3.2 Balneological Wells with a Net Discharge

One systemic difference in the plant operation strategies of geothermal energy production versus balneological spas is the categorical lack of reinjection of cooled-off waters into the aquifer in the case of medicinal wells (subsection 1.3.3). Since humans consume these waters directly, either as mineralized drinking waters, in swimming pools, or in specialized applications such as sulfur baths, reinjecting the used waters would risk biochemical contamination of the aquifer. Instead, the used waters are usually disposed of through the public sewage system, where they are transported to a treatment plant like any other wastewater. Further, balneological applications do not depend on high temperatures quite as much as geothermal power generation plants do and only require minimum temperatures of 20 °C to be officially certified as a thermal bath in Germany [22]. Typically, the hydrochemical composition is the most important factor to consider in balneology. Consequently, thermal breakthroughs and long temperature regeneration processes do not play a major role in the sustainability of balneology.

Instead, balneological wells impact the overall quantity of groundwater available to them. Theoretically, and in a worst-case scenario, a well could run dry if the net discharge exceeds the recharge rate of that aquifer. However, as presented in section 2.1, deep groundwater aquifers pose an immense resource of available water, and the complete exhaustion of an aquifer is highly unlikely. Instead, balneological wells operating at volume rates that are too demanding for a given well run the risk of activating or deactivating neighboring strata and the aquifers within them. In the case of these waters exhibiting chemical signatures that differ from their main aquifer, the additional waters might lead to a dilution of the mineralization or a different change in the produced water's chemical signature. Thus, to provide a sustainable use of a balneologically used well, it must ensure its production regime does not exceed natural aquifer recharge rates. This is usually covered by stringent withdrawal rate permits, limiting the exploitation to discharge rates of around 2 - 3 L/s [11].

2.4 Efforts to Protect Deep Groundwater Aquifers in Germany and Europe

The following section discusses legislative efforts to protect geothermal resources. Before diving into the works of the legislation established to protect the quality and quantity of deep groundwater bodies, the German Federal Mining Act [13] shall be mentioned briefly. It affects deep geothermal mining if the

well bore exceeds a depth of 400 m and is the central tool for approving proposed geothermal working procedure plans (§ 57e).

2.4.1 The European Water Framework Directive

The European WFD [33] concerns water conservation, which, according to this legislation, does not constitute a commercial product like any other. Instead, the WFD views water and its many forms as a "heritage that must be protected, defended and treated as such" (preamble (1)). It recognizes that water faces increasing pressure from a growing demand and presents community-based approaches to protect this resource in qualitative and quantitative terms (preamble (4)). It views surface waters and bodies of groundwater, in principle, as renewable natural resources as long as good planning, exploitation, and protection strategies are followed to ensure a good quantitative and qualitative status (Preamble (28)). According to the WFD, this good status must be achieved by all river basins and by both surface water and groundwater bodies in the EU, since they are connected hydraulically and ecologically (Preamble (34)). Among the framework's purposes are the prevention of further qualitative and quantitative deterioration of aquatic ecosystems, the promotion of sustainable water use, and a significant reduction in pollution of groundwater (Article 1 (a), (b), and (d)). To achieve these goals, the program of measures (Article 11) includes actions like controls over the abstraction of groundwater, a requirement for prior authorization of artificial recharge or augmentation of groundwater, and a prohibition of direct discharges of pollutants into groundwater except for some specified purposes.

While the WFD pursues noble goals, there is one major problem with this framework: its definition of groundwater includes all water bodies below the surface in the saturation zone and in direct contact with the ground or subsoil (Article 2.2). The critical part of this definition is the second half: it was clearly not written with the unique characteristics of deep aquifers in mind since they are, by definition, not in contact with the subsoil or the underlying saturated zone. The unique geological features of deep groundwater bodies, as presented in section 2.1, are thereby not considered in this text, which weakens the impact its suggestion of protective measures has on deep groundwater bodies.

2.4.2 Definitions and Quality Standards for Balneological Wells

While the WFD focuses on protecting groundwater as a resource, the Definitions and Quality Standards for the Nomination of Health Resorts, Resort Towns and Curative Sources (DQS) [22] is explicitly concerned with maintaining the quality of waters used in (German) medicinal spas. These institutions are bound to a specific location and the waters and/or gases produced there. Based on their chemical composition and/or physical properties, they are deemed applicable in the operation of medicinal spas, and officially certified and recognized as healing wells. The waters' hydrochemical and physical features determine the fields of medicine in which the waters can be deployed (e.g., rheumatology, cardiology, or orthopedics) [22].

Since the mineralization of the healing waters determines the curative field for which they can be used, the DQS determine thresholds in which the mineralization may fluctuate: "For the preservation and protection of a medicinal spring, it is [...] imperative that the assessment of fluctuations be based solely on the individual characteristics of each respective medicinal spring" (translated from section 1.2.2 (13) in

[22]). Firstly, a certified healing well must contain at least 1 g/L of dissolved solid minerals [22]. Secondly, the closer chemical characterization is determined by the fractional composition of the total mineralization. Here, the minimum value is 20 meq-percent, which means that only the main ions (Na^+, Mg^{2+}, Ca^{2+}, Cl^-, $HCO_3{}^-$, and $SO_4{}^{2-}$) are considered in this characterization [22]. Waters with high concentrations of certain trace elements are awarded corresponding designations (e.g., iodine/fluoride/sulfide-containing water with > 1 mg/L iodine/fluoride/sulfide, respectively, waters with carbonic acid with thresholds of 1000 mg/L and 500 mg/L, and radon-containing waters with > 666 Bq/L radon). The DQS mandates an initial "certification analysis" followed by annual monitoring analyses. In addition, well operators typically have their quality control managers perform more frequent assessments of specific parameters, such as microbiological factors or S^{2-}, between these regular analyses. Natural fluctuations in the mineralization are allowable unless they exceed ranges of +/- 20 % of the certification analysis. This affects ions that contribute at least 20 % of the total concentration in equivalent terms. The trace elements relevant for certification, as mentioned above, are allowed to fluctuate within a larger range, however, their mean value is not allowed to dip below the prescribed minimum value.

2.4.3 Further Legislation

Further legislative efforts to protect deep groundwater bodies include the **Mineral and Table Water Ordinance** [14], which defines natural mineral water: it originates from protected underground water sources and is extracted from natural or artificially developed springs. While the ordinance does not require a minimum content of dissolved minerals and does not give an allowed range of fluctuation in its mineral composition, it states that mineral water is naturally pure, rich in minerals and trace elements, and may have specific nutritional benefits. Its composition, temperature, and key characteristics remain stable within natural variations, unaffected by fluctuations in flow rate (§ 2) [14].

The **guideline on deep groundwater** by the LfU [40] describes problems specific to deep groundwater aquifers, such as changes in hydraulic conditions, which might lead to the activation of inflow from shallow or fast-generating groundwater bodies. Deep aquifers are especially vulnerable to this as they're often characterized by much more complex hydrogeological conditions than shallow aquifers, potentially rendering conventional water management practices designed for shallow aquifers inefficient when applied to deep aquifers. The guideline emphasizes the need for evaluations of hydrogeological conditions on a case-by-case basis. Due to its natural purity, deep groundwater deserves special protection and shall only be used for purposes that rely on the specific characteristics of deep groundwater, e.g., balneology, mineral water, and thermal water. For further protection, the guideline states the demand for evaluating local and regional hydrochemical background data so that fluctuations in the hydrochemical composition and the occurrence of anthropogenic contaminants, e.g., chlorofluorocarbonss (CFCs), perfluorinated compoundss (PFCs), pharmaceuticals or sweeteners, can be detected early on [40].

3 Setting Sail: Aims and Scope of This Dissertation

3.1 General Hypotheses

3.1.1 Hydrochemistry Shows Sustainability

A well's hydrochemical fingerprint is an indicator of an aquifer's age, its flow paths, and the mixing ratios of individual groundwater components [89]. On the other end of the groundwater life cycle, hydrochemistry affects rates of scaling and corrosion and thereby significantly influences the longevity of a geothermal plant's hardware. It also determines the certification and classification of healing and mineral waters. By observing changes in a well's hydrochemical composition, determined by the ions contained in its water, EC, pH, and TDS, it is possible to gain insights into the magnitude of natural hydrochemical fluctuations and thus derive how sustainably the well is used. The first study presented in this thesis is based on the hypothesis that a sustainably used well will not display unusually large hydrochemical fluctuations since its flow regime is stable and does not activate or deactivate the inflow of other aquifers. Correspondingly, large fluctuations outside of a well's natural range are assumed to be triggered and/or exacerbated by stress on the aquifer, e.g., through local or regional competing exploitation. The first working hypothesis is thus that, based on long-term observations of deep groundwater wells, their hydrochemical composition will allow a definition of their natural fluctuation range as well as a threshold indicating an unsustainable aquifer exploitation regime.

3.1.2 Sub-Seasonal Fluctuations Exceed Known Yearly Dynamics

It is reasonable to assume that yearly analyses, typically taken around the same time of year, do not reflect the entirety of the hydrochemical dynamics taking place in the different seasons. They are merely a snapshot of the aquifer's momentary load condition or, in simpler words, of the stress put on the aquifer by means of exploitation rates. These production volumes depend heavily on seasonal demand, both in the case of district heating as well as medical spas, and could lead to seasonally changing stress states in the aquifer, resulting in sub-seasonal fluctuations in its hydrochemical signature. Consequently, the second working hypothesis is that correlations between sub-daily and yearly data will allow for the derivation of hydrochemical data with higher temporal resolution without actually increasing the sampling frequency, if the flow paths are well understood.

3.1.3 Reinjection Site Dissolution Patterns are Detectable Using Multi-Scale Microscopy

The third hypothesis regards the hydrochemical effects of cooled-off water after its reinjection into the aquifer. The cooling process leads to a decrease in SI, resulting in an environment that encourages

dissolution processes in the vicinity of the reinjection well. While these dissolution processes can be modeled by software like PhreeqC, the hypothesis is that they do not impact the rock matrix uniformly and that surface roughness and mineralogical rock heterogeneity can impact the dissolution patterns on a pore scale. These alterations need to be made visible to further fine-tune existing models, spanning our understanding of scaling and dissolution effects from pore-scale to field-scale. A controlled laboratory environment utilizing an autoclave set-up capable of producing high-pressure, high-temperature, and low-SI conditions should be able to produce comparable dissolution patterns. By focusing the dissolution on a limited area of a solid rock sample, dissolution depth and resulting rock surface roughness should become visible even to the naked eye. A selection of microscopy instruments will be able to quantify these parameters on a very small scale, which will produce input parameters to further calibrate existing hydrochemical models.

3.2 Aims and Objectives

Based on the presented state of the art (chapter 2) and the proposed working hypotheses, this dissertation aimed to reach the following research goals:

1. Develop a statistically robust and reproducible algorithm to determine the natural hydrochemical state of any given well on an individual basis, based on yearly hydrochemical data, to identify a well's unique unsustainable fluctuation range, and to enable an emergency exploitation protocol before severe damages to the well or the can arise.

2. Derive unequivocal, causal correlations between hydrochemical well data with high and low temporal resolutions, which can then serve to produce high-resolution data based on the resulting algorithm, and without the need to take more analyses, in order to better understand sub-seasonal hydrochemical fluctuations.

3. Systematically compare three methods of microscopy on a semi-quantitative level to visualize the dissolution patterns caused by injecting cooled-off water with a low SI with regards to the surrounding aquifer matrix by using an autoclave set-up able to produce an environment with similar SI conditions and by limiting the dissolution processes to small areas on the rock sample.

4 Published Article: Assessing the Sustainable Development of Deep Aquifers

4.1 Placement in this Dissertation's Context

As described in subsection 2.4.1, the WFD cannot be applied directly to deep groundwater bodies, as it neglects the unique features of deep groundwater aquifers. Due to its shielded nature, an unexploited deep groundwater aquifer does not usually display any significant fluctuations in its hydrochemical composition. This changes when deep wells produce water from these aquifers, causing the activation or deactivation of influx from connected aquifers or sources of contaminants such as deep oil fields or salinary waters, resulting in fluctuations in hydrochemical parameters measured at the wellhead.

The first publication in this thesis intends to use this behavior to develop an early warning system capable of detecting fluctuations in the hydrochemical composition of an individual well and determining whether these fluctuations are part of its inherent, natural variability or whether they indicate changes in the aquifer caused by unsustainable exploitation practices. This endeavor was based on 30 consecutive years of yearly hydrochemical data and a reproducible clustering algorithm that identifies natural fluctuation ranges and reports on values exceeding this range. The workflow was tested on a distinct hydrochemical event at the well Bad Füssing TH-1, and the outliers were detected with just five yearly data points leading up to the event.

4.2 Research Questions

The first publication of this dissertation aimed to answer the following research questions:

- How can the natural state of a deep groundwater well be determined based on its hydrochemical signature and changes within it, using a reproducible and statistically robust algorithm?
- What is the range in which the hydrochemical signature of a well's analyses indicates an unsustainable well exploitation regime?
- How can changes in the hydrochemical signature be detected before they pose a problem for the well operator?

4.3 Author Contributions

Annette Dietmaier developed the theory, performed the computations, and wrote the manuscript with support from Thomas Baumann.

Prof. Dr. Thomas Baumann conceived the presented idea, verified the analytical methods, encouraged Annette Dietmaier to investigate clustering analysis methods, and supervised the findings of this work.

Both authors discussed the results and contributed to the final manuscript.

Water Resources Management (2023) 37:3857–3874
https://doi.org/10.1007/s11269-023-03529-6

Assessing Sustainable Development of Deep Aquifers

Annette Dietmaier[1] · **Thomas Baumann**[1]

Received: 29 April 2022 / Accepted: 27 April 2023 / Published online: 16 May 2023

Abstract

Deep groundwater aquifers are exploited for a variety of purposes. In general, impermeable rock layers protect these aquifers from anthropogenic influences. As such, they are a last resort for groundwater in a pre-industrial state, and a crucial resource in cases of emergency, such as floods contaminating shallow groundwater. The EU Water Framework Directive (WFD) provides the regulatory framework to protect its quality and quantity. Recent monitoring of the hydrochemical state of Upper Jurassic wells in Bavaria and Austria has shown fluctuations that were connected to new exploitation activities and might indicate an unsustainable development of the aquifer. We propose a new workflow in accordance with the WFD which uses clustering algorithms to assess these fluctuations. Our data consists of 5 to 42 hydrochemical analyses per well with yearly sampling intervals spanning up to 30 years. From the cluster analysis we derived thresholds for two corridors: Natural Range Corridor (NC) and Action Corridor (AC). While the NC represents a well-specific natural variation range, the AC hints towards unsustainable development and should trigger a detailed (re)assessment. To show the potential of the new method, the workflow was applied to two wells with different geological characteristics. Distinct fluctuation events were clearly recognized and can be used in the context of an early warning system, such that malign hydrochemical variations can be detected before they become legally problematic to well operators. Our workflow thus provides a novel, robust, and reproducible method to assess the grade of sustainability at which a well is exploited and ensures a good status of a unique and important resource.

Keywords Sustainable exploitation · Cluster analysis · Deep groundwater · Early warning system

1 Introduction

Deep groundwater is protected from anthropogenic influences by hundreds of meters of rock matrix with limited permeability and high retardation potential. Under this premise, deep groundwater reservoirs constitute an extraordinary source of clean water, especially

✉ Thomas Baumann
tbaumann@tum.de

Annette Dietmaier
annette.dietmaier@tum.de

[1] TUM School of Engineering and Design, Chair of Hydrogeology, Technical University Munich, Arcisstr. 21, Munich 80333, Bavaria, Germany

during times in which more shallow and surface water bodies are contaminated or depleted. The importance and wide range of applications of this resource results in conflicts over concurrent exploitation, e.g. large net discharge for technical purposes, geothermal energy, and drinking water production (Wycisk et al. 2003; Goldscheider 2005; Panagos et al. 2013; Baiocchi et al. 2013).

An aquifer is considered under stress if the cumulative withdrawal rate exceeds 20 % of the annual recharge rate (Arle et al. 2017). This value primarily ensures quantitative sustainability. However, groundwater flow velocities in deep aquifers are usually very slow. Thus, any withdrawal will change the age structure of the water body as more recent water replaces the water withdrawn. Analyzing age structures among bottled waters and evidence of pesticides present in these waters, Baumann (2013) shows that the exploitation of deep groundwater can change the age of the produced water from more than 1000 years to less than 30 years. Thus, on human time scales, deep groundwater bodies should be considered as a non-renewable resource (Ungemach et al. 2005). Nevertheless, aquifer-specific sustainable management plans currently do not exist for many deep aquifers.

Using groundwater age as a direct input parameter to assess the impacts of local exploitation schemes might seem intuitive. However, current age determination methods exhibit a range of uncertainties and therefore a lack of sensitivity when assessing small changes in the age structure, making groundwater age a questionable indicator for groundwater sustainability (Ferguson et al. 2020). Instead, we propose to use the hydrochemical signatures of individual wells and their changes as a sensitive indicator for (non-)sustainable well development. This premise assumes that over-exploitation of aquifers results in hydrochemical changes (Li et al. 2013).

The European Water Framework Directive (WFD; European Parliament and Council (2000)) sets the legal context for the assessment of groundwater bodies. It states that a "good quantity and quality status" must be reached for all specified groundwater bodies until 2027 (Foster and Custodio 2019). It also defines the good chemical status using electric conductivity (EC) to examine the effects of saline or other intrusions, and emphasizes anthropogenic influences and pollutants (European Parliament and Council 2000). These guidelines have had positive impacts on shallow groundwater bodies vulnerable to anthropogenic activities (Foster and Custodio 2019). However, deep aquifers underlie vastly different stressors and are less affected by anthropogenic influences, given their location of 150 m to 7000 m underground (Kang et al. 2019). Deep groundwater aquifers, such as the Upper Jurassic of the North Alpine Foreland Basin (NAFB), are at a small risk of receiving pollutants directly from anthropogenic sources. However, they may assume a "bad" chemical state (according to the WFD) e.g. through the intrusion of oil, gas or saline waters from higher or lower strata (European Parliament and Council 2000; Kang et al. 2019).

Examples of national industry standards implementing the WFD's core ideas are the EU mineral water directive (European Parliament and Council 2000) or the German Spa Association's (GSA) *"Definitions and quality standards for the nomination of health resorts, resort towns and curative sources"* (Deutscher Heilbäderverband and Deutscher Tourismusverband 2016). There are other national equivalents of WFD implementations with similar shortcomings. The characteristics discussed here are thus not limited to this German legal framework but can be extrapolated internationally. The GSA framework denotes threshold values for ingredients with balneo-therapeutical use, and allows

a $\pm$ 20 % and $\pm$ 50 % variation in the concentrations of characteristic ingredients and of ingredients with a concentration of$<$ 20 mg/L, respectively. However, these thresholds are detached from a well's natural variability. Hence, fluctuation characteristics which are clearly not part of the well's natural fluctuation, might go unnoticed in the mandatory

yearly hydrochemical analysis, if they lie within the allowed corridors. Thus, the generic value of ± 20 % fails to detect unsustainable well developments.

Temporal variations in hydrochemical parameters indicate the response of a heterogeneous inflow regime to varying withdrawal rates. This might be caused by, among other factors, seasonal fluctuations in heating demand or in the number of guests in balneological treatments, unpredictable events such as lock-downs during the COVID-19 pandemic, or pump malfunctions. Furthermore, reinjection of cooled-off waters or lack thereof must be considered. Most yearly sampling campaigns are scheduled within a ± 2 - 3 week time window during the calendar year, hence the sampling takes place at a similar operational state of the well.

The paramount importance of maintaining the quantitative and qualitative integrity of deep groundwater aquifers stands in contrast to a lack of suitable monitoring and management solutions. The result of this contradiction is the need for sound and reproducible methods to assess malign changes of a well's hydrochemical signature whilst determining its natural fluctuation range. These methods must also be robustly applicable to rudimentary data sets at unequal time intervals.

Determining the natural range must be achieved through clustering data points representing the well's natural fluctuation. Clustering algorithms follow the premises of pattern recognition, grouping data points with similar characteristics, and subdividing large data sets into smaller clusters in an unbiased fashion (Fu et al. 1976; Kaufman and Rousseeuw 1990). Difficulties arise when applying clustering methods on sparse training data. In other words, one aims to group data into homogeneous clusters without using any information pertaining to the groups of the samples (Lee 1981). Thus, having good knowledge of the data structure and the purpose of clustering is imperative. Two clustering algorithms from opposite sides of the clustering algorithm spectrum are DIvisive ANAlysis (DIANA) and k-means. DIANA is a hierarchical (top-down) clustering approach. It splits the initial data set into two clusters defined by their Euclidian distance to the most different data points. The resulting clusters are split up until each remaining cluster contains only one single data point (Patnaik et al. 2016).

K-means analysis, an agglomerative, bottom-up algorithm, approaches the clustering process in the reverse order (Kaufman and Rousseeuw 1990; Patnaik et al. 2016). As one of the simplest unsupervised learning algorithms (Kodinariya and Makwana 2016), it partitions a data set into k groups, k being set by the user (Wagstaff et al. 2001). This requires the investigator to have good prior knowledge off the data's structural characteristics. The locations of these k cluster centers are then iteratively refined using the Euclidian distance of the instances to the respective cluster center (Wagstaff et al. 2001).

Cluster analysis in combination with hydrogeochemical analyses have been established in examining spatial and temporal patterns of groundwater chemistry (Yang et al. 2020; Heine et al. 2021; Kim et al. 2003; Wang et al. 2015). Most studies, including recent investigations, utilizing this approach, focus on spatial hydrogeochemical zonation and use temporal averages representing the entire sampling period (Yang et al. 2020), neglecting temporal dynamics (Sayemuzzaman et al. 2018; Heine et al. 2021). Studies which focus on temporal analysis tend to apply cluster analysis to data of separate sampling periods in order to track changes between these periods over a larger geographic area, rather than at individual well sites (Pacheco Castro et al. 2018; Yang et al. 2020; Thyne et al. 2004; Hussain et al. 2008). Cluster analysis has also been used in groundwater monitoring programs. Ribeiro and Macedo (1995) employ a hierarchical cluster analysis (HCA) in order to establish groups of stations characterized by similar temporal patterns, after applying principal component analysis to the data set in order to define intercorrelation structures between the variables, and then analysing temporal variations of the resulting indices by the Mann-Kendall test. Daughney and Reeves (2006) apply HCA on

the temporal trends in groundwater chemistry which they previously determined by using the Mann-Kendall test. They emphasize the importance of defining baseline rates of changes in groundwater quality at the national scale, since a given well "cannot be defined as 'affected' or 'abnormal' unless the threshold limit of normality (baseline) has been previously defined" (Daughney and Reeves, 2006). Considering the range of conditions groundwater may encounter in natural systems, e.g. aquifer lithology, confinement, recharge source and age, it is important to define baselines as ranges of values rather than as single numbers. In their study, they define these ranges using percentiles (5th, 25th, 75th and 95th (Daughney and Reeves 2006)). At the time of writing (April 2022), we are not aware of any attempts to utilize clustering analysis methods to define dynamic natural temporal ranges of water quality at individual wells, rather than on aquifer level or through arbitrary value ranges.

Thus, based on data gathered in the Lower Bavarian and Upper Austrian part of the NAFB, the primary research question for this study was to define a well's natural state (considering its total concentration of main ions and trace substances), using reproducible statistical analysis methods and rudimentary data sets. Further, we test the functionality of the developed framework as an early warning system for changes in the well's hydrochemistry.

This study offers a novel approach of determining the typical inherent fluctuation ranges at each individual well in the NAFB, rather than employing an arbitrary value. Knowing this characteristic fluctuation is at the heart of our understanding of how sustainable geothermal groundwater exploitation is and how competing well operators using the same aquifer can coexist sustainably.

2 Methods

2.1 Study Area and Data

We selected 8 out of 22 geothermal wells (Fig. 1) exploiting the Upper Jurassic in the Northern Alpine Foreland Basin (NAFB) in Germany and Austria for analysis (Fig. 1). Previous studies (Mayrhofer et al. 2014; Heine et al. 2021; Birner et al. 2012) have shown that these carbonates are connected and constitute one deep groundwater body.

The selected wells produce hot water for balneological, district heating, and power generation purposes. The number of available analyses ranges from 5 to 42. While the earliest analysis was sampled in 1939 at BF1, only a few historic analyses were available. Yearly sampling started in the 1990s. Data include physical parameters (such as flow rate, electric conductivity (EC), temperature and pH) and hydrochemical parameters (main ions and trace ions relevant for balneotherapy). While most analyses at the German wells were performed by the Institute of Hydrochemistry at the Technical University of Munich, various other laboratories were involved. All data were stored in a PostgreSQL database and connected to QGIS through PostGIS for spatial representation (PostgreSQL Global Development Group (2021); PostGIS Project Steering Committee (PSC) (2021); QGIS Development Team (2021)).

2.2 Descriptive Statistics

Descriptive statistics were calculated using R (R Core Team 2020) for total dissolved solids (TDS), main ions, ions with relevance for balneotherapy and physical parameters. For

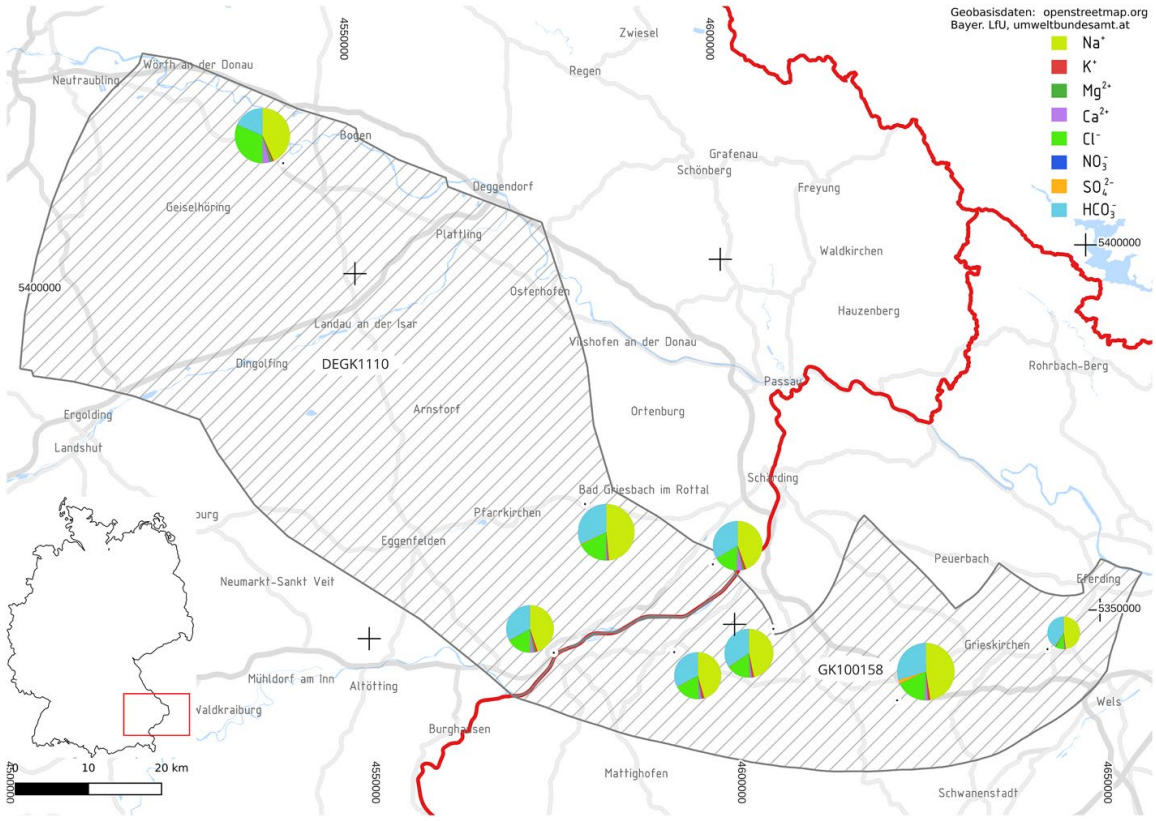

Fig. 1 Study area: DEGK1110 in Lower Bavaria and GK100158 in Upper Austria. The size of the pie charts representing the hydrochemical characteristics of the examined wells indicates TDS

all following analyses, we define TDS as the sum of the eight main ions and characterizing trace ions (Na^+, K^+, Ca^{2+}, Mg^{2+}, F^-, CI^-, SO_4^{2-} and HCO_3^-). An aggregated Schoeller diagram and two Piper diagrams (Online Resource 1) describe the wells' general hydrochemical characters. In order to describe the hydrochemical signatures in more detail, we must consider the inflow pathways affecting hydrochemical processes in the rock matrix and thereby TDS and individual parameter concentrations.

2.3 Cluster Analysis

This study employs two clustering algorithms: DIANA and k-means. By employing two methods from opposite ends of the clustering methods spectrum (bottom-up vs. top-down, unconditioned vs. preconditioned), we cover a broad array of approaches. Both methods were performed using the R packages "stats", "factoextra" (Kassambara and Mundt 2020), "cluster" implementing methods developed by Kaufman and Rousseeuw (1990) and Maechler et al. (2021), and "gridExtra" (Auguie and Antonov 2017).

Aiming to discern data points characterized by low TDS, those with TDS values higher than usual, and a value range between these two extremes, we grouped the data sets into three clusters ($k = 3$) for the k-means analysis. DIANA presents its results in a dendrogram which displays the similarity between two clusters. The larger the vertical distance between two clusters, the more dissimilar they are to each other (Kaufman and Rousseeuw 1990). The number of clusters thus depends on the vertical height value defined as a cut-off. Thus, we determined an appropriate height value for each well.

We ran both clustering algorithms on data without prior normalization because the absolute concentration is an important feature on which local implementations of water regulation standards are based (Länderarbeitsgemeinschaft für Wasser (LAWA) 1998). Additionally, we aimed at detecting changes in the hydrochemistry including dilution processes. If the relative concentrations of cations and anions does not change, but the total concentration does, these would go unnoticed using normalized data.

We compared the results of both clustering methods and assessed the congruence between them by comparing how many data points are grouped in the same cluster by both clustering methods. Both methods were tested for their sensitivity by removing one of the eight ions at a time before running the clustering algorithm with the remaining data.

The resulting workflow groups yearly data points into a natural state before defining corridors which represent "within the natural fluctuation range", and "outside of the natural fluctuation range" based on the mean and standard deviation (SD) of the cluster representing the natural state. Once the proposed workflow was checked to detect the outliers of distinct fluctuation events, we tested it for its suitability as an early warning system. To do so, we applied the workflow to a discernible fluctuation event in three iterations, increasing the data points available to the clustering algorithm with each iteration. We then assessed whether the proposed corridors would have allowed the distinction of the fluctuation event before and during its occurrence.

3 Results

3.1 General Hydrochemical Characteristics

Figure 2 presents the hydrochemical composition of all 8 wells in an aggregated Schoeller diagram. Waters with identical characteristics but varying concentrations plot in parallel lines. The concentrations of the individual ions differ by one order of magnitude. While the general characteristics seem to be fairly similar, there are significant differences where lines cross and/or the slope of the lines deviates strongly from the general trends. Water from BS1 shows low TDS and a dominance of sodium over chloride, indicating ion exchange processes along the flow path and little contact to saline waters. In contrast, STR show high concentration values with sodium concentrations almost matching chloride concentrations. This suggests a contribution of saline waters and little ion exchange.

In general, SD is low except for sulfate, pointing towards analysis errors rather than changes in the reservoir. Most thermal waters contain reduced sulfur (HS-, H2S) in significant concentrations. These species can oxidize during sampling and sample transfer unless special treatment is applied (Mayrhofer et al. 2014).

STM, HAA and ALT produce sodium-bicarbonate-chloride thermal waters. Relative equivalent concentrations of chloride decrease from west to east. BS1 stands out with relative chloride concentrations of less than 20 % and very low TDS.

The hydrochemical characteristics show that the waters from DEGK1110 and GK100158 differ significantly. This suggests different lithostratigraphic settings and local flow paths to the wells, which might include contact with aquifers above and below the main flow path. Regional residence times are long compared to reaction kinetics in the carbonate matrix. Thus, local effects influence the hydrochemical stability more strongly than the regional flow regime.

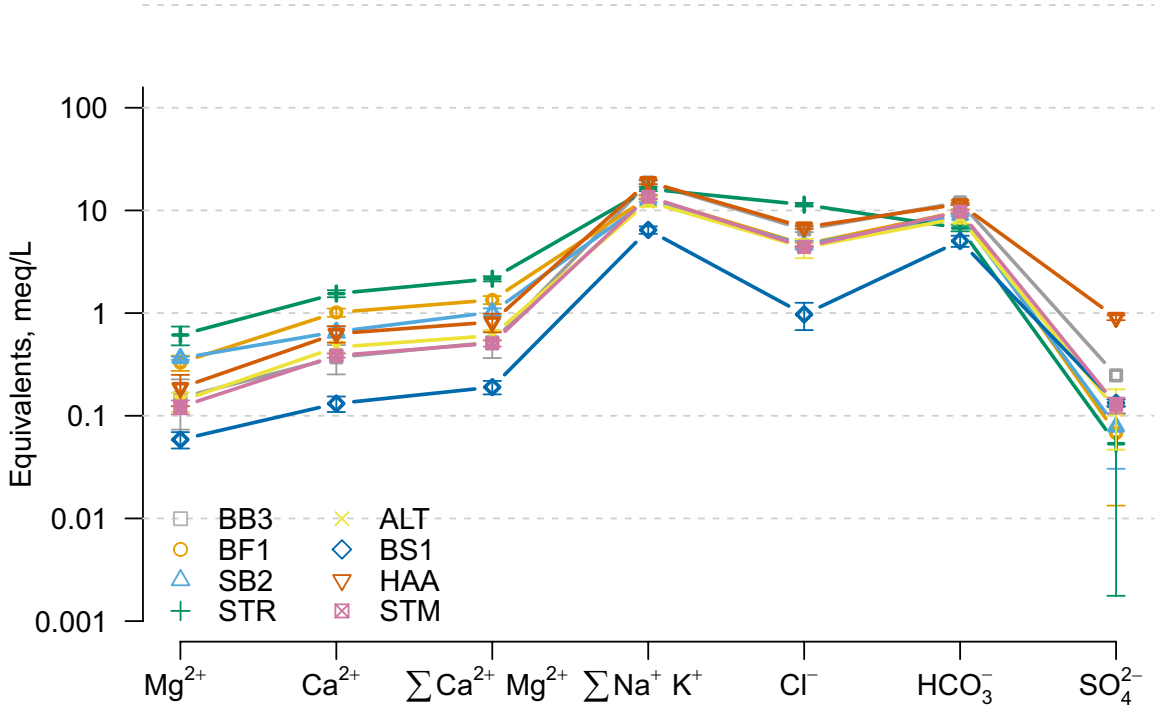

Fig. 2 Schoeller Diagram of all eight assessed wells. Connected points are the arithmetic mean of all analyses at this well, error ars show one standard deviation

3.2 Inflow Path Types

Based on drilling logs (Baumann and Nießner 2012; Institut für Wasserchemie TUM 1999, Elster et al. 2016) and the hydrochemical characteristics, we propose three inflow path types (Fig. 3). These simplified types experience effects of residence times, extraction volumes and pressure regime in different ways. Type A aquifers are enclosed between impermeable layers. Regardless of the withdrawal rates and hydraulic potential, the water flows only in the host rock of the aquifer. In Type B aquifers, hydraulic contact with adjacent layers is possible. The magnitude of this influx is a function of the permeability of the main aquifer and its neighboring strata, and the hydraulic potential in each layer. Type C represents a technical connection of different aquifers in strata which are otherwise separated. Here, the amount of mixing from the different aquifers is a function of the transmissivity of the different layers, the hydraulic potential and the production rates. While this exploration strategy is deprecated, some wells of this type still exist. These three inflow types provide a quick method for a first assessment of the robustness of the wells' exploitation. Out of all the wells in this study, 2 (SB2 and STR) belong to Type A, 4 (BF1, ALT, BS1, SB2) are Type B wells and 2 (BB3, HAA) are Type C wells. The majority of Type B wells are observed in the central part of the NAFB.

3.3 Well Specific Characteristics

For the remainder of this study, we will focus on two wells: BF1 (Type B) and SB2 (Type A), covering both variability in inflow types and the robustness of hydrochemical conditions. BF1 is used for heating and balneological purposes. It belongs to a group of wells

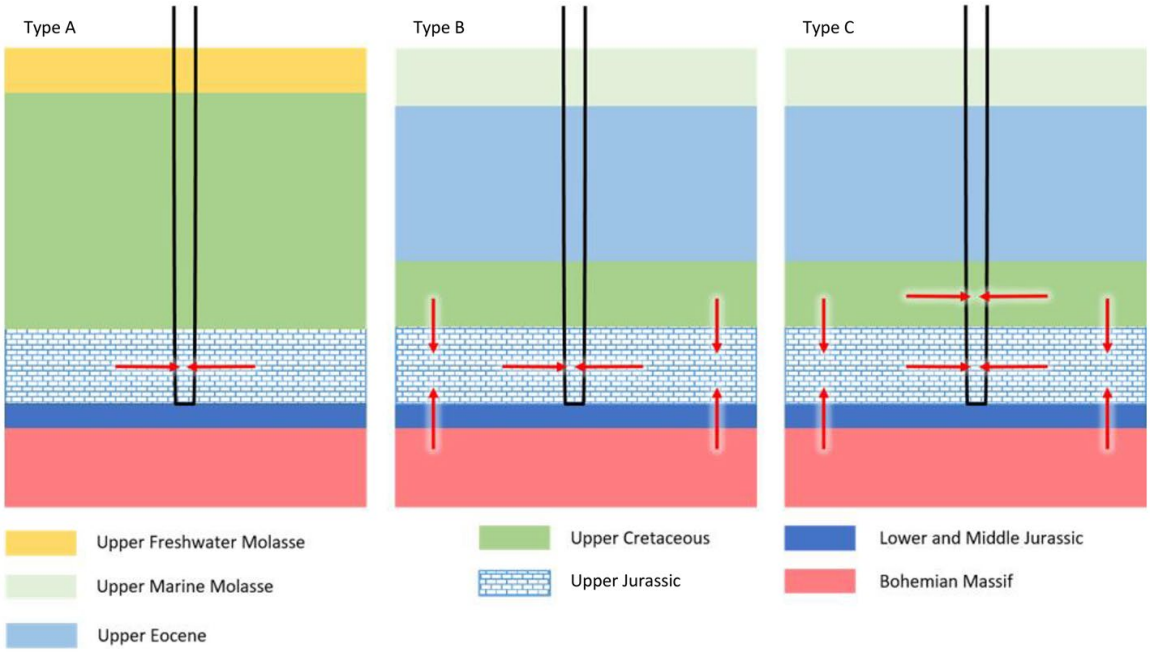

Fig. 3 Inflow path types in the study area

with a net discharge and no injection wells. SB2 exclusively generates heat for local district heating and is connected to an injection well to maintain the water balance.

On the left side of Fig. 4, selected ions and parameters for BF1 at all available sampling dates are shown. The temperature is constant without any discernible trend. The few low temperature data points were likely not measured at the well-head but elsewhere along the surface level production line.

Sodium and bicarbonate develop similarly over time. Between 1998 and 2011, sodium and bicarbonate display a highly dynamic behaviour, starting with an increase in concentration reaching maximum values of 296.5 mg/L and 646.8 mg/L, respectively. During the following years, the concentration values decrease until they reach minimum values of 260 mg/L and 515 mg/L, respectively, in 2006. After this development, sodium and bicarbonate values level off around a stable mean value with no apparent short-term trends.

Overall, BF1 is characterized by relatively large fluctuations in its chemical composition. This corresponds with its inflow path type (Type B). Here, the main inflow stems from the Upper Jurassic's carbonates, with contributions from the overlying Coniac/Cenoman carbonate formations. Figure 4 suggests a similar hydrochemical character with slightly lower mineralization for these two aquifers.

Since BF1 ion concentrations lie mostly within allowed limits, one might certify a good status for the aquifer. However, the dynamic behaviour around 2006 is striking (Fig. 4). The threshold of 1 g/L TDS was almost undercut and the concentration of sulfide undercut the allowed fluctuation range once. This illustrates that the criteria set by the current legal framework are not sensitive enough to detect changes possibly indicating unsustainable well development.

On the right side, Fig. 4 depicts the same selection of parameters as above for all available sampling dates at SB2. Most parameters are constant without any trend. Although TDS occasionally drops below 1000 mg/L, this is negligible because the water is not used for balneological purposes.

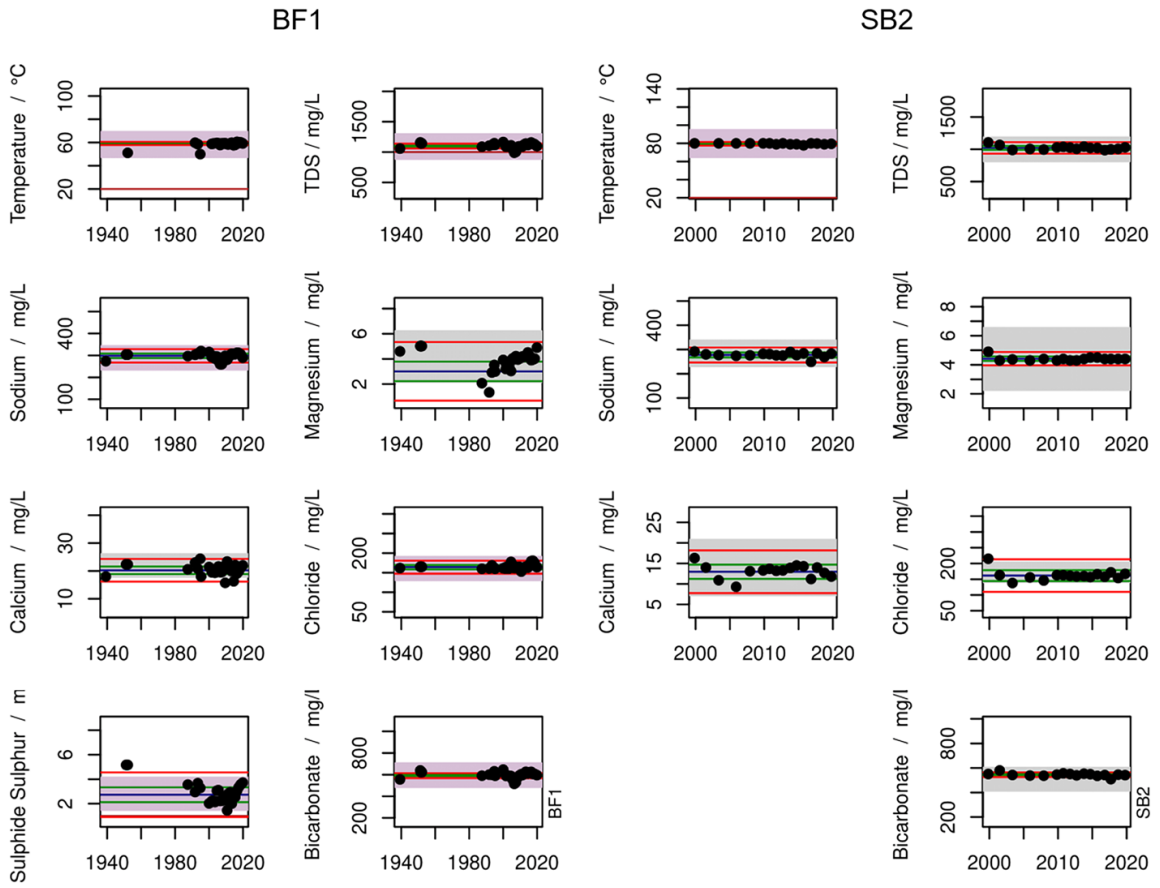

Fig. 4 Time series of characteristic ions at BF1 and SB2. The boxes show the allowed ± 20 % variation intervals (± 50 % for parameters with a relative concentration below 20 %) according to the legal framework (grey boxes: parameters not relevant to the hydrochemical characterization). The lines show the reference value (last official analysis; blue), the NC (green), and the AC (red)

In general, SB2 shows a stable development. TDS fluctuates only at the beginning of the recorded data and levels off at approximately 1000 mg/L. Calcium and chloride show the strongest variability, with their largest fluctuations occurring during the first ten years of the timeline. Their initial values are 16.3 mg/L and 215 mg/L, respectively. Within a decade, they decrease to minimum values of 9.3 mg/L in 2005 and 138 mg/L in 2003, before they settle on stable values at around 13 mg/L and 160 mg/L, respectively. Except for chloride, none of the parameters exceeds or undercuts the permissible fluctuation ranges.

SB2 generally presents a stable well representing its assigned inflow path type (Type A). Main inflow stems from the Upper Jurassic, which is shielded from the influence of waters from adjacent formations by impermeable layers. Thus, even increased production rates are unlikely to result in major changes in TDS or individual ion concentrations.

3.4 A New Workflow for Defining Baseline Fluctuations

It is in the interest of well operators and authorities to establish an early warning system with a high sensitivity to changes in the the overall state of the aquifer, such as presented in Fig. 4. It is not within the scope of this study to determine whether these changes are caused by additional exploration activities, over-use, or long-term changes of the hydraulic regime. The focus here lies on detecting fluctuations before they become legally relevant (e.g. by undercutting a minimum TDS threshold of 1000 mg/L), which is why our proposed

framework must function as an early warning system. We suggest a workflow which produces two corridors which shall be referred to as natural corridor (NC), representative for natural variations at sustainable use, and action corridor (AC) indicating unsustainable use, respectively. The latter should trigger further investigations and/or measures to retain a good state of the aquifer.

Both corridors are based on a specific well's hydrochemical character, including, where applicable, trace ingredients relevant to balneotherapy. We assume that every well has a natural hydrochemical variance which reflects its lithostratigraphic setting and inflow type. This natural variance includes production from the well, as there are usually no prior data from the aquifer itself.

The corridors are defined as 3 times (NC) and 6 times (AC) the SD around the Blank (mean values of the analyses representative for a natural state; Fig. 5c). This delineation of the corridors picks up the definitions of the limit of detection ($\bar{x}_b + 3\sigma$) and the limit of quantification ($\bar{x}_b + 6\sigma$) (Armbruster and Pry 2008). Here $\bar{x}_b$ is the mean of all samples

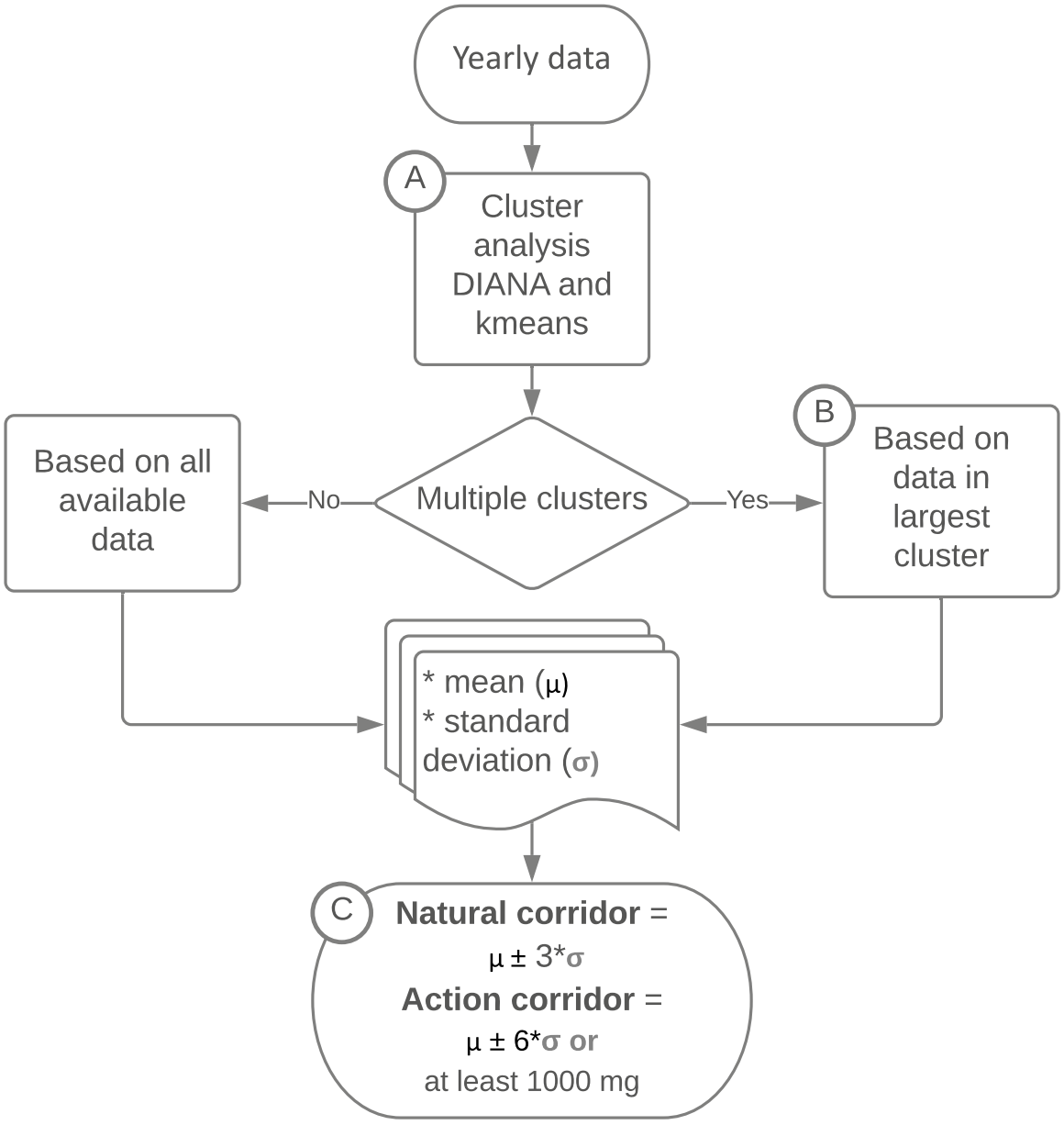

Fig. 5 Clustering workflow identifying the natural fluctuation range and action corridor of a given well

representing the natural fluctuation range and σ their SD. Following the three-sigma rule (or 68-95-99.7 rule) in probability theory (Hao et al. 2015) for a random variance with normal distributed values, 3 σ cover 99.73 %, while 6 σ cover 99.999998 % of the values.

This definition seems straightforward under the premise that the natural state of the well is known. If the hydrochemical signature of a given water is as constant as shown in Fig. 4, the natural state is evident. However, BF1 shows some features which apparently do not result from natural variation (Fig. 4). Therefore, the definition of the corridors requires the additional step of delineating the natural state first.

Using clustering algorithms (DIANA and k-means; Fig. 5a), we divide the data set into several groups of analyses. Historic data of all wells in the study area support the assumption that the natural state is represented by the largest resulting cluster (Fig. 5b).

Preliminary tests on whether there are any direct effects of the production rate on the hydrochemical characteristics are mandatory and can be obtained during pumping tests. Effects of the pumping rates and/or changes in the hydraulic potential on the hydrochemical composition are likely in inflow types B and C. Here, the concept of determining the natural variation is going to fail if the yearly samples are taken at different pumping rates. Table 1 and Fig. 4 display the results of the proposed workflow for all eight wells.

The mean of the NC and the mean of all data points available often lie close together. Differences arise in SD values which are typically much smaller for the NC than those of the entire data set. This underlines the importance of selecting the data points making up the well's natural range in the attempt of defining its baseline fluctuation.

Table 1 further shows the congruence of DIANA and k-means. K-means was run with $n = 3$ classes. Generally high congruence values are observed. ALT shows the lowest congruence value (64 %). For this data set, the k-means cluster analysis resulted in two equally large clusters. Increasing the number of clusters from three to four classes for both algorithms would increase the congruence value for ALT to 100 %. Excluding ALT, the minimum congruence value for all other wells is 77 % and the average congruence value, excluding ALT, is 94.57 %.

Table 1 Congruence of cluster assignment to each data point between DIANA and k-means and clustering results for DIANA

Well name	Available analyses	Sampled period	Congruence	Mean (NC)	Mean (total)	SD (NC)	SD (total)	n within NC
BB3	28	1973 - 2019	96	1457.99	1423.70	19.33	48.73	15
BF1	26	1939 - 2019	89	1106.10	1112.84	12.17	40.55	14
SB2	16	1999 - 2019	100	1024.80	1029.17	21.87	30.18	14
STR	26	1990 - 2019	77	1269.35	1236.55	39.55	50.79	14
ALT	11	1990 - 2010	64	1230.97	1236.55	7.48	50.79	10
BS1	5	1922 - 2003	100	527.77	502.15	27.40	40.15	3
HAA	5	1992 - 2009	100	1457.80	1432.14	48.47	71.09	4
STM	9	1999 - 2011	100	1096.97	1093.28	11.04	24.82	5

The results of the clustering were robust to the removal of most single ions from the data (Online Resources 3 and 4). The NC did not change when excluding $Ca^2+, K+, Mg^2+, F-$, and $SO4^2-$. Excluding Na+ or HCO3- did change the results because these ions are the main constituents of the water at these wells. K-means was sensitive to the removal of Cl- at BF1, which is attributed to the predefined number of clusters in k-means (SI). The two clustering algorithms are in accordance regarding the definition of the NC, and the absence of Na+ affects both clustering algorithms in the same way. In SB2, the number of data points in the largest cluster did not change when using DIANA. Using k-means, it changed from 16 to 11 when excluding Cl-, and to 10 when excluding HCO3-. Using k-means on BF1, the numbers of data points in the largest cluster increased from 14 to 16 when Cl- was excluded, and to 19 when Na+ was excluded. When using DIANA on BF1, these numbers changed from 14 to 19 when excluding Na+, and to 21 when excluding HCO3-.

3.5 Workflow Application

Figure 4 shows the resulting corridors for the two wells BF1 and SB2 based on DIANA clustering. Since 1939, TDS at BF1 was outside the NC with ten analyses, two data points are even outside the AC. For SB2, only one TDS data point is outside the NC and no data points cut the AC. With a TDS of 1112.8 ± 40.6 mg/L, BF1 generally reveals a larger variance compared to SB2 (TDS = 1029.17 ± 30.2 mg/L). However, their respective largest clusters reveal a different statistical signature: BF1's largest cluster exhibits a TDS of 1106.1 ± 12.2 mg/L, while SB2's largest cluster has a TDS of 1024.8 ± 21.9 mg/L. In BF1, the values attributed to the NC cluster lie much closer together. In SB2, there are only two values different enough from the other data points to form their own clusters. Thus, the entire remainder of the data set is grouped into one cluster, resulting in a larger NC for SB2. Our cluster analysis-based corridors are much narrower than the state of the art ± 20 % corridors around the last measurement. On the other hand, our corridors for single parameters, such as magnesium in BF1, might be more lenient than the ± 50 % corridors. This is because instead of relying on a single value, our corridors take into account the entire time series, providing a more robust assessment.

In order to address whether this workflow is apt to function as an early warning system, we assessed the development of corridors with increasing amounts of available data points for BF1 (SI), beginning with five data points covering the period from 1987 to 1995 (Online Resource 4). The DIANA clustering algorithm was chosen for this purpose because it allows insight into the development of the clustering structure through its visualization of dendrograms. The largest cluster contains four out of these five initial data points. By adding five more data points leading up to the fluctuation event (distinct and sudden decrease in total mineralization values in the early 2000s), the new thresholds based on now ten data points delineate slightly narrower corridors due to a lower SD in the newly formed largest cluster (Online Resource 4). After ten measurements we observe two data points exceeding the NC in 1994 and 2000. During the entire iteration, varying data points are clustered in the natural range, which explains the changes in SD and the NCs. When running the clustering workflow on 14 measurements, the data set covers the entire aforementioned sudden dip in TDS values observed between 2005 and 2007. The widths of the corridors change again very slightly, based on a new set of analysis data now making up the largest cluster. While the largest cluster's SD changes noticeably, the respective mean values, representing the well's range of TDS, stay relatively constant throughout the three scenarios. Both corridors based on the first and last scenarios would have managed to detect this fluctuation

event with their respective thresholds, proving the applicability of the proposed workflow for early warning purposes.

4 Discussion

The Upper Jurassic deep geothermal aquifer in the NAFB is an important source of geothermal water. Multiple well operators exploit it for both balneological and geothermal purposes. Even though this groundwater constitutes a non-renewable resource, the WFD is not an adequate tool to protect the Upper Jurassic aquifer, since the directive was designed to be used on shallow aquifers. Local implementations to monitor an aquifer's water quality (Deutscher Heilbäderverband and Deutscher Tourismusverband 2016; Daughney and Reeves 2006) are faced with the major problem of their application being based on arbitrary and generic thresholds in order to indicate problematic exploitation procedures. Daughney and Reeves (2006) stress the importance of defining the baseline fluctuation range in order to determine unnatural developments. Despite its easy and straight forward approach, the *Begriffsbestimmungen* (Deutscher Heilbäderverband and Deutscher Tourismusverband 2016) fail to delineate a given well's specific inherent and natural hydrochemical fluctuation range. Further, it offers no quantitative analysis of sudden changes in the hydrochemical signature as long as these, sometimes even distinct, events do not cross the aforementioned generic thresholds. Thus, significant yet not large enough fluctuations, which might indicate an unsustainable use of a well, remain unnoticed.

This study offers a new statistical approach to define a well's natural state. We propose a framework which, while slightly more time-consuming and complex than applying a generic percentage to a single data point, offers various advantages. By using clustering analysis, we found that we can robustly identify the specific natural fluctuation range of a well's hydrochemical signature, and detect changes in a well's hydrochemical composition which are not part of the natural fluctuation range. We identify these as data points that leave the previously defined NC. By applying well-specific corridors, it is no longer necessary for these unnatural events to exceed a threshold disconnected from the inherent natural fluctuation range of a well.

We used two clustering methods (DIANA and k-means). The k-means algorithm is relatively simple to implement and produces results that are easy to interpret. However, one has to have good knowledge of the data in order to choose the right value for k, a parameter on which the entire clustering mechanism then depends. Further, k-means tends to exhibit problems with defining clusters of varying densities (Likas et al. 2003) and the resulting clusters can be dragged by outliers (Wagstaff et al. 2001). DIANA, while being more complex than agglomerative clustering, does not require the user to define any initial parameters. Divisive algorithms take into account the global data distribution at the beginning of the clustering process, making them more accurate than agglomerative algorithms. A value to define the clusters, namely the height value from which the clusters are derived, must be defined by the user. We found that DIANA and k-means had a high congruence in the resulting cluster structures, which suggests that both algorithms are adequate tools to define the set of analyses representative for the well's naturals state. Four out of eight examined wells show a congruence of 100 %, and the lowest congruence is 64 %. Even this number can be improved once the number of clusters (k) is adjusted in the k-means clustering step. When assessing the robustness of the approaches regarding the absence of individual parameters, small changes in the resulting corridor widths were observed. The largest discrepancies occurred when leaving out HCO3-. Here, k-means includes a large

number of analyses values in the NC which seem to be part of fluctuation events. While both algorithms handle the data sets well, DIANA seems to be more robust compared to k-means. This is attributed to the fixed number of clusters in k-means. Although the clustering was robust to the exclusion of single ions, this only shows that the assessed wells react to stress with a change in multiple hydrochemical parameters. Trace metals, polycyclic aromatic hydrocarbons and isotopes could constitute additional parameters to detect changes in the overall flow pattern, however, too few analyses that included these parameters were available (regular intervals for the extended analyses were 10 years and are now 5 years). As the total concentration of the ions is a feature of the hydrochemical composition, clustering on non-normalized data is preferred.

The sensitivity of the newly developed framework to detect changes in the flow regime to the wells was tested on the well BF1. This well exhibits a clear fluctuation event which previously went unnoticed using the generic approach described by the GSA (Deutscher Heilbäderverband and Deutscher Tourismusverband 2016). In contrast, the new workflow was able to establish an NC and AC which would have detected the fluctuation events based on just five prior yearly data points. This is significant because it shows that the event was not only discernible retrospectively, but that the proposed workflow would have detected it by the time it occurred. It is important to consider that each new data point hones the precision of the clustering workflow and may thus change the well's natural fluctuation range slightly. This was observed when testing the workflow with differing amounts of data points at the same well. Nevertheless, this test produced significant conclusions regarding the minimum sample size of a data set which is to be used for this framework. According to our findings, a minimum of 5 yearly data points may offer a good base to establish a well's natural fluctuation range. Regarding data quality, a certain variance and offset has to be expected due to updated sampling and analysis protocols, as well as improved analytical methods, when using older measurements, and/or from different laboratories. This must be considered in the quality of the clustering structure.

5 Conclusion

This paper set out to design a robust statistical workflow by which the natural state of an individual well's hydrochemical signature can be defined and unsustainable operation strategies determined and avoided. A major goal was to discern unnatural fluctuation events, which might hint towards unsustainable well development before it becomes legally problematic for the operators. We propose a cluster analysis-based workflow using agglomerative and divisive algorithms as a substitute for the state-of-the art generic approach of arbitrarily-set thresholds for allowed minimum and maximum concentrations of certain hydrochemical parameters. Our framework is a practical approach to address the conflict of intensive geothermal water extraction and deep groundwater being a limited resource, and offers the following key features:

1. The proposed cluster analysis-based workflow offers well-specific identification of the natural hydrochemical fluctuation range focusing on total mineralization (sum of eight main ions and additional characterizing trace ions). In addition to the natural fluctuation range, it determines two corridors, delineated by a natural threshold and an action threshold. These thresholds can be utilized by surveyors tasked with assessing the sustainability of a well's operation procedures.

2. The proposed framework proved to be successful in detecting unnatural fluctuation events that would have gone unnoticed by the state-of-the-art approach of setting generic minimum and maximum concentration values. It is thus sensitive to changes in a well's hydrochemical signature while at the same time considering its natural fluctuation regime. Every newly added data point hones the accuracy of the determined natural fluctuation. This is particularly important because deep geothermal data is notoriously scarce and difficult to sample on high spatial and temporal resolutions.
3. The presented framework is suitable for the application as an early warning system. Based on the case study of a well whose waters exhibited a strong fluctuation event, the corridors produced by our workflow would have been able to detect the fluctuation before and while it occurred. This assessment also showed that the minimum data set size for this workflow is 5 yearly data points.

Finally, the results of the proposed workflow indicate that the wells exploiting the deep groundwater aquifers DEGK1110 and GK100158 are robust and previous exploration activities have not led to changes in the general state of the aquifers.

Supplementary Information The online version contains supplementary material available at https://doi.org/10.1007/s11269-023-03529-6.

Acknowledgements The authors would like to thank J. Schneider, R. Goller, A. Graf and T. Fritzer from the Bavarian Environmental Protection Agency, C. Kolmer and M. Lunz from the Office of the Government of Upper Austria and M. Samek from the Federal Ministry of Agriculture, Forestry, Environment and Hydrology for the lively discussion, and I. Stober for her final comments.

Author Contributions Thomas Baumann conceived the presented idea. Annette Dietmaier developed the theory and performed the computations. Thomas Baumann verified the analytical methods. Thomas Baumann encouraged Annette Dietmaier to investigate clustering analysis methods and supervised the findings of this work. All authors discussed the results and contributed to the final manuscript. Annette Dietmaier wrote the manuscript with support from Thomas Baumann.

Funding Open Access funding enabled and organized by Projekt DEAL. his work was funded by the Bavarian State Ministry of Science, Research and Art in the Framework of the Geothermal-Alliance Bavaria and the Bavarian Environmental Protection Agency (LfU).

Data Availability Hydrochemical data from Bavarian and Austrian wells were provided through the Technical University of Munich and/or upon request by the respective well operators.

Code Availability All code was written using the statistical software R. The software as well as the relevant clustering packages can be downloaded under https://www.r-project.org/.

Declarations

Ethics Approval Not applicable.

Consent to Participate Not applicable.

Consent for Publication Not applicable.

Conflicts of Interest The authors certify that they have no affiliations with, or involvement in any organization or entity with any financial interest (such as honoraria; educational grants; participation in speakers' bureaus; membership, employment, consultancies, stock ownership, or other equity interest; and expert testimony or patent-licensing arrangements), or non-financial interest (such as personal or professional relationships, affiliations, knowledge or beliefs) in the subject matter or materials discussed in this manuscript.

References

Arle J, Bartel H, Baumgarten C et al (2017) Wasserwirtschaft in Deutschland. Grundlagen, Belastungen, Maßnahmen. Tech Rep Umwelt Bundesamt, Dessau-Roßlau. www.umweltbundesamt.de/publikationen

Armbruster D, Pry T (2008) Limit of blank, limit of detection and limit of quantitation. Clin Biochem Rev 29 Suppl:19–52. https://pubmed.ncbi.nlm.nih.gov/18852857/

Auguie B, Antonov A (2017) gridExtra: Miscellaneaous functions for "Grid" Graphics. https://cran.r-project.org/web/packages/gridExtra/index.html

Baiocchi A, Lotti F, Piscopo V (2013) Impact des prélèvements d'eau souterraine sur l'interaction avec un complexe d'aquifères dans la zone géothermique de Viterbo (Centre de l'Italie). Hydrogeol J 21(6):1339–1353. https://doi.org/10.1007/s10040-013-1000-5

Baumann T (2013) Organische Spurenstoffe in Tiefengrundwasserleitern. Jh Ges Naturkde Sonderband Carlé pp. 103–117

Baumann T, Nießner R (2012) Bad Füssing Therme I Heilquellenanalyse, unveröffentlichtes Gutachten (Institut für Wasserchemie) (unpublished)

Birner J, Fritzer T, Jodocy M et al (2012) Hydraulische Eigenschaften des Malmaquifers im Süddeutschen Molassebecken und ihre Bedeutung für die geothermische Erschließung. [Hydraulic characterisation of the Malm aquifer in the South German Molasse basin and its impact on geothermal exploitations]. Z Geol Wiss 40(2/3):133–156. http://zgw-online.de/en/media/133-122.pdf

Daughney CJ, Reeves RR (2006) Analysis of temporal trends in New Zealand's groundwater quality based on data from the National Groundwater Monitoring Programme. J Hydrol New Zeal 45(1):41–62. https://www.jstor.org/stable/43944938

Deutscher Heilbäderverband, Deutscher Tourismusverband (2016) Begriffsbestimmungen / Qualitätsstandards für Heilbäder und Kurorte, Luftkurorte, Erholungsorte - einschließlich der Prädikatisierungsvoraussetzungen - sowie für Heilbrunnen und Heilquellen. Tech Rep Deutscher Tourismusverband e.V. und Deutscher Heilbäderverband e.V

Elster D, Goldbrunner J, Wessely G et al (2016) Erläuterungen zur geologischen Themenkarte Thermalwässer in Österreich 1:500 000. Geologische Bundesanstalt

European Parliament and Council (2000) Directive 2000/60/EC I - The European Water Framework Directive

Ferguson G, Cuthbert MO, Befus K et al (2020) Rethinking groundwater age. Nat Geosci 13(9):592–594

Foster S, Custodio E (2019) Groundwater Resources and Intensive Agriculture in Europe - Can Regulatory Agencies Cope with the Threat to Sustainability? Water Resour Manag 33(6):2139–2151. https://doi.org/10.1007/s11269-019-02235-6

Fu KS, Cover TM, Diday E et al (1976) Digital Pattern Recognition. Springer, Berlin Heidelberg

Goldscheider N (2005) Karst groundwater vulnerability mapping: Application of a new method in the Swabian Alb. Germany. Hydrogeol J 13(4):555–564. https://doi.org/10.1007/s10040-003-0291-3

Hao Y, Cao H, Qi Y, et al (2015) Efficient keyword search on graphs using MapReduce. Proc - 2015 IEEE Int Conf Big Data pp 2871–2873. https://doi.org/10.1109/BigData.2015.7364106

Heine F, Zosseder K, Einsiedl F (2021) Hydrochemical Zoning and Chemical Evolution of the Deep Upper Jurassic Thermal Groundwater Reservoir Using Water Chemical and Environmental Isotope Data. Water 13:1162. https://doi.org/10.3390/w13091162

Hussain M, Ahmed SM, Abderrahman W (2008) Cluster analysis and quality assessment of logged water at an irrigation project, eastern Saudi Arabia. J Environ Manage 86(1):297–307. https://doi.org/10.1016/j.jenvman.2006.12.007

Institut für Wasserchemie TUM (1999) Begutachtung der Thermalbohrung 1 in Straubing (unpublished). Technical University Munich, Tech. rep

Institut für Wasserchemie TUM (1999) Begutachtung des Wassers der "Chrysanti-Quelle" in Bad Birnbach (unpublished). Technical University Munich, Tech Rep

Kang M, Ayars JE, Jackson RB (2019) Deep groundwater quality in the southwestern United States. Environ Res Lett 14(3). https://doi.org/10.1088/1748-9326/aae93c
Kassambara A, Mundt F (2020) factoextra: Extract and Visualize the Results of Multivariate Data Analyses. http://www.sthda.com/english/rpkgs/factoextra
Kaufman L, Rousseeuw P (1990) Finding Groups in Data: An Introduction to Cluster Analysis. Wiley, Brussels, Brussels
Kim JH, Yum BW, Kim RH et al (2003) Application of cluster analysis for the hydrogeochemical factors of saline groundwater in Kimje. Korea. Geosci J 7(4):313–322. https://doi.org/10.1007/bf02919561
Kodinariya TM, Makwana DPR (2016) Review on determining of cluster in K-means clustering review on determining number of cluster in K-means clustering. Int J 1(July):90–95. www.ijarcsms.com
Länderarbeitsgemeinschaft für Wasser (LAWA) (1998) Richtlinien für Heilquellenschutzgebiete
Lee RCT (1981) Clustering analysis and its applications. In: Tou JT (ed) Adv Inf Syst Sci Springer, Boston, Chap 4 p. 169–292
Li F, Feng P, Zhang W et al (2013) An Integrated Groundwater Management Mode Based on Control Indexes of Groundwater Quantity and Level. Water Resour Manag 27(9):3273–3292. https://doi.org/10.1007/s11269-013-0346-8
Likas A, Vlassis N, J. Verbeek J (2003) The global k-means clustering algorithm. Pattern Recognit 36(2):451–461. https://doi.org/10.1016/S0031-3203(02)00060-2
Maechler M, Rousseeuw P, Struyf A, et al (2021) cluster: Cluster Analysis Basics and Extensions. R package version 2.1.2. https://cran.r-project.org/package=cluster
Mayrhofer C, Niessner R, Baumann T (2014) Hydrochemistry and hydrogen sulfide generating processes in the Malm aquifer, Bavarian Molasse Basin. Germany. Hydrogeol J 22(1):151–162. https://doi.org/10.1007/s10040-013-1064-2
Pacheco Castro R, Pacheco Ávila J, Ye M et al (2018) Groundwater Quality: Analysis of Its Temporal and Spatial Variability in a Karst Aquifer. Groundwater 56(1):62–72. https://doi.org/10.1111/gwat.12546
Panagos P, Van Liedekerke M, Yigini Y et al (2013) Estimating soil organic carbon in Europe based on data collected through an European network. J Environ Public Health 24:439–450. https://doi.org/10.1016/j.ecolind.2012.07.020
Patnaik AK, Bhuyan PK, Krishna Rao KV (2016) Divisive Analysis (DIANA) of hierarchical clustering and GPS data for level of service criteria of urban streets. Alexandria Eng J 55(1):407–418. http://dx.doi.org/10.1016/j.aej.2015.11.003
PostGIS Project Steering Committee (PSC) (2021) PostGIS v. 3.1.4. https://www.postgis.net
PostgreSQL Global Development Group (2021) PostgreSQL Database System v. 13.5. http://www.postgresql.org/about/
QGIS Development Team (2021) QGIS Geographic Information System v. 3.22. https://www.qgis.org
R Core Team (2020) R: a language and environment for statistical computing. https://www.r-project.org/
Ribeiro L, Macedo ME (1995) Application of multivariate statistics, trend- and cluster analysis to groundwater quality in the Tejo and Sado aquifer. Groundw Qual Remediat Prot Proc Conf Prague, 1995 January(95):39–47. https://www.researchgate.net/profile/Luis-Ribeiro-33/publication/252068832_Application_of_multivariate_statistics_trend-_and_cluster_analysis_to_groundwater_quality_in_the_Tejo_and_Sado_aquifer/links/0f31753454ae3ace43000000/Application-of-multivariate-st
Sayemuzzaman M, Ye M, Zhang F et al (2018) Multivariate statistical and trend analyses of surface water quality in the central Indian river Lagoon area. Florida. Environ Earth Sci 77(4):1–13. https://doi.org/10.1007/s12665-018-7266-0
Thyne G, Güler C, Poeter E (2004) Sequential analysis of hydrochemical data for watershed characterization. Ground Water 42(5):711–723. https://doi.org/10.1111/j.1745-6584.2004.tb02725.x
Ungemach P, Antics M, Papachristou M (2005) Sustainable Geothermal Reservoir Management. Proc World Geotherm Congr April(05):24–29. https://d1wqtxts1xzle7.cloudfront.net/43589480/Sustainable_Geothermal_Reservoir_Managem20160310-10466-hkii8l-with-cover-page-v2.pdf?Expires=1646221751 &Signature=BwyQ2XXEKN8GyolI1lBwiY5uI5qprAbEZOo1du8t6GW9LIJjiN61T0QpIqYr4npR8oS3swDgvp34YHivm19jDKNxYmo-yO
Wagstaff K, Cardie C, Rogers S, et al (2001) Constrained K-means Clustering with Background Knowledge. Int Conf Mach Learn ICML pages:577–584. http://citeseerx.ist.psu.edu/viewdoc/download?doi=10.1.1.90.4624 &rep=rep1 &type=pdf
Wang H, Jiang XW, Wan L et al (2015) Hydrogeochemical characterization of groundwater flow systems in the discharge area of a river basin. J Hydrol 527:433–441. https://doi.org/10.1016/j.jhydrol.2015.04.063
Wycisk P, Weiss H, Kaschl A et al (2003) Groundwater pollution and remediation options for multi-source contaminated aquifers (Bitterfeld/Wolfen, Germany). Toxicol Lett 140–141:343–351. https://doi.org/10.1016/S0378-4274(03)00031-6

Yang J, Ye M, Tang Z, et al (2020) Using cluster analysis for understanding spatial and temporal patterns and controlling factors of groundwater geochemistry in a regional aquifer. J Hydrol 583(January). https://doi.org/10.1016/j.jhydrol.2020.124594

5 Published article: Forecasting Changes of the Flow Regime at Deep Geothermal Wells Based on High-Resolution Sensor Data and Low-Resolution Chemical Analyses

5.1 Placement in this Dissertation's Context

Following the assumptions from the first publication, namely that production regimes exert a substantial impact on the hydrochemical signature of the individual well, it was reasonable to hypothesize that these yearly samples fail to show sub-seasonal variations in ionic composition based on sub-seasonal changes in production volumes, which in turn are governed by changes in demand between the different seasons. A logical solution to this conundrum seemed to be an increase in sampling frequency. However, deep groundwater aquifers are plagued by data scarcity, with the low spatial resolution of deep groundwater data caused by the high costs of drilling deep wells. However, the low temporal resolution could be improved with much lower financial investment.

This thesis' second publication compared high-frequency data points (online monitoring) with yearly data (offline data) to derive causal correlations and extrapolate ionic composition from easy-to-monitor values like production rates, pH, EC, and temperature. One well previously equipped with such online sensors was used to test this hypothesis. While the offline data was insufficient to derive the desired correlations, it offered important insights into the actual sub-seasonal hydrochemical fluctuations, which far exceed commonly observed yearly fluctuations. The study concludes with a recommendation of an ideal sampling frequency of at least three samples per year in order to cover sub-seasonal fluctuations.

5.2 Research Questions

The second publication of this dissertation aims to answer the following research questions:

- Do state-of-the-art monitoring programs depict hydrochemical fluctuations in deep groundwater wells accurately?
- Are data sets currently gathered on deep wells sufficient to train virtual sensors?
- How frequently do groundwater wells have to be sampled to show a realistic picture of sub-seasonal fluctuations?

5.3 Author Contributions

Prof. Dr. Thomas Baumann conceived the presented idea.

Annette Dietmaier developed the theory and performed the computations.

Prof. Dr. Thomas Baumann verified the analytical methods and supervised the findings of this work.

Both authors discussed the results and contributed to the final manuscript.

Annette Dietmaier wrote the manuscript with support from Prof. Dr. Thomas Baumann.

Adv. Geosci., 58, 189–197, 2023
https://doi.org/10.5194/adgeo-58-189-2023

Advances in Geosciences
Open Access
EGU

Forecasting changes of the flow regime at deep geothermal wells based on high resolution sensor data and low resolution chemical analyses

Annette Dietmaier and Thomas Baumann

Chair of Hydrogeology, TUM School of Engineering and Design, Technical University of Munich, Arcisstr. 21, 80333 Munich, Germany

Correspondence: Thomas Baumann (tbaumann@tum.de)

Received: 13 July 2022 – Accepted: 3 May 2023 – Published: 26 May 2023

Abstract. Geothermal waters provide a great resource to generate clean energy, however, there is a notorious lack of high quality data on these waters. The scarcity of deep geothermal aquifer information is largely due to inaccessibility and high analysis costs. However, multiple operators use geothermal wells in Lower Bavaria and Upper Austria for balneological (medical and wellness) applications as well as for heat mining purposes. The state of the art sampling strategy budgets for a sampling frequency of 1 year. Previous studies have shown that robust groundwater data requires sampling intervals of 1–3 months, however, these studies are based on shallow aquifers which are more likely to be influenced by seasonal changes in meteorological conditions. This study set out to assess whether yearly sampling adequately represents sub-yearly hydrochemical fluctuations in the aquifer by comparing yearly with quasi-continuous hydrochemical data at two wells in southeast Germany by assessing mean, trend and seasonality detection among the high and low temporal resolution data sets. Furthermore, the ability to produce reliable forecasts based on yearly data was examined. In order to test the applicability of virtual sensors to elevate the information content of yearly data, correlations between the individual parameters were assessed. The results of this study show that seasonal hydrochemical variations take place in deep aquifers, and are not adequately represented by yearly data points, as they are typically gathered at similar production states of the well and do not show varying states throughout the year. Forecasting on the basis of yearly data does not represent the data range of currently measured continuous data. The limited data availability did not allow for strong correlations to be determined. We found that annual measurements, if taken at regular intervals and roughly the same production rates, represent only a snapshot of the possible hydrochemical compositions. Neither mean values, trends nor seasonality was accurately captured by yearly data. This could lead to a violation of stability criteria for mineral water, or to problems in the geothermal operation (scalings, degassing). We thus recommend a new testing regime of at least 3 samples a year. While not a replacement for the detailed analyses, under the right circumstances, and when trained with more substantial data sets, viertual sensors provide a robust method in this setting to trigger further actions.

1 Introduction

Facing an acute energy crisis and a global climate crisis, Europe must search for alternative energy sources to imported oil and gas. Deep geothermal waters can provide an important source of energy. However, there is a notorious lack of reliable data regarding these waters (Krieger et al., 2022): current exploitation of deep groundwater consists of clustered wells which are widely distributed over large areas, which limits the spatial resolution of available data points, while sampling and analysis costs (typically between EUR 1500 and more than EUR 10 000, depending on the number of parameters) limit the frequency at which hydrochemical assessments can be conducted (Alley et al., 2013; Hebig et al., 2012; Krieger et al., 2022). At meaningful sampling intervals the costs for conventional analyses are on the same order as the equipment for online-measurements. Since deep groundwater aquifers play a negligible role in daily

drinking water provision, these aquifers are not as present in public interest as, e.g., shallow ground water or surface water bodies. However, even the large number of hydrochemical analyses of groundwater wells available to this study, which includes research wells, display a similar data scarcity.

Insufficient in-situ data makes numerical modelling of subsurface dynamics difficult and limits the reliability of groundwater monitoring networks (Hebig et al., 2012; Caers and Castro, 2006). Furthermore, deep groundwater acts as a safety net for times when shallow groundwater resources are depleted. Monitoring the development of its hydrochemical quality is thus of utmost importance (Kang et al., 2019) and one of the main purposes of the European Water Framework Directive (WFD) (European Parliament and Council, 2000). This study focuses on a deep geothermal groundwater body exploited for heat and energy production and medical spas. In this setting, hydrochemical and geophysical information serves as an indicator of the geographical course of the groundwater's flow paths. It further helps describe processes taking place along these flow paths in the rock matrix (Birner et al., 2011; Mayrhofer et al., 2014; Heine et al., 2021). Additionally, fluctuations in the hydrochemical composition can have severe effects on the longevity of the geothermal power plant hardware (e.g. corrosion and scaling) and, in the case of medical wellness applications, on the certification as a medical thermal spa. This information is not only relevant for present conditions. Forecasts are highly valuable to well operators for long-term sustainable well exploitation strategies and are explicitly required by the WFD (European Parliament and Council, 2000).

The state of the art deep groundwater sampling procedure typically budgets for yearly physical and chemical analyses. This frequency is codified in national guidelines, such as the "Definitions and Quality Standards for Medical Wellness" in Germany (Deutscher Heilbäderverband and Deutscher Tourismusverband, 2016). However, optimal sampling frequency is not an arbitrary value, but can be defined in terms of providing as much information as possible with as few sampling points as necessary (Nelson and Ward, 1981). The term *information*, in turn, can be defined, in a statistical sense, in terms of the variance of the mean (Barcelona et al., 1989): $\mathrm{Var}(x) = \sigma^2 \cdot n$, where x is the sample mean, σ is the variance and n is the number of samples. While information content rises with an increase of samples, given the costs, redundancies must be avoided (Barcelona et al., 1989).

In 1989, the US Environmental Protection Agency published a report on sampling frequency for groundwater quality monitoring (Barcelona et al., 1989) in which the investigators used data from a bi-weekly sampling campaign to derive optimal sampling intervals for a shallow sand and gravel aquifer in Illinois, USA. Basing their investigation on the assessment of auto-correlation and information loss at different sampling intervals, they found an optimal groundwater sampling frequency of around 2 to 3 months (Barcelona et al., 1989). In contrast, Zhou (1996) names three quantitative components (trend detection, determination of seasonal variability and estimation of mean) through which diverging sampling intervals can be compared to each other. In their case study at Spannenburg Pumping Station in the Netherlands they derive an optimal sampling interval for hydrochemical and geophysical analyses of 1 month. Financially and logistically, this might pose an impossible sampling strategy for many deep wells. If increasing sampling frequencies is not an option, elevating information through virtual sensors (VS) might be a viable alternative. VS are a software sensor layer which produces signals as indirect measurements of process variables by combining signals from physical sensors or other VS, physical laws and statistical models (Martin et al., 2021; Kabadayi et al., 2006; Porter et al., 2000). Among the advantages of VS are lower initial and ongoing costs and their ability to be deployed in hostile environments where inaccessibility limits the application of physical sensors (Tegen et al., 2019), all of which aids in optimizing maintenance and management processes (Porter et al., 2000). VS have been applied to groundwater monitoring applications before: Porter et al. (2000) used data fusion modeling to construct a groundwater flow model of a local river site. They point out that data fusion modeling solves the problem of combining point data for hydraulic head and conductivity. In order to fill months long data gaps in time series of a geothermal heating plant's energy demand, Baumann et al. (2017) used daily mean air temperatures and a typical control function for domestic boilers to calculate produced geothermal energy and derive flow rates and injection temperatures. Seasonal fluctuations and effects of sudden changes in energy demand were also represented with high accuracy.

Given the common practice of yearly hydrochemical analyses for German deep groundwater wells, which oppose the points raised in the aforementioned studies regarding optimal sampling frequency determination, the question arises whether the current sampling strategy accurately represents true fluctuations taking place in the aquifer. It is important to note that all studies conducted on this question have focused on shallow aquifers. It is thus of vital importance to asses the information content of yearly data in comparison to high frequency data gathered in a deep geothermal aquifer and explore options of elevating it through VS. In this study, we compare yearly and daily hydrochemical and physical (e.g. temperature, pressure, volume) data gathered in a deep geothermal aquifer in Bavaria, Germany, in order to answer the following questions: (i) can yearly data adequately represent mean, seasonal variability and trends of quasi-continuous data? (ii) is yearly data a sufficient base for long-term forecasting of hydrochemical compositions of deep groundwater? (iii) can virtual sensors be used to elevate information content of rudimentary data sets in this environment?

2 Methods

2.1 Study Area and Geology

This study uses hydrochemical samples taken at two wells in the Northern Alpine Foreland Basin (NAFB). Most waters in the Upper Jurassic Aquifer in the northern and northeastern part of the NAFB are characterized as Ca-(Mg)-HCO_3 water with low salinity ($< 0.9\,g\,L^{-1}$), but there are waters with total dissolved salts (TDS) values of $> 2\,g\,L^{-1}$ at the edge of the helvetic facies close to hydrocarbon deposits (Birner et al., 2011; Birner, 2013). Inflow from underlying or overlying strata change the general characteristics. Waters from Dogger, Keuper and Lias carry water of the types sodium-sulfate-bicarbonate (sampled in Bad Überkingen), sodium-chloride-sulfate (sampled in Königshofen), and sodium-bicarbonate-chloride (sampled in Göppingen), respectively. Their salinities reach values of up to $11\,g\,L^{-1}$ in Königshofen (Carlé, 1975). A well in Bad Gögging produces a sodium-bicarbonate-chloride water with a TDS of $1.3\,g\,L^{-1}$ from the Lower Triassic and the crystalline basement (Käss and Käss, 2008). This information is vital for characterising inflow pathways, and, more importantly, for analysing changes in these pathways.

2.2 Data

Data was collected from the well BAK at the northern margin of the NAFB close to Bad Abbach, Germany. The well has a depth of 676.5 m b.s.l. (well head at 272.56 m a.s.l).

The casing of the well reaches down to 473.20 m and is cemented against the borehole. The lower part of the borehole from 496.5 to 676.5 m b.s.l. was also cemented. Thus, the filter screen of the well is located in the sandstones of the Late Triassic (Käss and Käss, 2008). The clayey strata of the Lower Jurassic and the lower part of the Middle Jurassic serve as impermeable cap rock. However, a connection to the waters in the crystalline basement can be expected. BAK produces water of the type sodium-bicarbonate-chloride with traces of fluoride (Käss and Käss, 2008) for spa applications only, which are affected by strong seasonal fluctuations.

For the purpose of comparing our outcomes to a well with a more continuous production regime, we extended our analyses to the data gathered at another NAFB well ("BF2"), which also produces water of the type sodium-bicarbonate-chloride with trace amounts of sulphur and fluoride from the Upper Jurassic (1142.30 m b.s.l.) for the purpose of a medical spa and year-round power generation. This well produces geothermal water year-round and thus has a more balanced production regime.

There are two data sets available for each well: since they are used for medical spas, they are subject to yearly controls of the hydrochemical composition (data from 2002–2020 for BAK and from 2000–2022 for BF2) gathered at the wellhead and analyzed by the lab of *T*. Baumann at the Institute for Hydrochemistry and Chemical Balneology at TUM, hereafter referred to as *offline data*). Sampling took place during the summer (±2 weeks) at comparable withdrawal rates. Samples were taken at the well head and stabilized as required (e.g. H_2S, NH_4^+, heavy metals). Temperature, electrical conductivity (EC) and pH were determined with sensor probes. Lab analyses were done using standardized lab equipment and methods (ion chromatography, flame absorption spectroscopy, atomic adsorption and titration). All samples presented in this study were taken and analysed by the same lab technicians. Recently, the wells were equipped with online sensors which monitor six parameters (Table 1) in 5 min increments, resulting in a high sampling frequency data set (hereafter referred to as *online data*, provided by the well operators). Table 1 offers detailed information on sampling frequency, sampling period and parameters of the two data set types.

2.3 Data analysis and forecasting

Although all assessments were calculated for both data sets, this article focuses on the well BAK. Detailed analysis results for BF2 can be found in the appendix. Statistical examination started with a visual comparison of the time series using EC values. Descriptive time series analysis serves the purpose of deriving information needed for the determination of an appropriate sampling interval (Zhou, 1996). EC was chosen as an indicator of total dissolved salts (TDS) and was available in all data sets. All assessments were conducted with the statistical software R (R Core Team, 2020). We conducted descriptive statistical assessments (calculation of mean, minimum, maximum, standard deviation; SD) and produced kernel density plots (*R* function geom_density::ggplot2) for a better understanding of the different EC value ranges. In accordance with the proposed framework by Zhou (1996), we calculated long-term trends using a linear regression (*R* function lm). Seasonality was assessed through time-series decomposition (*R* function decompose::stats) for a better understanding of signal fluctuation frequency.

In order to span gaps in the time series and create a temporally equidistant data set, missing data were projected by linear interpolation between neighboring analyses (*R* function stats::approx).

For the prediction of the development of the hydrochemical composition, an autoregressive integrated moving average (ARIMA) model forecast was chosen. This algorithm assumes the future value of a variable to be a linear function of a data time series' several past observations and random errors (Zhang, 2003). Due to its simplicity, it constitutes one of the most popular linear forecasting approaches (Ho and Xie, 1998; Zhang, 2003). We calculated the prognosis based on offline data by using the *R* function forecast::auto.arima (Hyndman et al., 2021), which automatizes the forecast given equidistant time series data. Equidistance in the data set was achieved, like before, through linear inter-

Table 1. Characteristics of online and offline data sets for the assessed well BAK near Regensburg, Germany.

Data set type	Temporal resolution	Time period	Physical parameters	Chemical parameters
Online	5 min	2013–2021	Drawdown, production rate, pump state (on/off), temperature, volume count value	EC
Offline	1 a	2002–2020	Drawdown, production rate, temperature	pH, EC and 15 individual ions

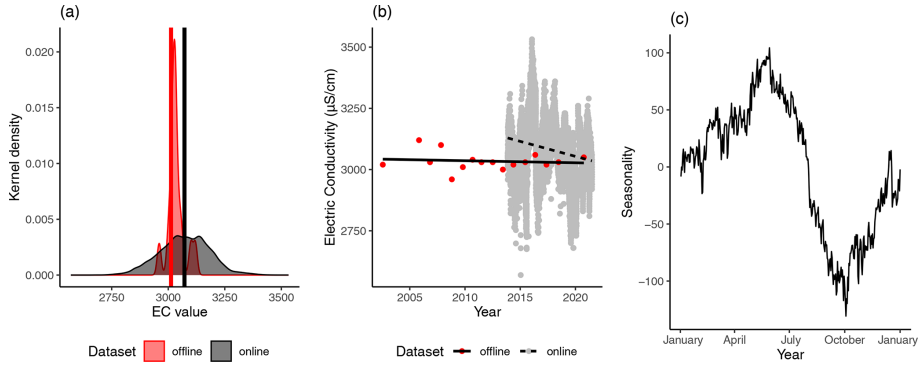

Figure 1. (a) Density histograms of both online and offline data at BAK. **(b)** Timelines and linear trend lines of EC-concentrations calculated for online and offline data. The dashed line shows the trend for the online data set. The solid line indicates the trend line for the offline data set. **(c)** Seasonal component of time series decomposition analysis based on the online data set.

polation between neighboring analyses (stats::approx). Using the same method, a forecast based on the online data was produced to compare resulting value ranges.

In order to elevate information on individual hydrochemical constituents to seasonal development, we conducted multiple linear regression analyses to assess the potential of these data sets for use in virtual sensors. This was done with the aim of discerning relationships between offline and online data in order to extrapolate high temporal resolution values of parameters which can realistically only be measured on a low temporal resolution. In addition to the individual parameters we defined parameter groups and ratios: Ca^{2+}/Mg^{2+} discerning dolomite vs. calcite inflow, Na^{+}/HCO_3^{-} and $(Na^{+}-Cl^{-})/HCO_3^{-}$ for discerning inflow of waters subject to ion exchange, Na^{+}/Cl^{-} to signal saline inflow dynamics, and $Na^{+}+K^{+-}-Cl^{-}/HCO_3^{-}$ for discerning saline versus ion exchange water inflow. The strongest correlations, as indicated by the Pearson correlation coefficient (PCC), were then further investigated through specific regression models. All regression models show a 0.99 confidence area and were computed using the default R package "stats" (R Core Team, 2020).

A calculation regarding mixing ratios was performed using the software PhreecC (Parkhurst and Appelo, 2013).

3 Results

In this chapter, results for BAK will be shown in detail and important results from the analyses of BF2 (Figs. S1 and S2 in the Supplement) are briefly presented.

3.1 Time series analysis

The density graph in Fig. 1a) shows differences in value ranges between the offline and the online data sets. The vertical bars indicate the mean values for each data set, which lie at $3071.72 \pm 109.63\,\mu S\,cm^{-1}$ for online data, and at $3012.35 \pm 97.63\,\mu S\,cm^{-1}$ for offline data (1471.66 ± 135.02 and $1434.28 \pm 38.05\,\mu S\,cm^{-1}$ respectively for BF2). The overlapping kernel density curves show a more evenly distributed curve for the online data set compared to the offline data set. The larger SD for the online data set represents the larger variability shown in Fig. 1b) which depicts the two time series and trend lines calculated for each data set. Both data sets are characterized by a negative trend, however, while the offline data resulted in an almost even but minimally negative trend line, the trend derived from the online data set shows a clearly negative course. Although sampling period is considerably shorter for the online data, this does not explain the differences in trend. When we restricted the offline data to the same sampling period as the online data, the offline trend became very slightly positive. Thus, online

and offline data systematically disagree on trend determination. In BF2, similar differences between the trend lines are observed, but in this case both trends are positive.

Time series decomposition resulted in Fig. 1c) which depicts the seasonal component for one year. A local maximum in late spring (104.36) and a local minimum in early autumn (−130.67) mark the seasonal variations. Obviously, offline data with yearly analyses can not exhibit any seasonal variations. BF2 did not show any clear seasonal variations.

Inter-annual fluctuations for eight individual ions (Na^+, K^+, Ca^{2+}, Mg^{2+}, F^-, Cl^-, SO_4^{2-} and HCO_3^-) were also examined. Over a time span of 20 years, the hydrochemical analyses show little variation. The highest relative SD values are displayed by Ca^{2+} (23.18 %), K^+ (20.50 %) and F^- (20.39 %), all of which exhibit low concentrations compared to the main ingredients.

3.2 ARIMA forecasting

The ARIMA forecasts differ strongly for online and offline data. Fig. 2a) shows an ARIMA forecast produced on the basis of offline data. The online data is depicted on top of the offline data. This shows that the forecast projects an expected value range which includes the measured offline data, however, it fails to cover even the currently measured online data. On the other hand, Fig. 2b) shows the ARIMA forecast based on online data. The projected value range covers a significantly wider area than the forecast based on offline data. Neither forecasts are able to produce a clear trend.

3.3 Correlation analysis

Among the assessed ions and physical parameters, such as temperature, extraction volume and drawdown, we found several strong correlations as indicated by the PCC and visualized them in scatter plots (Fig. 3). Due to the small sample sizes, many of these correlations were not statistically significant (based on the p-value and a significance level of 0.05), however, it is still worth to explore them as they can offer valuable insights into important hydrogeochemical dynamics. We found the obvious strong connection between drawdown and extraction volume ($R = 0.93$; Fig. 3a), but also between drawdown and EC ($R = 0.99$; Fig. 3b). Variations in TDS are covered by the concentration values of bicarbonate ($R = 0.86$) and sodium ($R = 0.90$). None of the calculated ratios showed any strong correlations with the physical parameters ($R > 0.6$) and only with their own constituents.

4 Discussion

This study set out to compare the information values of offline and online data gathered for a geothermal well, assess whether the current practice of yearly hydrochemical sampling is an adequate strategy on which a robust assessment of the status-quo and reliable forecasts can be based, and to use strong correlations between the two data sets to assess the applicability of virtual sensors to this setting where offline data fell short of providing critical information. For this, we assumed that a well's hydrochemical signature indicates flow paths, and changes in its signature indicate changes in flow paths.

One of the most striking pieces of information produced by this study was the comparison of yearly data, which is the current sampling standard (e.g. in Germany as mandated by the German Spa Association (Länderarbeitsgemeinschaft für Wasser, 1998)), and online data measurements which still remain scarce. While one could argue that the data sets agree on similar mean EC values, they differ vastly in their covered time period, seasonality and trends (Fig. 1).

The higher variation in the online data is not caused by a change of the operation conditions of the well, which is evident from the data from 2013 to 2020. Information on operating conditions was provided by the operators of the well. Lockdowns due to Covid-19 only affected contained time spans in 2020 and there were extensions or changes made to the infrastructure of the medical spa. Accordingly, visitor numbers stayed relatively constant. It is interesting to note that the application type of the well is probably responsible for the amplitude of seasonal variations.

The seasonal fluctuations are controlled by changes in the spa operation: the number of visitors is highest in winter and spring and therefore the volume withdrawn is also higher for these seasons compared to summer months (Fig. 1c). In contrast, BF2 does not show seasonal variations in the same way, because the well produces water continuously for balneological uses and heating which leads to more constant production rates. On the other hand, it might also indicate less inflow from above and below (Fig. S1). However, most aquifers are structurally heterogeneous and connected to the adjacent strata above and below. Inflow from these strata is a function of pressure in the main aquifer, even if their connection is weak. Increasing production rates lead to a decrease in the pressure in the main aquifer, which results in a pressure gradient to the adjacent stratigraphic units. If the hydrochemical composition in these units is different from the main aquifer, or if the main aquifer is strongly heterogeneous, changes in TDS (measured by EC probes at the well head) are to be expected. However, this correlation shows temporal dependencies which span over long periods, i.e. correlation between production rate and EC differ depending on the production regime leading up to the sampling date. This is a clear sign that the offline data fail to represent the hydrochemical state of the groundwater well at seasonally varying operating conditions. An assessment based on offline data alone will thus underestimate the contribution of other strata to the main aquifer.

Variability of the online data does show changes within the recorded time span. This corresponds with the trends detected in both data sets which differ starkly (Fig. 1b).

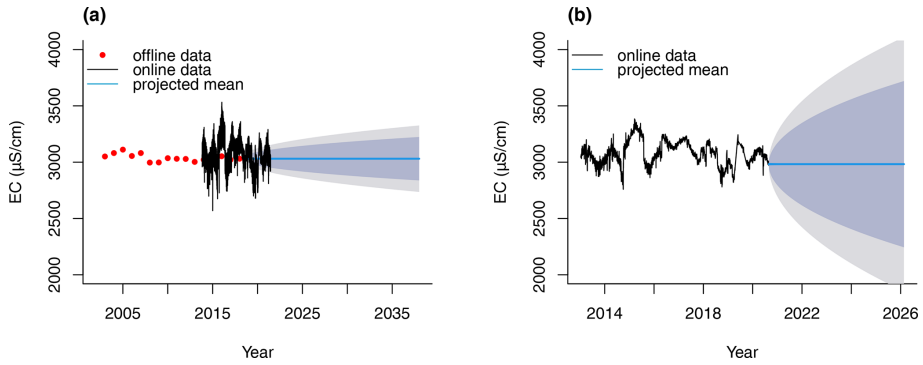

Figure 2. ARIMA forecasts for EC values at BAK. The forecast ranges are depicted in light blue: 85 % confidence interval; light grey: 95 % confidence interval. **(a)** forecast based on offline EC data, as well as overlaid online EC data. **(b)** forecast based on online EC data.

Overall, by omitting sub-yearly, seasonal fluctuations, the offline data set merely offers a snapshot of the well's hydrochemical state. The snapshot is limited in its informative value to the sampling date and does not provide any information on between-sampling fluctuations. This can lead to misjudgments on the hydrochemical stability of the well and seasonal activation of additional inflow pathways. Time series decomposition derived a seasonal variation frequency of 1 year (Fig. 1b). Accordingly, the Nyquist-Theorem demands that the sampling frequency be higher than one sample every six months in order to adequately represent the fluctuations with a 12 month period. We thus suggest a sampling frequency of 4 to 5 months which is higher than the current practice of one sample a year, but lower than the suggested frequencies by Zhou (1996) of 1 month, and by Barcelona et al. (1989) of 2 to 3 months. Their high sampling frequencies are likely due to stronger sub-seasonal variations in shallow ground water aquifers, by which deep ground water aquifers, such as the one in this study, are less impacted. However, this study showed that clear seasonal variations can also be found in deep ground water aquifers. The proposed scheme is applicable to all deep groundwater wells except for cases where the confining layers prevent any inflow from above or below at the well and in its vicinity. In this case, the water originates only from the reservoir and will not show any change in the flow pattern due to changes.

We further demonstrated that the ARIMA forecast for EC values, built upon offline data, neglects to consider even currently observed, sub-yearly EC concentration fluctuations. Due to the sampling bias, the forecast based on offline data (Fig. 2a) shows a rather small prediction interval and no trend. This is in line with very little variations of the hydrochemical composition observed over the years. The forecast based on online data reveals a great uncertainty but still no trend. This indicates that changes in the flow patterns to this particular well are fully reversible and points to a hydraulic activation of flow paths in a heterogeneous reservoir, rather than an influx from overlying or underlying stratigraphic units as seen e.g. at the Pullach Th2 well (Baumann et al., 2017). Part of the uncertainty can also be attributed to the shorter time span of online data. In the case of this well, we showed conclusively that a forecast, as required for many deep ground water aquifers by the WFD, based on yearly measurements, fails to represent sub-yearly variations in EC, and only represents one very specific state of the well. Thus, forecasting needs to be conducted with higher-resolution data in order to take these developments into account.

Having shown that yearly groundwater sampling does not adequately represent real hydrochemical fluctuations in the reservoir, the possibilities of applying VS in this field were tested. While we found some correlations with a high PCC, the correlations were rarely statistically significant (Fig. 3). This is due to the small size of the available data sets. There was an expected correlation between the production rate (or drawdown) and temperature. The correlation between water temperature and TDS might point to different flow patterns. The correlation between EC and drawdown allowed insights into some hydrochemical dynamics. The hydrochemical signature of the two most divergent analyses in our correlation assessment show slightly lower TDS: Na^+, Cl^-, and HCO_3^- show lower concentrations, K^+, Ca^{2+}, and SO_4^{2-} show higher concentrations. Assuming a minor change of the flow pattern at high production rate with an influx of 7 % of another water type, the calculated inflow water is a $K^+ - Ca^{2+} - HCO_3^- - SO_4^{2-}$ – type with a TDS of 1100 mg L^{-1}. The saturation indices calculated with PhreeqC show that the water is in equilibrium with dolomite, and under-saturated (saturation index $= -1$) with respect to gypsum. The calculated hydrochemistry of the in-flowing water does not fit waters of the crystalline basement or the overlying sandstones of the lower Jurassic (Carlé, 1975). Furthermore, the variations recorded by the online measurements are much larger compared to the analysis data. Therefore, the hydrochemistry of the in-flowing water would cause an even starker contrast to the assumed composition. Assuming a mix with 50 % of another water type leads to similar TDS and hydrochemical signature, and would indicate lithos-

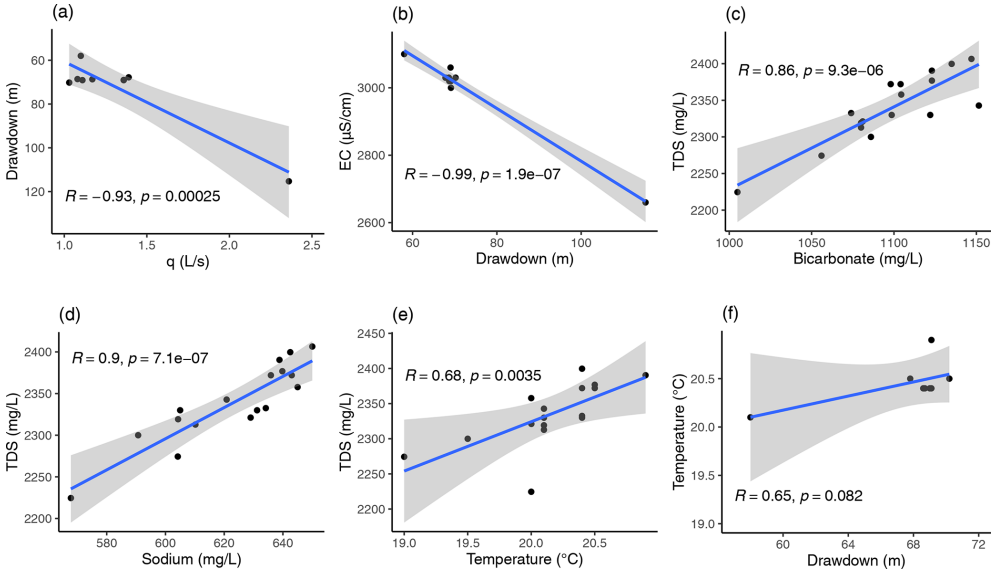

Figure 3. Selection of univariate regressions marked by a high Pearson correlation coefficients based on the offline data set at BAK. The blue line indicates the linear regression model, the grey shaded area shows the 99 % confidence interval.

tratigraphic heterogeneity or hydrochemical stratification in the reservoir.

To make use of VS to span data gaps and assess dynamic changes of the inflow pathways to the well, a number of prerequisites have to be met. The relationships between offline and online data sets must be based on larger data sets than are currently available to ensure statistically significant correlations. However, stronger data might also include the following: ideally, flow-meter logs and/or fibre optical measurements (Schölderle et al., 2021) are available to define the immediate inflow zones to the well at different production rates. To assess inflow from adjacent strata, pumping tests during exploration or information from wells close by and reaching into these strata can provide relevant information. The relation between production rate and hydrochemical characteristics can be obtained from pumping tests with different production rates. Long-term hydrochemical data can provide information about inflow zones further away from the well. Finally, under ideal conditions, a hydrogeochemical model framework to assess the interactions and reactions of the (mixed) waters along the flow paths is available.

5 Conclusions

This study showed that on the basis of two wells, one which is solely used for balneological purposes, and one which is exploited for balneology and constant energy production, the current state of the art practice of yearly hydrochemical measurements fail to accurately represent trend, mean and seasonality. It is thus of great importance that more data with high temporal resolution is made available. Since direct physical measurements of the variables in question are financially and physically impossible, virtual sensors could offer a viable alternative. We thus conclude that:

1. Yearly samples taken at the same stress state are underestimating the hydrochemical variations of the produced waters. This is relevant for balneological and geothermal applications with regards to the legal framework pertaining to recognition as medical spas, and predictive maintenance and prevention of corrosion and scaling, respectively.

2. Basing hydrochemical forecasting algorithms, such as ARIMA, on yearly data did not result in reliable value ranges. The calculated ranges failed to include even currently measured sub-yearly signal response variability when used on EC data.

3. Online data provide quantitative access to the nature of the processes responsible for changes in the hydrochemical conditions, and whether they are reversible or not. However, online data require careful hydrochemical characterization of the well (hydrochemical pumping tests, hydrochemical and hydraulic logs, depth oriented sampling) to make full use of their predictive potential, e.g. use in VS applications.

Knowing the precise fluctuations of the individual ions, TDS and overall hydrochemical composition is important knowledge for predictive maintenance and serves as an indicator and warning signal for unsustainable groundwater extraction schemes. For this, we estimate that sensor fusion in the framework of geothermal science is possible if there is a proper prior characterization of the reservoir, and the hydrochemical characteristics in the different parts of the reservoir

are known. In order to achieve larger training data sets, it is crucial that hydrochemical assessments take place more often than once a year.

Overall, more frequent sampling at different production scenarios, and learning algorithms in combination with mixing models will aid implementing VS to the field of geothermal water production.

Code and data availability. All code was written using the statistical software R and is available on request. The software as well as the relevant clustering packages can be downloaded under https://www.r-project.org/ (last access: 16 December 2022). Hydrochemical data is available on request.

Supplement. The supplement related to this article is available online at: https://doi.org/10.5194/adgeo-58-189-2023-supplement.

Author contributions. TB conceived the presented idea. AD developed the theory and performed the computations. TB verified the analytical methods and supervised the findings of this work. Both authors discussed the results and contributed to the final manuscript. AD wrote the manuscript with support from TB.

Competing interests. The contact author has declared that none of the authors has any competing interests.

Special issue statement. This article is part of the special issue "European Geosciences Union General Assembly 2022, EGU Division Energy, Resources & Environment (ERE)". It is a result of the EGU General Assembly 2022, Vienna, Austria, 23–27 May 2022.

Disclaimer. Publisher's note: Copernicus Publications remains neutral with regard to jurisdictional claims in published maps and institutional affiliations.

Acknowledgements. The authors would like to thank the reviewers and Ingrid Stober (Karlsruhe Institute of Technology) for their very helpful comments and the operators of the wells BAK and BF2 for supplying data. We also would like to thank the lab technicians Birgit Apel and Joachim Langer.

Financial support. This study was funded by the Bavarian State Ministry of Science, Research and Art in the Framework of the Geothermal-Alliance Bavaria.

This work was supported by the Technical University of Munich (TUM) in the framework of the Open Access Publishing Program.

Review statement. This paper was edited by Gregor Giebel and reviewed by two anonymous referees.

References

Alley, W. M., Bair, E. S., and Wireman, M.: "Deep" Groundwater, Groundwater, 51, 653–654, https://doi.org/10.1111/gwat.12098, 2013.

Barcelona, M., Wehrmann, H., Schock, M., Sievers, M., and Karny, J.: Sampling Frequency for groundwater Quality Monitoring, US Environmental Protection, Office of Research and Development, Environmental Monitoring Systems Laboratory, EPA/600/4-89/032, 1989.

Baumann, T., Bartels, J., Lafogler, M., and Wenderoth, F.: Assessment of heat mining and hydrogeochemical reactions with data from a former geothermal injection well in the Malm Aquifer, Bavarian Molasse Basin, Germany, Geothermics, 66, 50–60, https://doi.org/10.1016/j.geothermics.2016.11.008, 2017.

Birner, J.: Hydrogeologisches Modell des Malmaquifers im Süddeutschen Molassebecken, PhD thesis, https://refubium.fu-berlin.de/handle/fub188/1492 (last access: 12 May 2023), 2013.

Birner, J., Mayr, C., Thomas, L., Schneider, M., Baumann, T., and Winkler, A.: Hydrochemie und Genese der tiefen Grundwässer des Malmaquifers im bayerischen Teil des süddeutschen Molassebeckens Hydrochemistry and evolution of deep groundwaters in the Malm aquifer in the bavarian part of the South German Molasse Basin, Z. Geol. Wiss., 39, http://www.zgw-online.de/en/media/291-113.pdf (last access: 12 May 2023), 2011.

Caers, J. and Castro, S.: A Geostatistical Approach to Integrating Data From Multiple and Diverse Sources: An Application to the Integration of Well Data, Geological Information, 3d/4d Geophysical and Reservoir-Dynamics Data in a North-Sea Reservoir, Subsurf. Hydrol. Data Integr. Prop. Process. Geophys. Monogr. Ser., 171, https://doi.org/10.1029/171GM07, 2006.

Carlé, W.: Die Mineral- und Thermalwässer von Mitteleuropa: Geologie, Chemismus, Genese, Wissenschaftliche Verlagsgesellschaft, Stuttgart, ISBN 3 80470461 1, 1975.

Deutscher Heilbäderverband and Deutscher Tourismusverband: Begriffsbestimmungen/Qualitätsstandards für Heilbäder und Kurorte, Luftkurorte, Erholungsorte – einschließlich der Prädikatisierungsvoraussetzungen – sowie für Heilbrunnen und Heilquellen, Tech. Rep., Deutscher Tourismusverband e.V. und Deutscher Heilbäderverband e.V., 2016.

European Parliament and Council: Directive 2000/60/EC I – The European Water Framework Directive, https://doi.org/10.2779/75229, 2000.

Hebig, K. H., Ito, N., Scheytt, T., and Marui, A.: Review: Deep groundwater research with focus on Germany, Hydrogeol. J., 20, 227–243, https://doi.org/10.1007/s10040-011-0815-1, 2012.

Heine, F., Zosseder, K., and Einsiedl, F.: Hydrochemical Zoning and Chemical Evolution of the Deep Upper Jurassic Thermal Groundwater Reservoir Using Water Chemical and Environmental Isotope Data, Water, 13, 1162, https://doi.org/10.3390/w13091162, 2021.

Ho, S. L. and Xie, M.: The use of ARIMA models for reliability forecasting and analysis, Comput. Ind. Eng., 35, 213–216, https://doi.org/10.1016/s0360-8352(98)00066-7, 1998.

Hyndman, R., Athanasopoulos, G., Bergmeir, C., Caceres, G., Chhay, L., O'Hara-Wild, M., Petropoulos, F., Razbash, S., Wang, E., and Yasmeen, F.: forecast: Forecasting functions for time series and linear models, R package version 8.15, https://pkg.robjhyndman.com/forecast/ (last access: 16 December 2022), 2021.

Kabadayi, S., Pridgen, A., and Julien, C.: Virtual sensors: Abstracting data from physical sensors, Proc. – WoWMoM 2006 2006 Int. Symp. a World Wireless, Mob. Multimed. Networks, 2006, 587–592, https://doi.org/10.1109/WOWMOM.2006.115, 2006.

Kang, M., Ayars, J. E., and Jackson, R. B.: Deep groundwater quality in the southwestern United States, Environ. Res. Lett., 14, 034004, https://doi.org/10.1088/1748-9326/aae93c, 2019.

Käss, W. and Käss, H.: Deutsches Bäderbuch, Schweizerb. Edn., ISBN 978-3-510-65241-9, 2008.

Krieger, M., Kurek, K. A., and Brommer, M.: Global geothermal industry data collection: A systematic review, Geothermics, 104, 102457, https://doi.org/10.1016/j.geothermics.2022.102457, 2022.

Länderarbeitsgemeinschaft für Wasser: Richtlinien für Heilquellenschutzgebiete, ISBN 3-88961-217-2, 1998.

Martin, D., Kühl, N., and Satzger, G.: Virtual Sensors, Bus. Inf. Syst. Eng., 63, 315–323, https://doi.org/10.1007/s12599-021-00689-w, 2021.

Mayrhofer, C., Niessner, R., and Baumann, T.: Hydrochemistry and hydrogen sulfide generating processes in the Malm aquifer, Bavarian Molasse Basin, Germany, Hydrogeol. J., 22, 151–162, https://doi.org/10.1007/s10040-013-1064-2, 2014.

Nelson, J. D. and Ward, R. C.: Statistical Considerations and Sampling Techniques for Ground-Water Quality Monitoring, Ground Water, 19, 617–625, https://doi.org/10.1111/j.1745-6584.1981.tb03516.x, 1981.

Parkhurst, D. L. and Appelo, C. A. J.: Description of input and examples for PHREEQC versoin 3: a computer program for speciation, batch-reaction, one-dimensional transport, and inverse geochemical calculations, in: Model. Tech., Chap. 43, U.S. Geological Survey, Reston, Virginia, https://doi.org/10.3133/tm6A43, 2013.

Porter, D. W., Gibbs, B. P., Jones, W. F., Huyakorn, P. S., Hamm, L. L., and Flach, G. P.: Data fusion modeling for groundwater systems, J. Contam. Hydrol., 42, 303–335, https://doi.org/10.1016/S0169-7722(99)00081-9, 2000.

R Core Team: R: a language and environment for statistical computing, https://www.r-project.org/ (last access: 16 December 2022), 2020.

Schölderle, F., Lipus, M., Pfrang, D., Reinsch, T., Haberer, S., Einsiedl, F., and Zosseder, K.: Monitoring cold water injections for reservoir characterization using a permanent fiber optic installation in a geothermal production well in the Southern German Molasse Basin, Vol. 9, Springer Berlin Heidelberg, https://doi.org/10.1186/s40517-021-00204-0, 2021.

Tegen, A., Davidsson, P., Mihailescu, R. C., and Persson, J. A.: Collaborative sensing with interactive learning using dynamic intelligent virtual sensors, Sensors (Switzerland), 19, https://doi.org/10.3390/s19030477, 2019.

Zhang, P. G.: Time series forecasting using a hybrid ARIMA and neural network model, Neurocomputing, 50, 159–175, https://doi.org/10.1016/S0925-2312(01)00702-0, 2003.

Zhou, Y.: Sampling frequency for monitoring the actual state of groundwater systems, J. Hydrol., 180, 301–318, https://doi.org/10.1016/0022-1694(95)02892-7, 1996.

6 Submitted article: Visualization and Semi-Quantitative Analysis of Dissolution Processes at Artificial Structures in Carbonate Rocks Using Optical, 3D Micro-Scanning and Confocal Laser Scanning Microscopy

6.1 Placement in this Dissertation's Context

This thesis' third publication follows the water's route through a geothermal doublet through the heat exchanger, down through the reinjection well, and back into the aquifer pore space, where it is no longer in equilibrium with the rock matrix. Cooling the hot water in the heat exchanger shifts the hydrochemical equilibrium by facilitating CO_2 dissociation, lowering the water's pH, and causing the calcium saturation index to drop. Consequently, when this water comes into contact with the aquifer, it can lead to dissolution processes affecting the carbonate rock matrix. In the context of sustainable groundwater management, these dynamics play an essential role as dissolution processes near the reinjection well can lead to a quicker spread of the cool water, possibly facilitating a shorter thermal breakthrough time.

This third publication (accepted with minor revisions) systematically compares three methods to visualize and quantify these dissolution effects on a pore scale. A new autoclave treatment protocol was developed that facilitated high temperature and pressure conditions and limited dissolution effects to a small, easily observable area in a representative carbonate rock sample by using an autoclave with continuous injection of CO_2 to artificially increase the water's acidity and lower the calcite saturation index. The effects were then examined using optical microscopy, confocal laser confocal laser scanning microscopy (CLSM), and 3D micro-scanning. This study found that each method has its unique advantages and shortcomings, ranging from financial accessibility to a very precise depiction of rock surface morphology and the ability to peek beneath overhangs, respectively.

6.2 Research Questions

The third publication of this dissertation aimed to answer the following research questions:

1. How can the visibility of chemical alterations to a rock's surface, induced in autoclave experiments, be enhanced for optical and 3D microscopic imaging methods?

2. How do optical microscopy, 3D micro-scanning, and CLSM differ in their ability to characterize surface roughness and depth changes resulting from dissolution processes?

3. What unique insights does each method provide, and how can they be combined to achieve a comprehensive understanding of surface alterations in the aquifer, and what are the practical considerations (e.g., resolution, cost, accessibility) for using these methods in both laboratory and applied geothermal settings?

6.3 Author Contributions

Thomas Baumann conceived the presented idea and acquired funding, verified the analytical methods, and supervised the findings of this work.

Annette Dietmaier and Justin Mattheis contributed equally to the writing of the first draft.

Annette Dietmaier prepared the samples, designed and performed the autoclave experiments, performed optical microscopy and 3D scans, evaluated the results, and coordinated author meetings.

Justin Mattheis performed 3D scans, assisted with the optical microscopy image acquisition and autoclave setup, and analyzed and interpreted the 3D data.

Daniel Weller performed the CSLM data acquisition, analysis, and interpretation.

Ingrid Stober supervised the study and contributed significantly to the discussion and introduction based on her previous works on this subject.

Michael Drews initiated the application of 3D micro-scanning for this purpose and provided support during the evaluation of the results.

All authors discussed the results and contributed to the final manuscript.

Dietmaier *et al. Geothermal Energy* (2025) 13:32
https://doi.org/10.1186/s40517-025-00355-4

Geothermal Energy

METHODOLOGY Open Access

Visualization and semi-quantitative analysis of dissolution processes at artificial structures in carbonate rocks using optical, 3D micro-scanning and confocal laser scanning microscopy

Annette Dietmaier[1†], Justin Mattheis[2†], Daniel Weller[3], Ingrid Stober[4], Michael Drews[5] and Thomas Baumann[1*]

[†]A. Dietmaier, J. Mattheis: These authors contributed equally to this work.

*Correspondence: tbaumann@tum.de

[1] Chair of Hydrogeology, Technical University Munich, Arcisstr. 21, 80333 Munich, Germany
[2] Chair of Engineering Geology, Technical University Munich, Arcisstr. 21, 80333 Munich, Germany
[3] Department of Earth and Environmental Sciences, Ludwig-Maximilians-Universität, Theresienstr. 41, 80333 Munich, Germany
[4] Institut of Geo and Environmental Sciences, University Freiburg, Albertstr. 23b, 79104 Freiburg, Germany
[5] Chair of Geothermal Technologies, Technical University Munich, Arcisstr. 21, 80333 Munich, Germany

Abstract

The Northern Alpine Foreland Basin in southeast Germany hosts more deep geothermal plants than any other region in the country. Its primary aquifer, the Upper Jurassic, is composed of permeable carbonates containing water with temperatures exceeding 150 °C in the southern margin and low total dissolved solids (≤ 2 g/L) at depths of up to 4000 m. Its sustainable use of geothermal energy depends on an efficient exploitation strategy concerning the entire reservoir, which is influenced by the development of flow paths between production and reinjection wells. The Upper Jurassic's waters show a carbonate signature with calcium and magnesium often replaced by sodium due to ion exchange along the infiltration pathways. These waters become undersaturated upon cooling, and dissolution around reinjection wells has been previously documented. Assessing short- to medium-term localized dissolution experimentally is challenging. While dissolution kinetics and overall volume changes have been studied in the field, microscopic changes to flow paths remain less under investigation. This study used a time-lapse experiment to evaluate microscopic changes during dissolution in limestone samples exposed to elevated CO_2 partial pressure in an autoclave. For an effective observation, we used artificial structures to localize the dissolution effects. Post-treatment analysis included Raman microscopy, 3D micro-scanning, confocal laser scanning microscopy (CLSM), and optical microscopy with image stacking, with a strong focus on the latter three. Each imaging method had distinct strengths and limitations. CLSM provided high-resolution surface roughness assessments but could not capture areas beneath overhangs. Optical microscopy is affordable and user-friendly and was effective for visualizing preferential dissolution pathways but lacked precise roughness information. 3D micro-scanning, despite lower resolution, uniquely resolved overhangs. The dissolution processes led to significant surface roughening, forming micrometer-scale moldic pores and preferential pathways. Artificial structures widened and deformed, with 3D micro-scanning quantifying these changes effectively and CLSM revealing fine-scale roughness details. Increased fracture surface roughness and widening of flow paths enhance water transport

and dissolution, potentially accelerating thermal breakthroughs at geothermal plants. Understanding these processes is essential for predicting reservoir behavior, improving geothermal energy extraction efficiency, and exploiting aquifers sustainably.

Keywords: Dissolution, Flow path dynamics, Thermal breakthrough, Microscopic surface analysis, 3D microscopy

Introduction

The "Clean Energy for All Europeans" package adopted by the European Union (EU) in 2019 aims to decarbonize the EU's energy provision by setting and improving standards regarding, among others, energy performance in buildings, renewable energy, and energy efficiency (European Commission, 2023). Decentralized geothermal wells, i.e., doublets, are used for district heating in Germany, most of which are situated in the carbonates of the Upper Jurassic in the Northern Alpine Foreland Basin (NAFB). The NAFB offers very favorable conditions given its highly permeable carbonate rock matrix located in 2000–4000 m depth, and suitably high aquifer temperatures (BayStMWI 2012).

In a geothermal doublet, a production well withdraws hot water that is in chemical equilibrium with the host rock from the reservoir. A surface-level heat exchanger extracts the heat, and the cool water is reinjected into the reservoir through an injection well (BayStMWI 2012). A reliable forecast of the expected thermal breakthrough time (governed by production volumes and the aquifer's permeability; Schmidt et al. 2018) is necessary to ensure these sites' long-term sustainable use. Porosity and permeability are affected by geochemical reactions between the fluid in the pores and fractures, and the rock matrix itself (Baumann et al. 2017; Ling et al. 2022; Schmidt et al. 2017; Singurindy and Berkowitz 2005). These dynamics, such as precipitation and dissolution of minerals, lead to changes in fracture and porosity propagation and reactive solute transport, and alter fluid chemistry as well as fracture and pore geometry (Stober and Bucher 2022; Ling et al. 2022). In the case of a geothermal doublet, the development of the permeability at the reinjection well site is controlled by an inherent hydrochemical shift: the produced water is assumed to be in chemical equilibrium with the surrounding rock matrix at reservoir depth, but during transportation to the surface level, the pressure decreases significantly, causing degassing and stripping effects (Zacherl and Baumann 2023). In the carbonate setting, the waters arrive at the surface level supersaturated, and precipitation of carbonates occurs along the whole production path. After the heat exchanger, however, the waters become undersaturated with typical saturation indices (SI) for Calcite between −0.26 (Pullach Th2 (98 ⟶ 55°C)) to −1.86 (Sauerlach, 137 ⟶ 55°C, values calculated with PhreeqC in previous studies Baumann et al. 2017; Köhl et al. 2020). Waters initially in equilibrium with dolomite show lower SI values compared to waters in equilibrium with limestone. This makes injection wells in the Upper Jurassic benign with regard to the precipitation of minerals. Ultimately, this can trigger dissolution processes in the rock matrix near the reinjection site, resulting in rougher pore surfaces, expanded pore space, or weakened structural matrix integrity at the reinjection well site (Su et al. 2018; Stober and Bucher 2022; Ling et al. 2022), which can deteriorate the reservoir's usability and diminish geothermal production (Rivera Diaz et al. 2016; Yang et al. 2022). In a worst-case scenario, these dynamics result in the early onset of thermal breakthrough between injection and production wells. The presented study focuses on

characterizing and visualizing the dissolution processes occurring at the reinjection site as it is a critical point to consider for researchers, decision-makers in urban energy planning, and geothermal plant operators to optimize production efficacy and general system longevity and ultimately to enable sustainable use of the geothermal resource.

Focusing mainly on reservoir materials different from the NAFB carbonates (e.g., halite, shale, granite, and sandstone), previous studies have analyzed dissolution and precipitation in aquifer rock fractures in laboratory experiments to assess fracture morphology, flow patterns (Dijk and Berkowitz 2002; Lu et al. 2016), preferential dissolution pathways (Wen et al. 2016), mineralogical and textural changes (Schmidt et al. 2017, 2018, 2019; Sun et al. 2016) and general reactivity between fluid and rock matrix (Drüppel et al. 2020; Ling et al. 2022; Singurindy and Berkowitz 2005) on pore scale.

Among these studies, many are based on one or both of two recurring types of experimental setups: flow cells, in which aquifer rock samples are injected with an undersaturated fluid (Dijk and Berkowitz 2002; Singurindy and Berkowitz 2005; Ling et al. 2022), and autoclave experiments, where the aquifer rock samples, either in a crushed or intact form, are submerged in a reactive fluid. Here, the undersaturation of the fluid is achieved through an adequate chemical composition of the fluid itself or CO_2 injections into the closed autoclave setup (Lu et al. 2012; Sun et al. 2016; Randi et al. 2014).

For example, flow cell experiments with undersaturated saline solutions injected into natural halite samples with an aperture of ~2 mm showed that flow patterns positively correlate to fracture size, aperture, and wall roughness (Dijk and Berkowitz 2002), leading to faster clogging of pores when walls were rougher. The results were obtained using 3D nuclear magnetic resonance imaging (NMRI) of water density and flow velocity with a spatial resolution of 0.16–0.18 mm, and 0.25 mm in x and y, and z directions, respectively. NMRI thus proved a powerful yet very expensive (initial investment costs: starting at more than USD 200,000; annual maintenance fee: starting at USD 40,000; Imaging 2025) tool for understanding dissolution processes in natural water-saturated rock fractures and flow paths using flow cells. To further improve the visual analysis of fracture alteration, Ling et al. (2022) exposed quasi-2D samples of highly heterogeneous shale (Marcellus carbonate-rich shale and Wolfcamp shale) to acidic fluid (1 % HCl) in microfluidic cells and analyzed alterations on pore and fracture scales (0.0001–0.001 mm and 0.001–1 mm, respectively). They found that fracture morphology and loss of rock strength were governed by the relative volume and distribution of reactive grains (mainly calcite and dolomite) (Ling et al. 2022). Their visualization was done using optical imagery and scanning electron microscopy (SEM). While flow cell experiments such as (Dijk and Berkowitz 2002) and Ling et al. (2022) allow for close visual inspection with a high temporal resolution and almost real-time image acquisition (e.g., 120–130 s intervals in Ling et al. (2022)), they are typically conducted at ambient temperatures of around 20°C and at low or unspecified pressures (Singurindy and Berkowitz 2005; Dijk and Berkowitz 2002; Ling et al. 2022).

To incorporate parameters such as high pressure and temperature (as they are typically found in deep thermal aquifers), autoclaves offer a good method of simulating these conditions. For example, Randi et al. (2014) used an autoclave setup on Lavoux limestone from the Paris Basin in the framework of CO_2-storage to assess chemical reactions in the near-injection well area between rock formation, the well's cement phases, and the

fluid containing CO_2. Their autoclave flow-through experiments were conducted at relevant temperature and pressure conditions (60 °C and 120 bar, respectively). Using X-ray tomography, the authors observed a complex wormhole network developing within 15 days from the injection point to the plug's exterior on a centimeter scale (Randi et al. 2014; Dijk and Berkowitz 2002). While visible holes in the wall of the core plug were described to have formed during the treatment, no quantitative information on mass loss or surface roughness was given in this particular publication. Stober et al. (2023) carried out high-temperature alteration experiments in highly concentrated NaCl solutions with limestone samples of the Muschelkalk. They found both dissolution structures on the original rock samples and the formation of new minerals on the original rock sample surfaces, which could be identified as calcite crystals through SEM. The main effect of the alteration process was a dissolution-precipitation process of limestone to calcite and to traces of dolomite, and the formation of depression zones (Stober et al. 2018). Thus, while autoclave experiments do not allow for high temporal resolution image/data acquisition, their strength lies in enabling a controlled increase of temperature and pressure during the treatment, facilitating the simulation of realistic aquifer conditions. Furthermore, fluid undersaturation can be achieved through ionic composition and the continuous injection of CO_2 throughout a treatment cycle.

While prior studies have investigated dissolution and precipitation dynamics in aquifer rocks using techniques, such as SEM, X-ray tomography, NMRI, and CT imaging, there is limited systematic comparison of surface characterization methods for dissolution-induced changes. Specifically, the ability to quantify surface roughness and fracture morphology across different scales remains important to advancing our understanding of reactive transport processes critical for sustainable geothermal plant operation. Building upon the results of controlled autoclave experiments by Schmidt et al. (2017), Schmidt et al. (2018), Schmidt et al. (2019), Randi et al. (2014) and Sun et al. (2016), and bridging the gap between the mineralogical and structural centimeter scale, this study aims to make 3D pore-level alterations visible. We address this gap by assessing three methods that have not yet been put in a general comparison: optical microscopy, 3D micro-scanning, and confocal laser scanning microscopy (CLSM) on rock samples having been exposed to an undersaturated fluid in an autoclave setup.

Relying on a high-intensity source of visible light and a combination of magnifying lenses (objectives), optical microscopy has been a long-standing method of producing magnified 2D images of the object at hand. For decades, it has been used to examine mineral and rock samples from the earth, the moon, and meteorites (Davidson and Lofgren 1991) and still serves to characterize micro-mechanical properties of these samples (Jensen et al. 2010; Laurich et al. 2014). Optical microscopy allows insights into transparent/absorbing phases (through transmitted-light microscopy on thin sections), grain boundaries, fractures, and artifacts (Gribble 2012). Reflected-light microscopy is commonly applied to polished rock samples (Gribble 2012), minimizing image blurs due to the rock sample leaving the microscope's field of depth.

3D imaging provides a new and promising method to quantify the observed changes in depth. Optical 3D imaging is already state-of-the-art in various geological applications (Kersten et al. 2018). Through laser scanning and photogrammetrical analyses, outcrops and larger surface structures can be captured digitally and further processed (Pless et al.

2015; Gaich and Pötsch 2016; Erharter et al. 2018; Francioni et al. 2019; Rechberger 2022; Garcia-Luna et al. 2023). In geological engineering applications, this is particularly useful for mapping joints and faults or detecting surface movements through temporal monitoring. Although recent research has used this method on archaeological artifacts (Göldner et al. 2022; Diara 2023; Falcucci 2022), on a laboratory scale, optical 3D micro-scanning has not yet been established to analyze the surface properties of rock samples. 3D micro-scanning, as used in this study, is commonly used in the field of dental prostheses (Koban et al. 2020; August et al. 2024; Costello et al. 2024; Demirel et al. 2024; Limones et al. 2025), or for capturing precision of mechanical parts in engineering (Peng et al. 2017).

CLSM is an established tool in geo- and material science typically used to characterize surface properties of rocks, metals, ceramics, and manufactured materials (Fredrich et al. 1995; Petford et al. 1999; Menéndez et al. 2001; Lohbauer et al. 2008; Weller et al. 2024). Due to the application of a pinhole in front of the detector, only the focal plane is measured, resulting in high data quality with up to nanometer resolution. By adjusting the distance between the sample and lens, several 2D measurements can be stacked to create a 3D data set that can be used to measure the volumetric and surface properties of rocks. From the generated topographical data, surface roughness can be calculated through the arithmetical mean height, which is crucial for the characterization of reservoir rocks (Singer et al. 2023; Ma et al. 2021).

As criticized by Sun et al. (2016), typical autoclave experiments with rock plugs result in a thin "skin-depth" zone of chemical alterations. In this study, we complement our assessment of the aforementioned methods with a new experiment protocol to make these chemical alterations to the rock matrix directly visible by controlling the exposed rock matrix area through water- and heat-resistant coating and concentrating chemical alterations to the samples in a controlled autoclave environment at increased temperatures and partial CO_2 pressures. Our protocol results in a time-lapse simulation of the slow hydrochemical kinetics at a typical reinjection site in the NAFB. Thus, this study intends to answer the following research questions:

1. How can the visibility of chemical alterations to a rock's surface, induced in autoclave experiments, be enhanced for optical and 3D microscopic imaging methods?
2. How do optical microscopy, 3D micro-scanning, and CLSM differ in their ability to characterize surface roughness and depth changes resulting from dissolution processes?
3. What unique insights does each method provide, and how can they be combined to achieve a comprehensive understanding of surface alterations in the aquifer, and what are the practical considerations (e.g., resolution, cost, accessibility) for using these methods in both laboratory and applied geothermal settings?

This study evaluates three characterization techniques—optical microscopy, 3D micro-scanning, and CLSM—to better understand their relative advantages and limitations in visualizing and quantifying dissolution-induced changes in carbonate rocks. To achieve this, we propose a novel approach to investigating rock–water interactions in an autoclave setting by limiting dissolution processes to specific areas on the rock sample,

shielding the rest from exposure to acidic fluid. By adding CO_2 to simulate undersaturation caused by shifts in the lime–carbonic acid equilibrium, our controlled autoclave setup produces a time-lapse simulation of conditions and processes found in the geothermal aquifer around injection wells. Through a combination of high-resolution structural data from 3D and microscopic imaging, hydrochemical analysis, and mass balance calculations, we aim to localize dissolution processes, characterize changes to the rock matrix, and link these findings to the evolving chemistry of the fluid. This integrative approach enhances our understanding of reactive transport processes and helps improve the basis of hydrogeochemical models, moving beyond singular-crystal kinetics toward a more accurate representation of aquifer dynamics.

Methods

Rock matrix characterization and sample preparation

Our experiments were carried out on limestone samples representing the NAFB's carbonates. The limestone samples were prepared from a block of "Solnhofener Plattenkalk" that was extracted from a limestone quarry in Solnhofen in the Franconian Alb (quarry Steinbruch Solnhofen, proprietor: A. Kress). Stratigraphically belonging to the Upper Altmühltal formation of the Upper Jurassic (lower Tithonian–upper Kimmeridgian), the limestone was formed as ultra lagoon facies in the southern German basin (Niebuhr and Pürner 2014). While macroscopically a homogeneous, light beige to grey limestone, few recrystallized micro-fossils classify the micritic rock as a wackestone to mudstone (Mraz et al. 2018). $CaCO_3$ (96–98 %) and $MgCO_3$ (0.5–2 %) make up the bulk of the mineral composition, with metal oxides covering the remainder to 100 % (Sonat 2024).

Using a UniPrec saw equipped with a TS 30/7 saw blade, the rock sample was cut into roughly cubic shape with side lengths of approximately 15 mm with mostly smooth surfaces. The cube was further prepared by being covered entirely with two layers of water- and heat-resistant 2K-PU-paint (PU 250-90, MIPA SE, Essenbach, Germany), resulting in a 0.02–0.03 mm thick coating. It was then dried and tempered at 60 °C for 4 h after each coating. Using a Dremel mini drill and a precision drill bit (Dremel 628), we created two artificial structures in the lacquer and the underlying rock material (one point-shaped = hole, one line-shaped = cut; Fig. 1). The sample cube was weighed with a precision scale (ABP 200-5DM, Kern & Sohn GmbH, Balingen-Frommern, Germany) before and after being coated. This before value, in combination with the cube's respective volume derived from the 3D scans, served to calculate the sample's density, which amounted to 2.6 g/cm^3.

Autoclave experiment setup

The study design uses an autoclave setup to simulate the reactions between rock matrix and geofluids near an injection well in a time-lapse experiment, in which elevated CO_2 pressures serve to reproduce local saturation indices (Table 1). The experiment was conducted using a stainless steel midiclave 4E autoclave (Büchi AG, Uster, Switzerland) which holds a total volume of 1.0 L and facilitates high-temperature, high-pressure condition experiments (max. temperature = 150 °C; max.

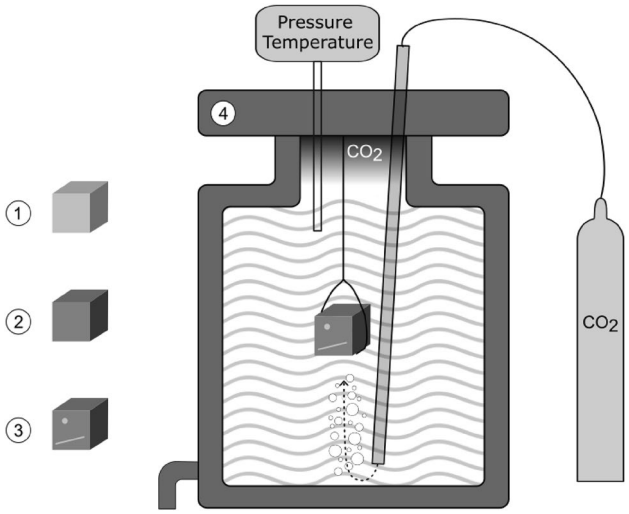

Fig. 1 Schematic of the autoclave setup, including the added CO_2 bubbling up through the entire water column from the bottom to a gas pocket above the water surface, an external pressure and temperature monitor, and a water outlet at the bottom. (1) untreated sample; (2) coated sample; (3) coated sample with artificial fractures; (4) exposure of the sample to undersaturated liquid in the autoclave

pressure = 200 bar) with the possibility of continuous CO_2 injection into the system while running an experiment (Table 1).

The experiment setup is presented in Fig. 1. At the beginning of each treatment cycle, the autoclave was filled with ultra-pure water (UPW; EC: 0.055 μS/cm; produced by SIEMENS UltraClear, Munich, Germany). To allow for a sufficient air pocket to form on top of the fluid, the autoclave was filled with only 820 mL of UPW. It should be noted that the use of UPW with CO_2 injection results in a more aggressive fluid compared to natural geothermal waters, due to the absence of dissolved $Ca_2{}^+$ and $HCO_3{}^-$, which would otherwise buffer calcite dissolution. This results in a time-lapse experiment of the same dynamics that are to be expected when using waters that more closely resemble actual local aquifer conditions.

The sample was fixed to the lid and submerged in the fluid using stainless steel wire, allowing it to be surrounded by water on all sides. We continuously added CO_2 to the autoclave through a stainless steel capillary to facilitate the undersaturation. After closing the autoclave and a pressure check, CO_2 was injected into the bottom of the autoclave and passed through the water for 5 min with the top autoclave valve still open. This removed all remaining air from the headspace before the top valves were closed and the autoclave was heated up, forming a pocket of CO_2 and water vapor in the autoclave's headspace. Finally, the headspace was connected to a CO_2-supply ($\geq$ 99.995 %, Linde) at a pressure of 5.9 bar via a backflow preventer. At a temperature of 80 °C and a recorded pressure of 5.9 bar inside the chamber, the partial pressure of CO_2, pCO2, was 5.5 bar.

The pressure and temperature in the reaction chamber of the autoclave were continuously monitored with a PTE7300 pressure sensor (Mouser, Germany) connected to a Raspberry Pi via I^2C-bus and the data output of the Buechi autoclave connected to the Raspberry Pi via RS232, respectively. The effective CO_2 partial pressure values

were calculated using PhreeqC and taking the vapor pressure of water into account. Before use, the autoclave was cleaned with distilled water and concentrated citric acid to remove possible carbonate precipitates. At the end of the treatment cycle, the pressure valves were opened to release the gas from the headspace. To avoid new crystal formation during the cooling process of the autoclave, all fluid was immediately drained at experiment temperature without prior cooling and captured in a clean vessel, where it was weighed and distributed for the following analysis steps (Sect. 2.7).

Optical microscopy

The preliminary analysis and an initial visual overview of potential mineral precipitation and dissolution were conducted via optical microscopic images of the artificial structures. The images were captured at 10x magnification using an Olympus BX-60 microscope paired with a monochromatic Teledyne DALSA M2420 (Ontario, Canada) camera (pixel size = 0.34×0.34 μm^2). The samples were securely mounted on a ThorLabs MTS50 (Newton, NJ, USA) 3D stage, enabling positioning with 0.05 μm resolution and 1.6 μm reproducibility. A custom python script was developed to automate the image acquisition process, capturing image stacks with a depth resolution of 0.02 mm. These image stacks were processed using the Picolay stacking software (Cypionka 2023), which generates mosaic tiles through focus stacking. The tiles were then assembled into comprehensive mosaics representing all the artificial structures, complete with color-coded depth maps. The resulting images provided the basis for optical comparison, facilitating assessments of the structures' size, shape, and color. In addition, they enabled visual evaluation of depth changes and surface roughness induced by the treatment cycles.

Raman microscopy

To determine mineral precipitation during the experiment, samples were analyzed after the treatment cycle at 10 evenly distributed points across the surface of the exposed area with Raman microscopy (XploRA PLUS, HORIBA, Horiba France SAS). A 100x objective (LM Plan FL N/NA=0.8) was used (wavelength: 532 nm; grating: 1200 (750 nm); filter: 10 %), and the resulting spectra were compared to the RRUFF (Lafuente et al. 2015) database.

Confocal laser scanning microscopy

The exposed surfaces of the hole and the cut were analyzed with a KEYENCE VK-X1050 Confocal Laser Scanning Microscope (Keyence Osaka, Japan) at LMU (Department of Earth and Environmental Sciences; Weller et al. (2024)). Images were taken in focus-variation mode, using a combination of coaxial and ring light for proper illumination, color, and contrast. The measurements were then repeated with confocal laser light to obtain volume, area, and surface roughness data. All measurements were performed in manual mode with automatic brightness detection for the laser. Resolution was set to 2048 × 1536 pixels at a field of view of 2.700 × 2.025 mm^2 and 0.675 × 0.506 mm^2 (at 5x and 20x magnification, respectively) to ensure high image and data quality. The resulting xy-resolution is $3 \cdot 10^{-4}$ mm, and the z-resolution is $4 \cdot 10^{-5}$ mm. The 5x magnification (aperture 0.13) lens was used for volume measurements, and the 20x magnification (aperture 0.46) lens was used for surface roughness. Several measurements of 5x and 20x

images were stitched together to measure a representative area of both the hole and the cut.

The generated 3D data was processed with the Analyzer program of the microscope (Keyence 2023). A reference plane was defined through four points selected on the coating around the hole and the cut for the 5x magnification measurements. Surface roughness was obtained by measuring a square and a circle with 0.5 mm in length/diameter. From these two measurements, the average and the standard deviation (SD) were calculated. The results were then compared with data obtained after correcting the surface curvature inside the two structures. Surface roughness is represented by the arithmetical mean height (Sa) as a function of area (A), and integrated height information for every pixel z(x, y) on the topography (Eq. 1).

$$\mathrm{Sa} = \frac{1}{A} \iint_{A} |z(x,y)| \mathrm{dxdy} \tag{1}$$

Volume and area measurements of the exposed artificial structures were performed with the Analyzer software by defining the height threshold at 0.025 mm depth beneath the reference plane (before applying the surface shape correction). The volumetric change was visualized, and CLSM topography data was exported to ASCII to compare results with those obtained from 3D micro-scanning to correlate changes in volume and roughness with both methods.

3D micro-scanning

To create a differential map, locate areas affected by strong dissolution, calculate volumetric changes to the rock matrix, and compare surface roughness within the artificial structures, 3D images of the rock samples at 10 μm point accuracy were taken before and after the experiment, using the fully automatic Artec Micro 3D micro-scanner (Artec 3D, Luxembourg) and the proprietary software Artec Studio Professional 16.

The default scan path for small and complex structures with a total of 42 single pictures was selected, and the brightness was adjusted so that the sample area was neither over- nor underexposed. After the first scan, the sample was rotated by 90° in the fixture, and the procedure was repeated. The resulting point clouds were cleaned from unintended surrounding information, and both compilations of pictures were merged via auto alignment, global registration, and sharp fusion (3D resolution of 0.05 mm). The generated mesh of the cube was covered with the recorded texture information ($16,384^2$ pixels) of both scans and then further processed in CloudCompare (version 2.12.4 Kyiv, EDF R&D, Paris, France). This measuring method reproduces the cube's surface area with an error of 0.06 % and the enclosed volume with an error of 0.01 %.

All scans before and after the experiment were directly compared to one another by finely registering them to a final overlap of at least 90 %, including scaling. This achieved better results than a theoretical overlap of 100 % as the surface changed in some areas (e.g., artificial fractures) between treatment cycles, where the scans do not and should not align. Subsequently, the nearest orthogonal difference of the point clouds is computed by the iterative-closest-point algorithm default settings after (Besl and McKay 1992). For every scan, the body volume enveloped by the mesh is calculated. The exact

volume loss at the prepared exposed surfaces was determined by the 2.5 D volume tool in the Cloud Compare software. Since overhangs were not represented correctly in the vertical projected distance between the point clouds before and after the experiment used for volume calculation, pre-processing of the point clouds was necessary: the point clouds were split into five sub-clouds along the walls. The four wall segments were aligned with the coordinate system, and artificial planes of points were added along the cutting planes to avoid points being projected to empty cells. The sub-volumes were calculated twice by projection in the x-direction, twice by projection in the y-direction, and once in the z-direction for the bottom part. The size of the unit cell for transferring distance values to volumetric values had a precision of 0.001 mm^2. Multiplied with the depth of these cells (precision of 0.01 mm) the cumulative volume of the cut and hole structure is calculated.

Textural information was mainly processed to determine the exposed surface interacting with the fluid during the autoclave treatment. To increase the accuracy of the surface boundaries, 1–10 million points were sampled on the mesh of the rough cut-out areas around the exposed surfaces. In some cases, the texture information was insufficient, so the mesh's topological information was used to identify exposed surfaces. The identified surface areas not coated by paint were then cut out and exported as an ASCII cloud file.

Using the software MeshLab (version 2023.12; Cignoni et al. 2008), the point clouds were meshed by the ball pivoting algorithm (Cignoni et al. 2008; Bernardini et al. 1999). Depending on the size of the surface to be generated and the point cloud density, the ball radii of the algorithm were between 0.01 and 0.1. If existent, minor holes in the generated mesh were filled with plane surfaces, and the geometric measures of the mesh were calculated. The size and topology of the cut, the hole, and the other minor exposed areas due to paint exfoliation vary strongly. Those three cases were analyzed individually for both scanned states.

To assess the surface structure along the artificial hole and cut, vertical sections through those structures were obtained by slicing the point cloud with a slice thickness of 0.01 mm. Both the cut and the hole were cut along a profile trace, where the structure's maximum depth was expected. Reducing the complex three-dimensional shapes to 2D profiles allows for a better description of overhangs and preferential dissolution patterns.

In addition, the surface roughness, given by the mean arithmetical height (Sa) of the hole structure, was determined for both states analogously. First, the hole was isolated from the cube's meshes and transformed to ASCII cloud (1×10^6 points each) in Cloud Compare. In MeshLab, the clouds were imported, and normals were computed using the default settings of the "compute normals for point sets" algorithm. For both, a medium surface was constructed that follows the structure's curvature but not the smaller-scale roughness with the "Screened Poisson" reconstruction tool. To achieve this, a reconstruction depth of 5 and a minimum number of samples of 10 were used for the pre-experiment state. For the post-experiment state, a reconstruction depth of 4 and a minimum number of samples of 15 were used. All other settings were kept at default. These surfaces were exported to Cloud Compare as an OBJ file, on which point clouds were sampled (1×10^6 points each) to compute the cloud-to-cloud distance between the

scan's surface and the constructed medium surface. The average value of the computed scalar field corresponds to the roughness Sa as described in Sect. 2.5.

Fluid analysis

At the beginning of the treatment cycle, the autoclave contained 820 mL of UPW. The post-cycle solution was weighed, and its pH and electric conductivity (EC) values were measured using the digital pH sensor PHEHT probe for ODEON and the digital conductivity sensor C4E for ODEON on a portable ODEON pH-Conductivity meter (Aqualabo, Champigny-sur-Marne, France), respectively, with automatic temperature correction to 25°C. The concentrations of cations and anions were quantified using ion chromatography (Dionex ICS-1100 Autosampler AS-AP, Thermo Fischer Scientific, Waltham, Mass., USA). Bicarbonate was quantified immediately via manual titration after the fluid extraction from the autoclave using 0.1N HCl and methyl orange (both from CarlRoth, Karlsruhe, Germany) as an indicator. All statistical analysis was performed using the software R (R Core Team 2020).

Results

Optical microscopy

While the surface alterations resulting from dissolution processes in the autoclave were already clearly visible to the naked eye without any instrumentation, optical microscopy images allowed for a semi-quantitative assessment. Figure 2 shows depth maps resulting from the focus stacking process before and after the experiment. The in-plane resolution is $0.34 \times 0.34\,\mu m^2$, and the vertical distance between images is 0.02 mm. The depth map is based on the z-steps of the microscopic stage with a virtual base plane. Green shades show deeper points in the sample, while the blue shades signify higher points in

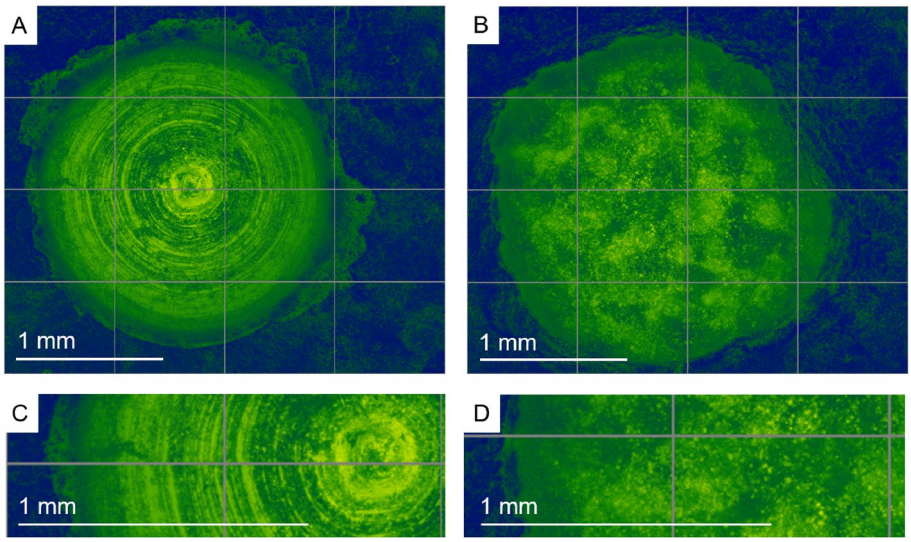

Fig. 2 Optical microscopy images are stacked and assembled into depth maps; color coding indicates the highest (blue) and lowest (green) topography (z values). The left column shows the hole before the autoclave exposition with C zooming into A and showing the scratch lines from the drill bit ($\Delta z = 1.02$ mm); the right column shows the hole after the autoclave exposition with D zooming into B, displaying a crystal structure instead of scratch lines ($\Delta z = 1.40$ mm)

the sample. The deepest point in the hole before exposure was 1.02 mm below the surface plane and 1.40 mm after the autoclave treatment.

Before the autoclave treatment, the hole and the cut displayed circular/linear scratch marks, respectively, caused by the drill bits. After the experiment, the depth in both disruptions increased uniformly, and the scratch marks vanished. The hole, which previously displayed angular walls and a pointed dip in the middle (mirroring the drill bit's shape), turned into an approximately sphere-shaped hole with a rough bottom, which was later confirmed by the 3D micro-scan (Fig. 5). Toward the edges of the hole and the cut, the walls became steeper. The observed dissolution patterns were not aligned with the scratch marks in either the hole or the cut. Instead, zooming into the microscopic images suggests that the post-experiment roughness followed individual crystals, with larger crystals standing out. Both disruptions showed changes in the topmost images, which extended slightly into the matrix and seemed to be enabled by the chipping of the protective coating.

CLSM results

The optical images taken with the CLSM (Fig. 7) complement those taken by the optical microscope. The depth resolution of 4×10^{-5} mm was sufficient to identify single calcite crystals sticking out at the bottom of the structures after exposure (Fig. 3). The size of the crystal cumulates was 0.1–0.15 mm, and they consisted of smaller (scalenohedral) crystals of mostly 0.01–0.05 mm in length and hyp-idiomorph to idiomorph habitus, respectively.

For the quantification of the surface roughness, surface shape corrections were necessary to avoid an overestimation caused by the change from, e.g., a spherical to cylindrical bottom of the hole. This affects smooth but shaped surfaces (i.e., the initial state

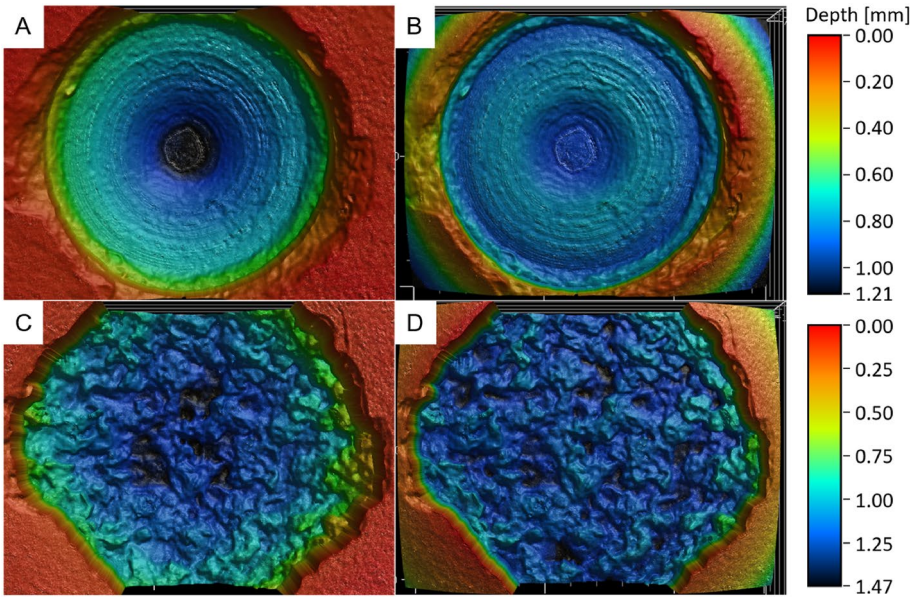

Fig. 3 Topographical change at the bottom of the drilled hole before (**a**, **c**) and after (**b**, **d**) the autoclave treatment. Changes in surface roughness became more visible after applying corrections to the surface curvature (B, D). Color coding indicates the highest (red) and lowest (black) topography

in our experiment). Without this correction, surface roughness in the hole increased moderately from 0.018 mm to 0.042 mm after exposure. With correction, there was a significantly higher increase from 0.007 mm to 0.042 mm. Surface roughness in the cut changed from 0.005 mm to 0.042 mm after corrections.

The visible surface was calculated to be 7.134 mm^2 before and 12.140 mm^2 after the autoclave treatment and 14.075 mm^2 before and 25.036 mm^2 after the treatment for the hole and the cut, respectively; this included surface roughness.

The acquired 3D-CLSM images supported the calculation of the volume of individual structures, taking the coated plane surface as a reference plane. The initial volume of the hole of the sample was 2.338 mm^3. After the autoclave treatment, this volume increased to 4.014 mm^3 (71.66 %). The cross-sectional area (CSA) increased from 4.054 to 4.502 mm^2 (11.05 %). Optical examination and the 3D micro-scanning images suggested that the dissolution might have crept beneath the coating, which could not be measured using orthophotos. Therefore, the hollow volume beneath the coating was extrapolated from the maximum depth (0.988–1.347 mm) of the hole as the radius of a half sphere. This results in an additional volumetric increase, which cannot be reproducibly quantified due to heterogeneous surface topography and unknown curvature of the disturbance.

3D-scanning

3D renderings of the sample before and after the autoclave treatment with a point accuracy of up to 10 µm are shown in Fig. 4, as well as the cloud-to-cloud distances between the initial cube surface and the surface after the autoclave treatment for the aligned data of the sample cube. This scalar field of orthogonal distance is displayed by a color scale ranging from blue (slight volume increase) via green and yellow to red (large volume decrease).

The flat surface of the sample cube showed a minimal increase in the z-direction of 0.12 mm compared to the reference (the cube showed a larger volume after treatment). This increase was extremely homogeneous, with only a few areas slightly protruding from the plane with very gentle slopes. Both the hole and the cut stood out with significant deepening of up to 0.48 mm in the features. The cut showed a deepening of 0.44 mm and the hole 0.41 mm. This deepening is the minimal distance between the point clouds before and after the experiment and is not to be confused with the change

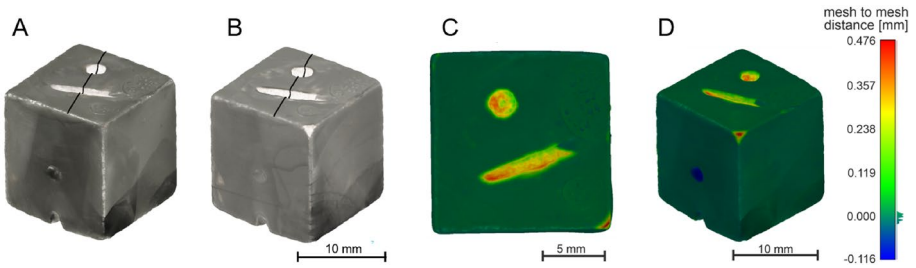

Fig. 4 3D renderings of the cube before (**a**) and after (**b**) the autoclave treatment. The black lines indicate the profile traces corresponding to Fig. 5. C, D Orthogonal mesh-to-mesh distances between the 3D scans before and after the autoclave treatment. The exposed areas show a retreat of the rock surface. In the paint-coated areas, only a slight variation is observed

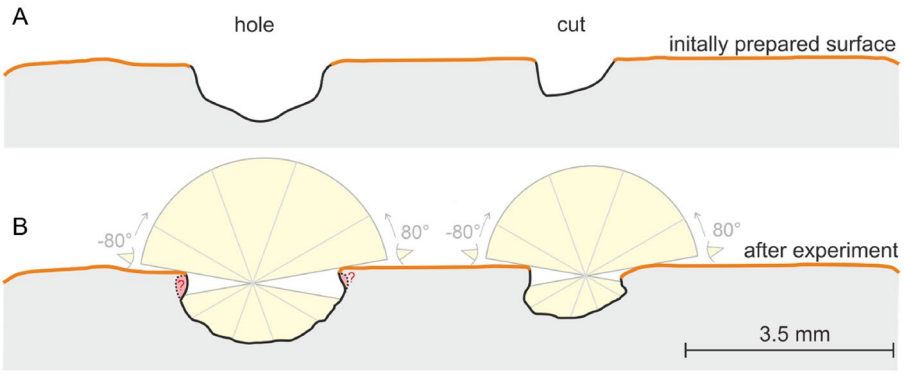

Fig. 5 Cross section of the sample at both features (Fig. 4) and the theoretical representation of the 3D micro-scanning image acquisition capability with the given feature opening and coating thickness (orange). (**a**) Cross sections before the autoclave treatment; (**b**) cross sections after the autoclave treatment

Table 1 Chemical, physical and structural results of parameters measured before and after the autoclave treatment.

Parameter	Before treatment	After treatment
pCO_2/bar	–	5.9
Water volume/L*	–	0.820
EC/μS/cm*	0.055	167
pH*	7.0	5.5
Sample mass/g	8.329	8.276
Exp. surface/mm^2	20.78	35.53
Volume/mm^3	3150.13	3149.10
Ca^{2+}/mg/L*	0.0	20.04
Ca^{2+}/mmol/L*	–	0.505
Ca^{2+}/mmol*	–	0.41
HCO_3^-/mg/L*	0.0	128
Depth, hole/mm (3D scan)	0.916	1.198
Depth, cut/mm (3D scan)	0.675	0.958

EC and pH values were corrected to 25°C. * parameters measured in the autoclave fluid. Unmarked parameters concern the sample cube itself

in z-direction. Here the depth of the cut increased from 0.675 mm to 0.958 mm and of the hole from 0.916 mm to 1.198 mm depth in z-direction. Volume loss was further detected near the corners and edges of the cube. Physical inspection showed that some of the coating had exfoliated and gave way to dissolution underneath.

Due to the multi-angle image acquisition of the 3D micro-scanner, data is available from overhanging and bridging structures to some extent. The depth behind the overhang is geometrically controlled by the opening of the structure and the angle at which the sample is scanned. Assuming a perfectly flat outer surface and a scanning angle deviating from the vertical (0°) with up to 80° and −80°, respectively, the shaded areas form small wedges that lead to interpolation of an arbitrary surface directly below the coating. From the 3D data, a cross section was constructed covering both the hole and the cut (Fig. 5). In addition to the deepening suggested by Fig. 4, both the hole and the cut also displayed effects of dissolution beneath the coating, which led to apparent overhangs at the cube's surface and a bulged

shape of the 2D section at the hole and the cut. In both structures, the shapes resembled an upside-down mushroom, being largely determined by the theoretical imaging capabilities (Fig. 5). Assuming the rock surface's shape continues in the shaded areas similarly up until directly underneath the coating, the additional volume loss not detected by the scanner can be computed. By measuring the cross-sectional area along two orthogonal profiles through the hole, the medium shaded area amounts to 0.036 mm^2. Multiplied with the circumferential distance of the hole (using r=1.24 mm), this area corresponds to an additional volume loss of 0.28 mm^3 (11.7 %). Since optical examination of the cut disturbance shows substantially less dissolution beneath the coating, an even lower error is expected here.

When comparing both entire cubes before and after the treatment, the 3D scans showed a volume difference of $-6.55\,mm^3$. This volume loss was attributed to the hole ($-2.39\,mm^3$), the cut ($-4.13\,mm^3$), chipped edges and corners ($-4.08\,mm^3$), and minor bubble formation under the coating ($+4.05\,mm^3$). The bubble formation during the autoclave treatment lowers the value of overall volume loss as the bubbles increase the post-experiment cube's volume.

The volume loss that took place precisely at the disturbances due to the dissolution of the uncoated rock matrix was 10.61 mm^3, translating to 0.028 g ($\varrho = 2.6\ mg/mm^3$). The surface available for this dissolution in the cut and hole structures was measured to be 20.78 mm^2 before the experiment. The resulting dissolved volume per initial surface ratio of the whole sample ($0.51\,mm^3/mm^2$) was slightly lower at the hole ($0.32\,mm^3/mm^2$) and at the cut structure ($0,32\,mm^3/mm^2$). The surface area of the exposed rock after the experiment increased to 35.53 mm^2 overall (18.46 mm^2 at the cut, 11.27 mm^2 at the hole and 5.8 mm^2 at the previously coated areas). The initially regular and smooth surface line increased during the autoclave treatment. The effect of the detectable resolution on the resulting roughness needs to be considered here. This method revealed an increase in the surface roughness from 0.0047 mm to 0.0168 mm.

The exposed area includes every exposed surface on the cube, determined by the 3D scans' texture information and optical examination (including occasional, very small areas, where the coat had chipped off).

Hydrochemical analysis

Table 1 shows the hydrochemical composition of the fluid in the autoclave after the treatment, which was used to assess the mass balance of the experiments. The bulk ion contents in the sample fluid consisted, as expected, of Ca^{2+} and $HCO_3{}^-$. The pH values measured shortly after each experiment show a slightly acidic value.

Table 1 further shows the mass loss and the mass balance based on the hydrochemical analyses. The cube lost 0.28 mmol Calcite. The mass loss based on the hydrochemical analyses is 0.41 mmol. (−11 %). The Raman scanning of the features did not reveal any newly formed crystals on or inside the features nor traces of minerals that were not already present in the original rock sample.

Discussion

Technical aspects

Our comparison of the three image acquisition methods, optical microscopy, CLSM, and 3D micro-scanning, resulted in an overview of their technical aspects and notes on usability (Table 2).

The theoretical depth resolution of optical microscopy depends on the resolution of the microscopic stage and the depth-of-field of the setup. Higher magnification leads to improved xyz-resolution, but it also results in longer scanning times as a trade-off. Furthermore, the precision of the depth measurement using focus stacking depends on the features of the sample. Highly heterogeneous samples with large contrast (e.g., a large number of clearly defined individual crystals) allow for a higher resolution compared to matrices with low image contrast (e.g., bulk micro crystals beyond optical resolution). The area in focus is positively correlated with the possible z-resolution: areas close to vertical edges are difficult to measure because of a very small area being captured by the focal plane. Correspondingly, completely vertical edges cannot be put into a depth context. Overhangs are shadowed due to the orthographic image acquisition and cannot be depicted. The insufficient depth resolution causes a blurred depth map when single crystals protrude. With a monochrome camera (Fig. 8), the optical microscopic images seem redundant to the depth maps. This might change in matrices with higher image contrast, e.g., granite.

CLSM inherently shares the limitations of optical microscopy with regard to the visualization and quantification of overhangs and vertical features. However, with 3D-image acquisition, the depth profiles are much more detailed than images resulting from

Table 2 Technical aspects of the assessed image acquisition methods at applied magnifications

Technical specification	Optical microscopy	3D micro-scanner	CLSM (20x Mag.)
xy resolution	0.34 x 0.34 μm^2	29 μm^2 x 29 μm^2	0.1 x 0.1 μm^2
z resolution	0.02 mm	29 μm^2	0.04 μm
Field of view	816 × 680 μm^2		924 × 693 μm
Initial acquisition cost	approx. USD 10,000	approx. USD 36,000	approx. USD 80,000
Sample preparation	Fixation to the stage using industrial putty (Hama Haftpast)	Fixation to the rotary stage using the included screws	no special sample preparation necessary
Data output format	.png	.obj, .ply, .wrl, .stl, .aop, .asc, .ptex, .e57, .xyzrgb, .step, .iges, .x_t, .csv, .dxf, .xml	.jpg, .tiff, .png, .xlx, .cag, .vk4, .vk6, ASCII
Multimodal capability	Limited multimodal capability; .png files as input for image stacking software	Very good multimodal capability. Data can be exported and edited in open source software such as CloudCompare	3D data and images need to be exported—otherwise limited to KEYENCE software
Time required per analysis	30–45 min per disturbance	40 min per sample (both disturbances)	1–2 min for hole, 5–10 min for cut
Usability	Very user-friendly, requiring minimal setup and training; intuitive controls for magnification, focus, and lighting. Image stacking and mosaic assembly depend on software.	Very user-friendly and intuitive image acquisition; time-consuming and sometimes complex/difficult data analysis through a combination of further software	Very user-friendly, requiring minimal setup and training; mostly automated; intuitive controls for magnification, focus, and lighting

focus-stacking (depending on the capabilities of the chosen stacking software, depth labels can be added to the stacked images). The color images provided by CLSM add significantly to the information content. For instance, the hypothesis that the chipping of the coating partially controls the development of the structure can be clearly verified through the CLSM images. The benefit of using CLSM is the reduction of noise via the application of a pinhole in front of the detector. The automated measurements, in combination with a high xy-resolution, allow for fast analyses with high image and data quality. By applying the laser, a spatial resolution of up to 5 nm can be achieved at the highest magnification, allowing precise characterization of various topographies (Fig. 6). A notable drawback of CLSM image acquisition lies in the vertically cut 3D data: the orthogonally positioned laser cannot view underneath any overhangs, which makes the dissolution effects under the coating overhangs inaccessible via this method (Fig. 6).

Out of the three examined methods presented here, 3D micro-scanning is the only one that records information from multiple scanning angles and, therefore, allows for a representation of areas that are shaded from the camera or the laser by other material. This can be seen in the concave spaces underneath the hole's edge in Fig. 6, where CLSM produces no data under the overhangs. While this is essential for describing the cube's total volume and the volume loss due to dissolution, it does not work for every 3D structure. The scanning path records in steps of turning the sample by 20°. The area beneath the sharp edges around the hole and cut could, therefore, not be captured entirely (Fig. 5). This leads to an underestimation of volume loss, especially at the hole structure that is not quantifiable using optical methods. This explains the difference in volumes calculated from hydrochemistry versus 3D micro-scanning: assuming 36,93 cm^3/mol, 41 mmol calcite translates to 15.14 mm^3 versus the measured 10.61 mm^3, respectively. In addition, the 3D micro-scanner's resolution neglects fine-scale morphology, which would add to the calculated volume. Assuming typical surface gradients, comparable to the visible parts of the surfaces, the expected error is negligible. Only tomographic analyses as carried out by Randi et al. (2014) could provide more precise information but require substantial additional resources. Furthermore, the scanning point accuracy

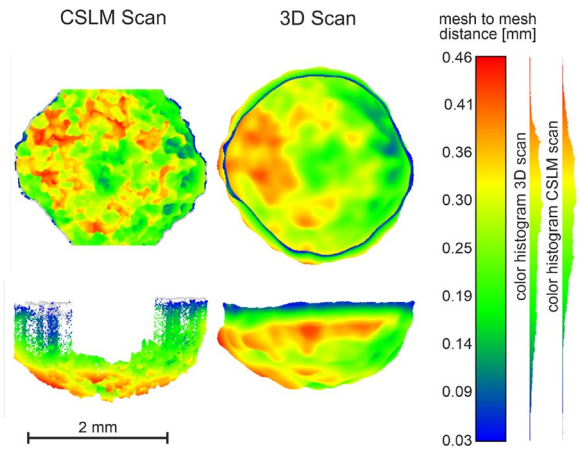

Fig. 6 Point cloud data of the hole structure recorded by CLSM (left column) and 3D micro-scanner (right column) in top and side view. Colors indicate the vertical distance of the initial surface compared to after autoclave treatment

of 10 μm is not as precise as that of other methods. This leads to a "smear-effect", where sharp edges are smoothed out, and some detailed structural information is lost.

The strengths of CLSM versus 3D micro-scans become apparent in Fig. 6. While the 3D scans produced information underneath overhangs, which is not feasible with optical microscopy or CLSM, the resolution of texture information was remarkably lower than the structural resolution (which is already lower than that of CLSM). Thus, information on crystal sizes and habitus is only available if the crystals stick out of the matrix. The texture information proved useful for determining the areas of the prepared cut and hole structure and the exfoliation of the coating. Using the Artec Studio Professional 16 software, scanning one sample is comparably fast, but the post-processing of the scanned point cloud using a combination of the open-source software CloudCompare and MeshLab, calculations of various surface areas, volumes, and roughnesses took several days.

Processes accessible with the described methods

This paper set out to assess the impacts of reinjecting cooled-off water at geothermal doublets on the structural integrity of the reservoir matrix. A widening and deepening of the artificially imposed disturbances, which would translate into a net enlargement of flow paths in the reservoir, became visible after the autoclave treatment, even to the naked eye. They were successfully quantified using the 3D micro-scanner thanks to its multi-angle image acquisition technique, allowing the scanner to peek underneath overhangs. Its relatively coarse spatial resolution (compared to optical and confocal laser scanning microscopy) did not impact the initial assessment of the widening of flow paths too heavily. In fact, its ability to peek beneath overhangs makes 3D micro-scanning a very good method for this purpose. However, the calculation of detailed dissolution kinetics requires information with a higher spatial resolution. Regarding surface roughness and matching the results of Ling et al. (2022), all three techniques showed a noticeable roughening of the exposed rock matrix surfaces due to dissolution processes forming micrometer-sized moldic pores, where calcite grains were dissolved. This leaves a surface characterized by preferential dissolution pathways, a development strongly visible in the images acquired by optical microscopy. This corroborates the findings of Wen et al. (2016) and Stober et al. (2023), who observed highly localized preferential dissolution regions, where calcite was abundant. In contrast to the 3D micro-scanner, the CLSM proved to be of superior usefulness in the quantification of surface roughness, given its high spatial resolution. Its inability to assess the surface underneath overhangs is to be noted. However, the surface roughness underneath these overhangs can only be assumed to be similar to the assessed roughness of accessible areas. The increasing surface roughness enhances the reactive surface area and must, therefore, be considered in kinetic calculations. Unlike microtomography (μCT) and despite their individual advantages, neither method is able to penetrate the rock sample. The effects of this shortcoming are small for rock matrices with little porosity and disconnected pores but significant for porous media with connected pores.

The composition of the solution in the autoclave served as an independent validation of the changes visualized with the three image acquisition methods. The general composition of the solution indicates a net dissolution at the sample surface, and the mass balance is closed. A slightly acidic pH value underlined that the reactions in the autoclave

were not at equilibrium yet. At the observed pH value, precipitation at the surfaces of the reaction chamber, which would have led to losses in the mass balance, can, thus, be ruled out.

The mass balance suggests that the calculation of volume losses based on the three methods is precise (CLSM) to conservative (3D micro-scanner). It has to be pointed out that the reactive surface of the samples was restricted to small features. Running the same experiments on samples without coating will likely fail to produce the same outcome as the volume changes are distributed across a large area and thus appear below the resolution of either method. Therefore, the development of an experimental setup by which all dissolution processes were confined to easily observable areas was critical to the successful evaluation of the three methods.

Potential for further studies

The development of overhangs, which are visible in the 3D micro-scans, is relevant to the general development of the flow channels in porous structures with dead-end pores. While pore surface roughness affects practically all natural stones and their permeability, reactive transport, and dispersion dynamics, surface roughness is still somewhat neglected in the study of multi-phase flow models (Mehmani et al. 2019). Higher fracture surface roughness could lead to slower water flow, increased eddies in the available water, and even capillary trapping (Mehmani et al. 2019). In contrast, smoother fractures facilitate unhindered water flow with less turbulence and a lower residence time in a given pore. The exact effects of pore surface roughness resulting from reinjecting cool water depend on various site- and reservoir-specific parameters, such as interfacial tension, contact angle, and viscosity ratios (Mehmani et al. 2019).

In addition to increasing surface roughness, the dissolution processes resulted in the hollowing out and, thereby, enlarging of the existing artificial structures. Similar effects were observed during alteration experiments carried out by Stober et al. (2023). The virtual sections of the 3D images show that not only micro-structures, like the drilling lines left over from the drilling process, are completely erased, but structures like the drill bit's angular profile are smoothed out until there is a relatively round, concave profile left (Fig. 5). The initial structure's profile is not only smoothed but deformed. The hollowing effect leads to the formation of an upside-down mushroom profile, hinting at the preferential dissolution pathways observed in the optical microscopy images. This dynamic can affect dissolution kinetics, as the development of "dead spaces" that are less easily reached by new, still undersaturated waters can trap the saturated fluid, slowing down further dissolution.

Assessment of applicability to geothermal reservoirs

The roughening of the pore surfaces causes a deceleration of water flow and an increase in highly localized eddies, which might lead to concentration- and diffusion-limited dissolution processes. This interpretation is supported by Dijk and Berkowitz (2002), who found that fracture aperture and fracture wall roughness significantly govern flow rates. Preferential dissolution of the rock matrix surrounding the artificial structure causing mushroom-shaped cavities can reinforce this dynamic (Dijk and Berkowitz 2002), which was also observed in the alteration experiments of Stober et al. (2023). In an extreme

case, the water at the inner-most end of this cavity is entirely saturated, which leads to concentration-limited diffusion until the saturated water can diffuse out of the cavity (Wen et al. 2016).

In contrast, when fracture walls are rather smooth, and the hollows are straight-walled or concave, the undersaturated water could reach the exposed fracture structure and, therefore, replace any slightly saturated fluid much more easily, creating rate-limited dissolution conditions. This was observed by Singurindy and Berkowitz (2005), who identified the residence time of the fluid in their column samples as a key parameter in determining reaction rates and, thus, the relative dominance of precipitation and dissolution mechanisms. In addition, Dijk and Berkowitz (2002) found fracture morphology, especially local apertures and wall roughness, to be the biggest factor determining flow patterns.

For geothermal reservoirs, quantification of these processes is vital for the assessment of long-term behavior. The longevity of heat mining heavily depends on a homogeneous exploitation of heat-in-place. Thus, preferential flow paths developing from the injection well and possibly leading to an early onset of thermal breakthrough are undesired.

Fracture surface roughness can play a critical role in mineral precipitation. Conducting flow-through experiments on Calcite material, Singurindy and Berkowitz (2005) observed enhanced gypsum precipitation on rougher fracture surfaces, leading to faster clogging of these fractures compared to smooth (polished) fractures. They found that the two most critical factors influencing mineral precipitation and, thus, hydraulic conductivity of fractures are fracture wall roughness and the chemical composition of the fluid (Singurindy and Berkowitz 2005). To mimic these conditions in our setup, the solution has to be changed from UPW to waters containing sulfate or to rock matrices containing more than traces of gypsum.

In providing access to morphological changes at surfaces exposed to undersaturated geothermal fluids, our workflow offers important insight into the long-term effects and evolution of fracture wall dissolution: assuming higher roughness and larger cavities in Calcite aquifers, they might experience a stronger oscillation between precipitation and dissolution, given an undersaturated, highly mineralized fluid.

Conclusion

At first glance, the autoclave setting seems disconnected from any real-world example. Using ultra-pure water at elevated CO_2 partial pressures and temperatures seems to contradict the conditions around the injection wells in carbonate rocks (lower temperature and partial pressure). The experimental conditions, however, nicely match the expected saturation state of the geothermal waters, and the elevated temperature enables time-lapse experiments.

With regard to our main research questions, we conclude that by focusing the dissolution processes on artificial disturbances and shielding the rest of the sample from acidic exposure by means of a 2K paint coat, the effects became more easily observable through a combination of optical microscopy, confocal laser scanning, and 3D micro-scanning. Optical microscopy, while the most affordable and user-friendly method, was unable to assess areas underneath overhangs. CLSM is limited in the same way. However, it provides very fine-scale information on surface roughness. 3D micro-scanning displayed the

coarsest xy-resolution but uniquely solved overhangs to a certain degree and was thus able to paint a more complete image of the changes in the artificial disturbances. Combining these methods allows for a holistic assessment of the widening of flow paths, as well as changes in surface roughness and morphology on various scales. Our experimental results can be transferred to actual reservoirs and provide information on the temporal development of the surface area and roughness, which has to be included to make the transition from equilibrium (Baumann et al. 2017) and kinetic (Ueckert and Baumann 2019) hydrogeochemical models to combined reactive flow models with changing geometry of the flow paths.

Appendix Additional microscopy images

See Figs. 7 and 8

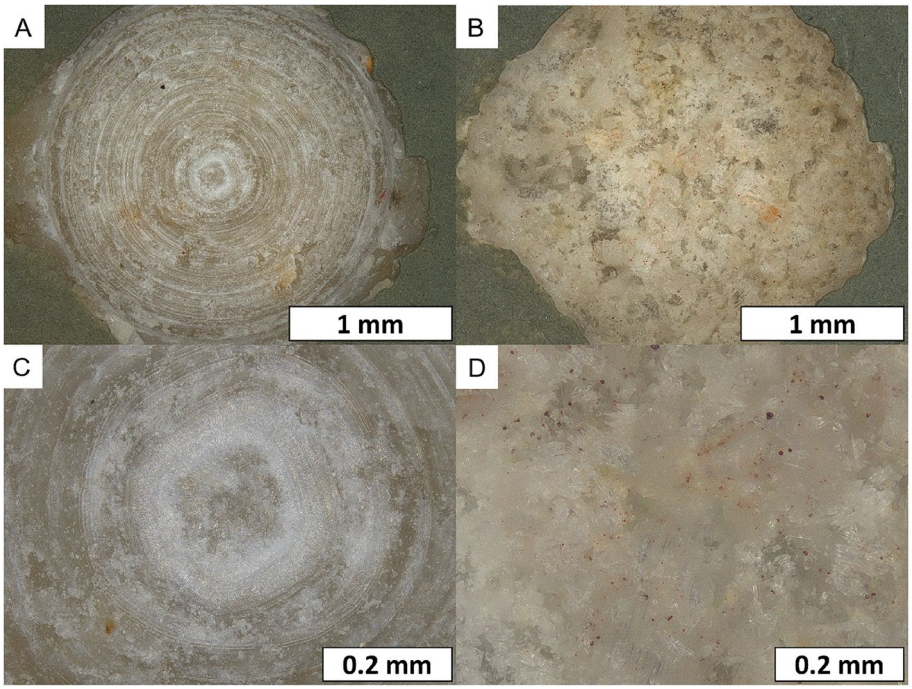

Fig. 7 Optical microscopy images of the hole as acquired through CLSM

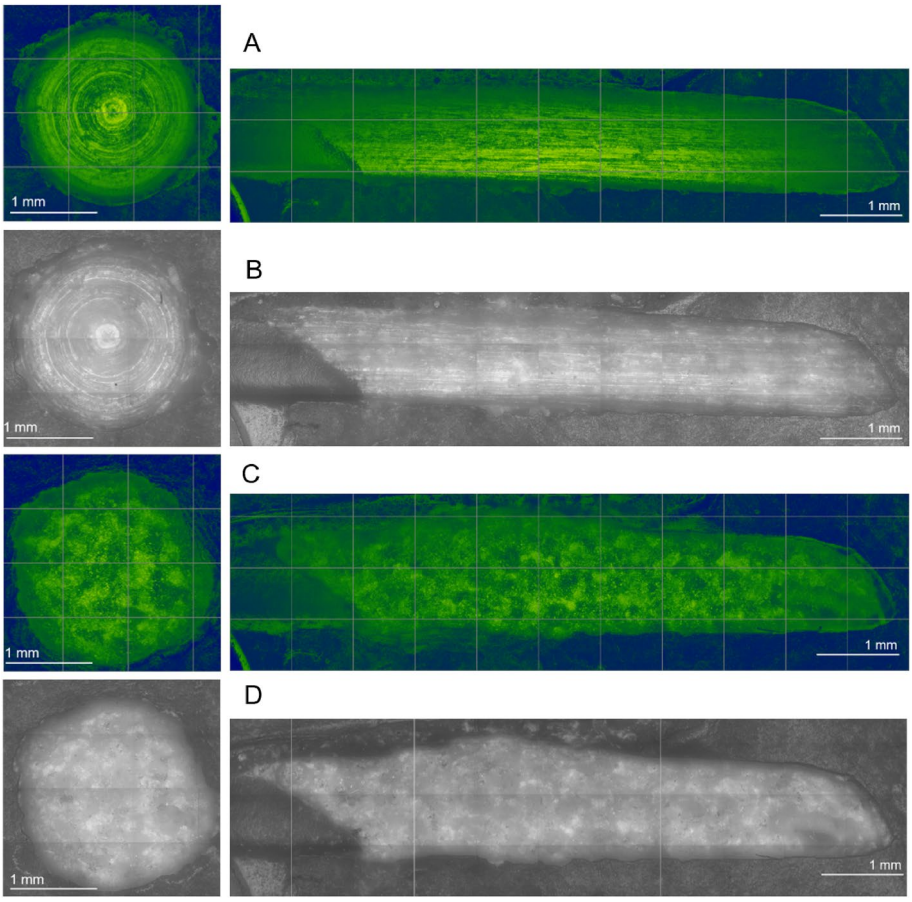

Fig. 8 Stacked optical microscopy images and depth images of the hole and the line as acquired through optical microscopy and image stacking. The colour indicates sample morphology, with shades of green indicating lower z values and shades of blue indicating higher z values. The image show the disappearance of the linear/circular drill bit scratch lines in the rock matrix due to dissolution processes

Supplementary Information

The online version contains supplementary material available at https://doi.org/10.1186/s40517-025-00355-4.

Additional file

Supplementary file 1.

Supplementary file 2.

Supplementary file 3.

Acknowledgements
The authors would like to thank the laboratory assistant Sophia Bachmayer, the laboratory technician Jaroslava Obel, and Marlis Hegels for their help in the laboratory. Lena Able contributed to the 3D micro-scanning methodology and Peter Obermeier conducted the initial training with the 3D micro-scanner.

Author Contributions
Thomas Baumann conceived the presented idea and acquired funding, verified the analytical methods, and supervised the findings of this work. Annette Dietmaier and Justin Mattheis contributed equally to the writing of the first draft. Annette Dietmaier prepared the samples, designed and performed the autoclave experiments, performed optical microscopy and 3D scans, evaluated the results, and coordinated author meetings. Justin Mattheis performed 3D scans, assisted with the optical microscopy image acquisition and autoclave setup, and analyzed and interpreted the 3D data. Daniel Weller performed the CLSM data acquisition, analysis, and interpretation. Ingrid Stober supervised the study and contributed significantly to the discussion and introduction based on her previous works on this subject. Michael

Drews initiated the application of 3D micro-scanning for this purpose and provided support during the evaluation of the results. All authors discussed the results and contributed to the final manuscript.

Funding
Open Access funding enabled and organized by Projekt DEAL.

Data Availability
The data sets used and/or analyzed during the current study are available from the corresponding author on reasonable request.

Declarations

Ethics approval and consent to participate
Not applicable.

Consent for publication
Not applicable.

Competing interests
The authors declare that they have no Competing interests.

Received: 28 January 2025 Accepted: 2 June 2025
Published online: 12 July 2025

References

August D, Byram I, Forrestal D, Desselle M, Stevenson N, Iyer K, Davies MW, White K, Cobbald L, Chapple L, McGrory K, McLean M, Hall S, Schoenmaker B, Clement J, Lai MM. Assessing the feasibility of handheld scanning technologies in neonatal intensive care: trueness, acceptability, and suitability for personalised medical devices. Aust Crit Care Off J Conf Aust Crit Care Nurses. 2024. https://doi.org/10.1016/j.aucc.2024.09.012.

Baumann T, Bartels J, Lafogler M, Wenderoth F. Assessment of heat mining and hydrogeochemical reactions with data from a former geothermal injection well in the Malm Aquifer, Bavarian Molasse Basin, Germany. Geothermics. 2017;66:50–60. https://doi.org/10.1016/j.geothermics.2016.11.008.

BayStMWI: Bayerischer Geothermieatlas, 2012;1–96.

Bernardini F, Mittleman J, Rushmeier H, Silva C, Taubin G. The ball-pivoting algorithm for surface reconstruction. IEEE Trans Vis Comput Graph. 1999;5(4):349–59. https://doi.org/10.1109/2945.817351.

Besl PJ, McKay ND. A method for registration of 3-D shapes. IEEE Trans Patt Anal Mach Intell. 1992;14(2):239–56. https://doi.org/10.1109/34.121791.

Cignoni P, Callieri M, Corsini M, Dellepiane M, Ganovelli F, Ranzuglia G. MeshLab: an Open-Source Mesh Processing Tool. 2008. https://doi.org/10.2312/LocalChapterEvents/ItalChap/ItalianChapConf2008/129-136.

Costello LF, McMenamin PG, Quayle MR, Bertram JF, Adams JW. Applying 3d surface scanning technology to create photorealistic three-dimensional printed replicas of human anatomy. Future Sci OA. 2024;10(1):2381956. https://doi.org/10.1080/20565623.2024.2381956.

Cypionka H. Picolay. 2023. www.picolay.de

Davidson MW, Lofgren GE. Photomicrography in the geological sciences. J Geol Edu. 1991;39(5):403–18.

Demirel M, Diken Trksayar AA, Donmez MB, Yilmaz B. Effect of 3d printing technology and print orientation on the trueness of additively manufactured definitive casts with different tooth preparations. J Dent. 2024;148: 105244. https://doi.org/10.1016/j.jdent.2024.105244.

Diara F. Structured-light scanning and metrological analysis for archaeology: quality assessment of artec 3d solutions for cuneiform tablets. Heritage. 2023;6(9):6016–34. https://doi.org/10.3390/heritage6090317.

Dijk PE, Berkowitz B. Measurement and analysis of dissolution patterns in rock fractures. Water Resour Res. 2002;38(2):5.

Drüppel K, Stober I, Grimmer JC, Mertz-Kraus R. Experimental alteration of granitic rocks: Implications for the evolution of geothermal brines in the Upper Rhine Graben. Germany Geothermics. 2020;88(May): 101903. https://doi.org/10.1016/j.geothermics.2020.101903.

Erharter GH, Kieffer DS, Prager C. Uav-based discontinuity analyses and rock fall source mapping in alpine terrain (pletzachkogel/tyrol/austria). In: Shakoor, A. (ed.) IAEG/AEG Annual Meeting Proceedings, San Francisco, California vol. 1, 2018. p. 317–323. Springer, Cham. 2018. https://doi.org/10.1007/978-3-319-93124-1_39.

Falcucci A. Microstone: exploring the capabilities of the artec micro in scanning stone tools, v1. 2022. https://doi.org/10.17504/protocols.io.81wgb6781lpk/v1.

Francioni M, Simone M, Stead D, Sciarra N, Mataloni G, Calamita F. A new fast and low-cost photogrammetry method for the engineering characterization of rock slopes. Remote Sens. 2019;11(11):1267. https://doi.org/10.3390/rs11111267.

Fredrich J, Menéndez B, Wong T-F. Imaging the pore structure of geomaterials. Science. 1995;268(5208):276–9.

Gaich A, Pötsch M. 3d images for digital tunnel face documentation at tbm headings-application at koralmtunnel lot kat2/3d-bilder zur digitalen ortsbrustdokumentation bei tbm-vortrieben-anwendung beim koralmtunnel baulos kat2. Geomech Tunnell. 2016;9(3):210–21. https://doi.org/10.1002/geot.201600018.

Garcia-Luna R, Senent S, Jimenez R. Applications of the structure from motion photogrammetric technique to solve geotechnical problems at different scales to solve geotechnical problems at different scales. IN: 15th ISRM Congress 2023 and 72nd Geomechanics Colloquium. 2023;965–970.

Göldner D, Karakostis FA, Falcucci A. Practical and technical aspects for the 3d scanning of lithic artefacts using micro-computed tomography techniques and laser light scanners for subsequent geometric morphometric analysis. Introducing the styrostone protocol. PLoS ONE. 2022;17: e0267163.
Gribble CD. Optical Mineralogy: principles and Practice. Berlin: Springer; 2012.
Imaging B. 2024 MRI MACHINE PRICE GUIDE. 2025. https://www.blockimaging.com/bid/92623/mri-machine-cost-and-price-guide
Jensen LRD, Friis H, Fundal H, Mller P, Jespersen M. Analysis of limestone micromechanical properties by optical microscopy. Eng Geol. 2010;110(3):43–50. https://doi.org/10.1016/j.enggeo.2009.10.004.
Kersten TP, Lindstaedt M, Starosta D. Comparative geometrical accuracy invesitigations of hand-held 3d scanning systems—an update. Int Arch Photogramm Remote Sens Spat Inf Sci XLII-2. 2018. https://doi.org/10.5194/isprs-archives-XLII-2-487-2018.
Keyence: keyence Analyzer. 2023. https://www.keyence.com/
Koban KC, Perko P, Etzel L, Li Z, Schenck TL, Giunta RE. Validation of two handheld devices against a non-portable three-dimensional surface scanner and assessment of potential use for intraoperative facial imaging. J Plast Reconstruct Aesthet Surg JPRAS. 2020;73(1):141–8. https://doi.org/10.1016/j.bjps.2019.07.008.
Köhl B, Elsner M, Baumann T. Hydrochemical and operational parameters driving carbonate scale kinetics at geothermal facilities in the Bavarian Molasse Basin. Geotherm Energy. 2020. https://doi.org/10.1186/s40517-020-00180-x.
Lafuente B, Downs RT, Yang H, Stone N. The power of databases: the rruff project. In: Armbruster T, Danisi RM, editors. Highlights in Mineralogical Crystallography. Berlin: W. De Gruyter; 2015. p. 1–30 (https://rruff.info).
Laurich B, Urai JL, Desbois G, Vollmer C, Nussbaum C. Microstructural evolution of an incipient fault zone in opalinus clay: insights from an optical and electron microscopic study of ion-beam polished samples from the main fault in the mt-terri underground research laboratory. J Struct Geol. 2014;67:107–28.
Limones A, Akmak G, Fonseca M, Roccuzzo A, Cobo-Vzquez C, Gmez-Polo M, Molinero-Mourelle P. Impact of scanning interruptions on accuracy of implant-supported full-arch scans: an in-vitro pilot study. J Dent. 2025;153: 105503. https://doi.org/10.1016/j.jdent.2024.105503.
Ling B, Sodwatana M, Kohli A, Ross CM, Jew A, Kovscek AR, Battiato I. Probing multiscale dissolution dynamics in natural rocks through microfluidics and compositional analysis. PNAS. 2022;119(32):1–9. https://doi.org/10.1073/pnas.2122520119/-/DCSupplemental.Published.
Lohbauer U, Müller FA, Petschelt A. Influence of surface roughness on mechanical strength of resin composite versus glass ceramic materials. Dental Mater. 2008;24(2):250–6.
Lu J, Kharaka YK, Thordsen JJ, Horita J, Karamalidis A, Griffith C, Hakala JA, Ambats G, Cole DR, Phelps TJ, Manning MA, Cook PJ, Hovorka SD. CO2-rock-brine interactions in Lower Tuscaloosa Formation at Cranfield CO2 sequestration site, Mississippi, USA. Chem Geol. 2012;291:269–77. https://doi.org/10.1016/j.chemgeo.2011.10.020.
Lu J, Nicot J-P, Micker PJ, Ribeiro LH, Darvari R. Alteration of Bakken reservoir rock during CO2-based fracturing—an autoclave reaction experiment. J Unconv Oil Gas Resour. 2016;14(2016):72–85.
Ma SM, Singer G, Chen S, Eid M. Objective-driven solid-surface-roughness characterization for enhanced nuclear-magnetic-resonance petrophysics. SPE J. 2021;26(05):2860–79.
Mehmani A, Kelly S, Torres-Verdín C, Balhoff M. Capillary Trapping Following Imbibition in Porous Media: microfluidic Quantification of the Impact of Pore-Scale Surface Roughness. Water Resour Res. 2019;55(11):9905–25. https://doi.org/10.1029/2019WR025170.
Menéndez B, David C, Nistal AM. Confocal scanning laser microscopy applied to the study of pore and crack networks in rocks. Comput Geosci. 2001;27(9):1101–9.
Mraz E, Bohnsack D, Stockinger G, Käsling H, Zosseder K, Thuro K. Die bedeutung von analogaufschlüssen des oberjura für die interpretation der lithologie der geothermalen tiefbohrung geretsried. Jber Mitt Oberrhein Geol Ver. 2018;100:517–48.
Niebuhr B, Pürner T. Plattenkalk und frankendolomit? lithostratigraphie der weißjura?gruppe der frankenalb (außeralpiner oberjura, bayern). Schriftenreihe der Deutschen Gesellschaft für Geowissenschaften. 2014;83:5–72. https://doi.org/10.1127/sdgg/83/2014/5.
Peng F, Lin SC, Guo J, Wang H, Gao X. The application of sfm photogrammetry software for extracting artifact provenience from palaeolithic excavation surfaces. J Field Archaeol. 2017;42(4):326–36.
Petford N, Davidson G, Miller J. Pore structure determination using confocal scanning laser microscopy. Phys Chem Earth Part A Solid Earth Geodesy. 1999;24(7):563–7.
Pless JC, McCaffrey KJW, Jones RR, Holdsworth RE, Conway A, Krabbendam M. 3d characterization of fracture systems using terrestrial laser scanning: an example from the lewisian basement of nw scotland. Geol Soc London Spec Publ. 2015;421(1):125–41. https://doi.org/10.1144/SP421.14.
R Core Team. R: a language and environment for statistical computing. R Foundation for Statistical Computing, Vienna. 2020. https://www.r-project.org/
Randi A, Sterpenich J, Morlot C, Pironon J, Kervévan C, Beddelem MH, Fléhoc C. CO2-DISSOLVED: a novel concept coupling geological storage of dissolved CO2 and geothermal heat recovery-Part 3: design of the MIRAGES-2 experimental device dedicated to the study of the geochemical water-rock interactions triggered by CO2 laden brine i. Energy Procedia. 2014;63:4536–47. https://doi.org/10.1016/j.egypro.2014.11.487.
Rechberger C. Deep-seated rock slides in foliated metamorphic rock masses: characterising, monitoring, and modelling. Dissertation, BOKU Wien, Wien. 2022.
Rivera Diaz A, Kaya E, Zarrouk SJ. Reinjection in geothermal fields—a worldwide review update. Renew Sustain Energy Rev. 2016;53:105–62. https://doi.org/10.1016/j.rser.2015.07.151.
Schmidt RB, Bucher K, Drüppel K, Stober I. Experimental interaction of hydrothermal Na-Cl solution with fracture surfaces of geothermal reservoir sandstone of the Upper Rhine Graben. Appl Geochem. 2017;81:36–52. https://doi.org/10.1016/j.apgeochem.2017.03.010.
Schmidt RB, Bucher K, Stober I. Experiments on granite alteration under geothermal reservoir conditions and the initiation of fracture evolution. Eur J Mineral. 2018;30(5):899–916. https://doi.org/10.1127/ejm/2018/0030-2771.

Schmidt RB, Göttlicher J, Stober I. Experiments on sandstone alteration under geothermal reservoir conditions and the formation of zeolites. Eur J Mineral. 2019;31(5–6):929–44. https://doi.org/10.1127/ejm/2019/0031-2870.
Singer G, Ma SM, Chen S, Eid M. 2d surface roughness quantification for enhanced petrophysical applications. SPE J. 2023;28(03):1117–34.
Singurindy O, Berkowitz B. The role of fractures on coupled dissolution and precipitation patterns in carbonate rocks. Adv Water Resour. 2005;28(5):507–21. https://doi.org/10.1016/j.advwatres.2005.01.002.
Sonat: Solnhofener Naturstein. 2024. https://www.sonat.de/de/select/solnhofener-naturstein/
Stober I, Bucher K. Geothermal Energy-from House Heating Applications to Electrical Power Production. 2nd ed. Heidelberg: Springer; 2022. p. 390.
Stober I, Grimmer J, Kraml M. The Muschelkalk aquifer of the Molasse basin in SW-Germany: implications on the origin and development of highly saline lithium-rich brines in calcareous hydrothermal reservoirs. Geotherm Energy. 2023. https://doi.org/10.1186/s40517-023-00270-6.
Stober I, Kohl T, Schmidt R, Egert R. Verbundvorhaben "GeoFaces": Charakterisierung geothermischer Ressourcen unter Berücksichtigung von Grenz- und Trennflächen, Teilvorhaben "Systematische Untersuchung von Fluidwegsamkeiten im Bereich von Trennflächen in Süd-Deutschland." Technical report, Bundesministerium für Wirtschaft und Energie (BMWi) Projektträger Jülich (PtJ-EEN): Final report; 2018.
Su Y, Yang F, Wang B, Jia Z, Duan Z. Reinjection of cooled water into sandstone geothermal reservoirs in China: a review. Geosci J. 2018;22(1):199–207. https://doi.org/10.1007/s12303-017-0019-3.
Sun Y, Aman M, Espinoza DN. Assessment of mechanical rock alteration caused by CO2-water mixtures using indentation and scratch experiments. Int J Greenh Gas Control. 2016;45:9–17. https://doi.org/10.1016/j.ijggc.2015.11.021.
Ueckert M, Baumann T. Hydrochemical aspects of high-temperature aquifer storage in carbonaceous aquifers: evaluation of a field study. Geotherm Energy. 2019. https://doi.org/10.1186/s40517-019-0120-0.
Weller D, Colombier M, Cáceres F, Vasseur J, Dingwell DB, Scheu B. Confocal scanning laser microscopic (cslm) characterization of volcanic rocks. J Volcanol Geotherm Res. 2024;446: 107992.
Wen H, Li L, Crandall D, Hakala A. Where Lower Calcite Abundance Creates More Alteration: enhanced Rock Matrix Diffusivity Induced by Preferential Dissolution. Energy Fuels. 2016. https://doi.org/10.1021/acs.energyfuels.5b02932.
Yang J, Tao Y, Gao Y, Wang L, Kang B. Experimental study on the waterrock interaction mechanism in a groundwater heat pump reinjection process. J Water Clim Chang. 2022;13(3):1516–33. https://doi.org/10.2166/wcc.2022.393.
Zacherl L, Baumann T. Quantification of the effect of gaswaterequilibria on carbonate precipitation. Geotherm Energy. 2023. https://doi.org/10.1186/s40517-023-00256-4.

Publisher's Note

7 Discussion: Charting a Course for Sustainable Geothermal Systems

7.1 Synthesis of Key Research Findings

This dissertation took a holistic approach to assess how geothermal aquifers can be exploited in a sustainable manner. The three publications follow the path of geothermal water from the production site and beyond (chapter 4), through the above-ground heat exchanger and data available at the wellhead (chapter 5), down to the injection site where reintroducing the undersaturated cooled-off water causes dissolution processes in the rock matrix (chapter 6; Fig. 7.1).

The workflow introduced in [24] (Fig. 7.1 (1)) established a method for assessing whether a geothermal well operates sustainably based on its unique hydrochemical signature and historical data. A statistical analysis of yearly hydrochemical records from deep groundwater wells in Lower Bavaria and Upper Austria, including parameters such as ionic composition, pH, EC, temperature, and production volumes, resulted in the definition of two site-specific corridors: the natural corridor (NC), reflecting the expected variation under sustainable conditions, and the action corridor (AC), signaling potentially unsustainable use. The method accounted for individual well characteristics, particularly stratigraphy and inflow dynamics, which were categorized into three inflow types: a) no additional inflow, b) natural inflow from adjacent layers, and c) inflow from otherwise separated layers due to a technical connection (Fig. 1). Since hydrochemical composition and fluctuations are directly influenced by these factors, they were at the heart of the workflow's design. Beyond providing a quantifiable definition of sustainable hydrochemical variation, the method also functioned as an early warning system, allowing for intervention after five yearly data points and before severe and costly damage to the aquifer or geothermal infrastructure occurs.

Building on this, [25] examined whether standard annual sampling sufficiently captures short-term hydrochemical fluctuations by comparing it to high-resolution online data from two deep groundwater wells: one with a net discharge and one with reinjection (Fig. 7.1 (2)). The analysis revealed that the variation in online EC measurements was approximately four times greater than what was observed in annual data. Furthermore, discrepancies emerged between the two datasets regarding mean values and trend detection. Seasonal cycles were evident in the high-resolution data, with EC peaking in late spring and reaching their lowest values in early autumn, a pattern entirely neglected by the yearly measurements. These findings demonstrated that an annual sampling approach is inadequate for representing sub-seasonal hydrochemical variability; therefore, the study concluded with a statistically supported recommendation to increase sampling frequency to at least three times per year, providing a more accurate representation of the aquifer's actual stress state.

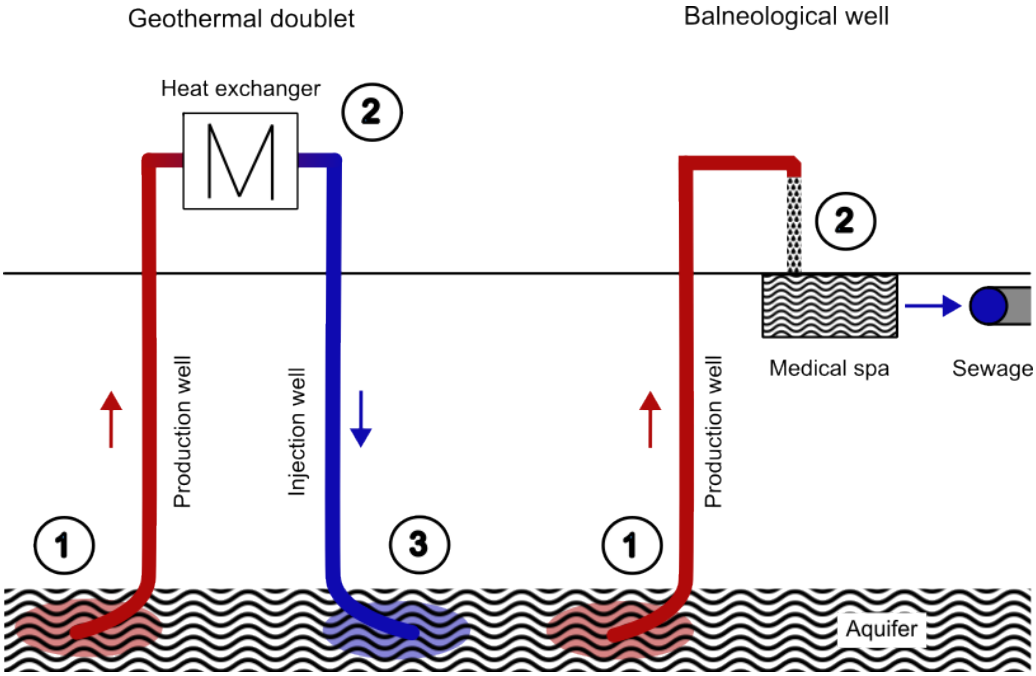

Figure 7.1 Logical and spatial links between the three publications presented in this thesis. Following the path of the water from the aquifer (first publication) through the production well up to the heat exchanger or wellhead (second publication) and back into the aquifer (third publication).

The final study [26] shifted its focus to the reinjection process, where the undersaturated geothermal fluid interacts with the aquifer rock matrix (Fig. 7.1 (3)). The study evaluated three imaging techniques (optical microscopy, CLSM, and 3D micro-scanning) regarding their ability to quantify and visualize pore-scale dissolution effects driven by pH shifts in the reinjected fluid. To isolate and intensify dissolution effects, a novel sample preparation method was developed: limestone samples were coated with a water- and heat-resistant lacquer, leaving only two artificial disturbances exposed to dissolution. The samples were then subjected to controlled CO_2 partial pressure and temperature conditions in an autoclave to simulate time-lapse aquifer conditions. All three imaging techniques confirmed the widening and geometric deformation of the artificial disturbances, as well as a marked increase in surface roughness, highlighting the impact of reinjection-induced dissolution processes.

7.2 Methodological Evaluation and Limitations

7.2.1 Challenges in Defining Sustainable Operation Ranges for Individual Deep Groundwater Wells

In the context of this thesis, a report was written in collaboration with the LfU to develop a basis for future national guidelines to identify a given well's individual baseline variation range, a.k.a. its natural hydrochemical fingerprint. The state-of-the-art approach of arbitrarily set values regarding allowed fluctuation ranges [22] has been proven to overlook glaring breaches of what "seems normal" to someone looking at multi-annual data with common sense. This was the case in Bad Füssing TH-1, where the well operator noticed stark changes in the well's hydrochemical signature, which had not triggered any response be-

cause the variation had not yet exceeded the threshold allowed by current regulations. Still, it was obvious that something was not right.

To offer a less arbitrary and instead a statistically reliable and reproducible approach to the question of what hydrochemical fluctuation range is “normal”, i.e., characteristic for a given well, and thus determine its baseline sustainable operation range, two clustering algorithms (DIANA and k-means) were applied to the annual hydrochemical data of two deep geothermal wells (Bad Füssing TH-1 and Bad Birnbach T-3). Both methods produced groups of data points that had been clustered on the basis of multiple parameters (main ions) and used these to determine the sustainable fluctuation range based on the largest cluster. The identified corridors were consistent between the two clustering algorithms. When considering additional wells in the NAFB, the congruence (agreement of the identified corridors) varied between 77 and 100 % (with the significance of the congruence dependent on the number of samples n). A causal relation between the number of available samples and the congruence was not identified (Table 7.1).

Table 7.1 Congruence of baseline variation clusters detected by DIANA and k-means at the eight assessed wells in the NAFB.

Well name	Number of yearly samples	Congruence, %
Bad Birnbach T-3	28	96
Bad Füssing Therme 1	26	89
Simbach Braunau TH-2	16	100
Straubing TH-1	26	77
Altheim TH-1	11	64
Bad Schallerbach TH-1	5	100
Haag TH-1	5	100
St. Martin TH-1	9	100

The high level of congruence is significant as these two algorithms cover both ends of the clustering algorithm spectrum (bottom-up vs. top-down, unconditioned vs. preconditioned). DIANA splits the data set into smaller and smaller clusters depending on their dissimilarities, eventually producing a dendrogram ending in clusters containing one data point each. The dissimilarity is based on the vertical distance between two clusters [60]. The number of clusters results from the *height* value at which the user determines to make the cut of the dendrogram’s branches. For example, in Fig. 7.2, when using 15 data points, three groups are determined at a vertical height of approximately 50. In contrast, k-means groups the dataset into clusters to achieve maximum similarity within each cluster. This is done in steps in which the centers of a predetermined number of clusters are moved around iteratively to find the placements with the smallest clustering error [61]. The number of clusters must be provided by the user beforehand.

This comparison shows that, based on the congruence of two vastly different clustering algorithms, the resulting clusters can be deemed reliable and reproducible. In addition, the presented workflow functions as an early warning system, which goes far beyond the capabilities of current regulations. Starting at a minimum of five annual samples, the workflow succeeded in defining the irregularity that was observed in

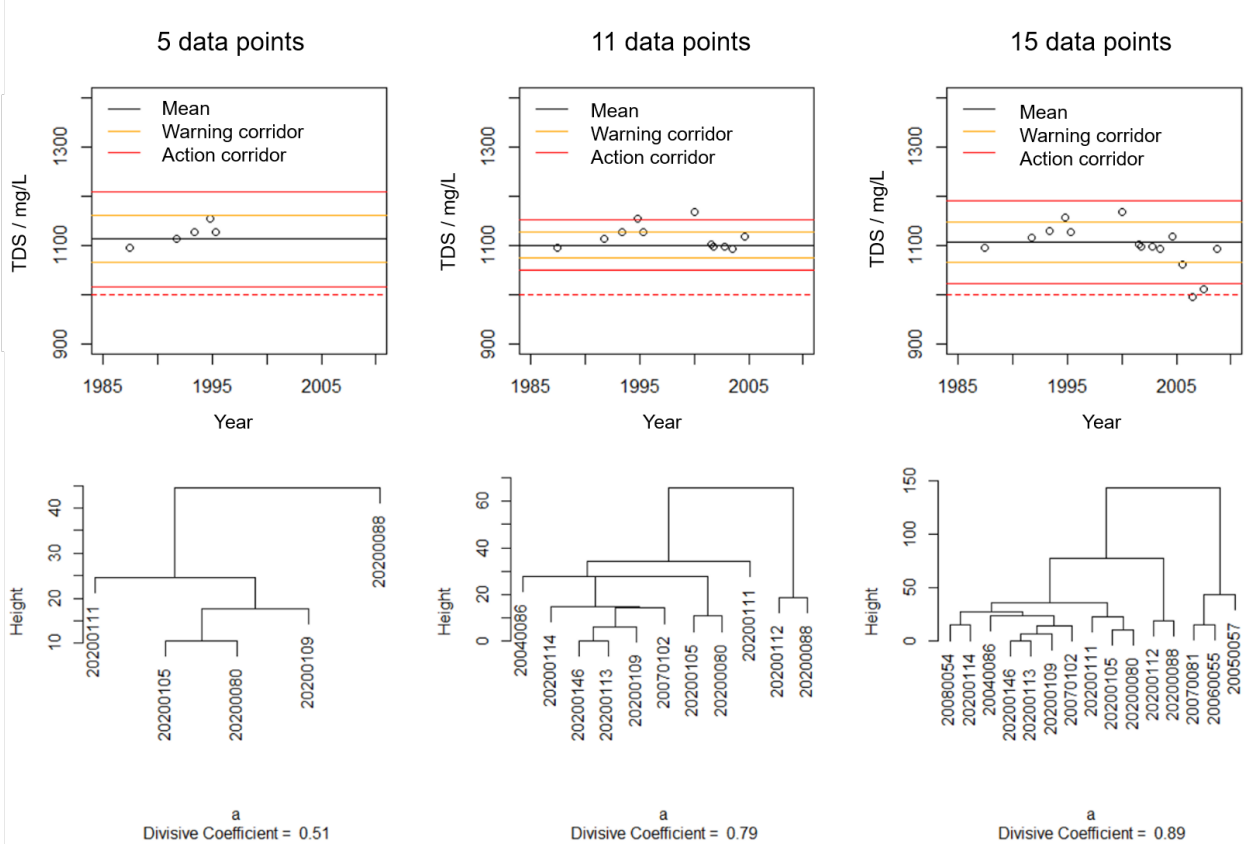

Figure 7.2 The increase in available sampling points from 5 to 10 to 15 continuously fine-tunes the determined corridor.

the data in Bad Füssing TH-1 (Fig. 7.2). Thus, we concluded that four to five years of yearly samples are sufficient to represent a well's inherent character and to determine its sustainable operational state, with every additional data point further fine-tuning the clusters and, thereby, the natural fluctuation range corridor. However, the most notable advantage of the proposed workflow compared to established sampling protocols such as the DQS [22] is that it is sensitive to minor yet uncharacteristic fluctuations in singular ions, TDS or EC, which occur within the arbitrarily allowed thresholds of current regulations, but indicate unsustainable well exploitation practices. These will no longer go unnoticed in the proposed workflow and can instead be utilized as indicators for an immediate and detailed reassessment of the current production strategy.

Some limitations apply to this method. The assessment observes medium- to long-term (inter-annual) sustainability and relies on the comparison of similar stress states. As such, it is critical to use data from the same time every year. Comparing a chemical analysis taken in early spring of one year to one taken in late autumn the next year would lead to a skewed image of the hydrochemical development, as seasonal fluctuations would superimpose long-term trends. Further, one must consider the fact that the input data should not be normalized, as absolute values of ions (making up total dissolved salts and trace ions) are important for the characterization of a well, especially of wells used for balneological purposes. Therefore, individual ions with high concentration values can exert a stronger weight on the clustering analysis than others. In the case of Bad Füssing TH-1, the clusters were heavily influenced by an irregular fluctuation

in HCO_3^-, which is available in high concentrations in that part of the NAFB. To assess the sensitivity of the algorithm to this effect, a leave-one-out analysis was conducted, which showed that the clustering workflow was resilient with regard to the elimination of singular ions, even the dominant ones.

The sustainable use of an aquifer can be determined based on long-term developments, especially using the proposed workflow in which every additional sample further fine-tunes our understanding of the well-specific acceptable natural corridors. In combination with classifications according to the inflow path types [24], this can result in a thorough understanding of individual deep groundwater wells. For example, a value belonging to inflow path type A (no connection to overlying or underlying aquifers) can be expected to display hydrochemical signatures with remarkable regularity, whereas the activation of additional inflow pathways is easier to trigger in Types B (hydraulic connections to adjacent aquifers) and C (intentional exploitation of multiple aquifers by one well). Well operators should make an effort to truly understand their respective geological settings to better be able to read the messages their wells convey to them in the shape of their hydrochemical signatures. While they might contend that observing fixed thresholds as stated by national guidelines is a much simpler approach, one should argue that this thesis' algorithm can be applied in a matter of seconds as long as the data are available in a suitable format (in a database or a .csv file adhering to some formatting criteria).

Regarding the methodology in this publication and future applications, it would be interesting to apply this method to wells outside the NAFB and assess its efficacy in different geological settings. As always, an improved database can be assumed to increase the accuracy of this method further. This includes additional parameters regarding the aquifer, e.g., temperature, flow rate, or pressure, and the execution of step-wise pumping tests. The latter could improve our understanding of the individual wells in a dynamic setting. Once additional hydrochemical information becomes available covering the time between the typical sampling dates in the summer months, one could expand this workflow to include seasonal developments and further assess the reliability of this workflow based on sub-yearly data. Then, when unsustainable indicators arise, the early warning system might be triggered up to nine months earlier than when based only on yearly data.

7.2.2 Ideas for Fixing the Notorious Lack of Deep Groundwater Data

As mentioned in subsection 2.1.3, hydrochemical sampling and the drilling of deep groundwater wells are time- and cost-intensive, resulting in data characterized by both low temporal and spatial resolution. The initial idea of fixing this problem was to apply VS trained on the available data. In the context of deep groundwater wells, this could be done by combining high spectral, low temporal resolution data (offline data: yearly complete hydrochemical analyses describing the ionic composition of the fluid) with low spectral, high temporal resolution data (online data: minute-based measurements of pressure, temperature, pH, EC, production volume, meta- and operational information). If successful, this approach would allow the well's ionic composition to be inferred from easily monitored parameters, such as pressure, temperature, pH, EC, and production volume, in real-time. This would enable continuous surveillance of hydrochemical stability, improving the temporal resolution of deep groundwater monitoring, without requiring frequent, costly, and labor-intensive hydrochemical sampling.

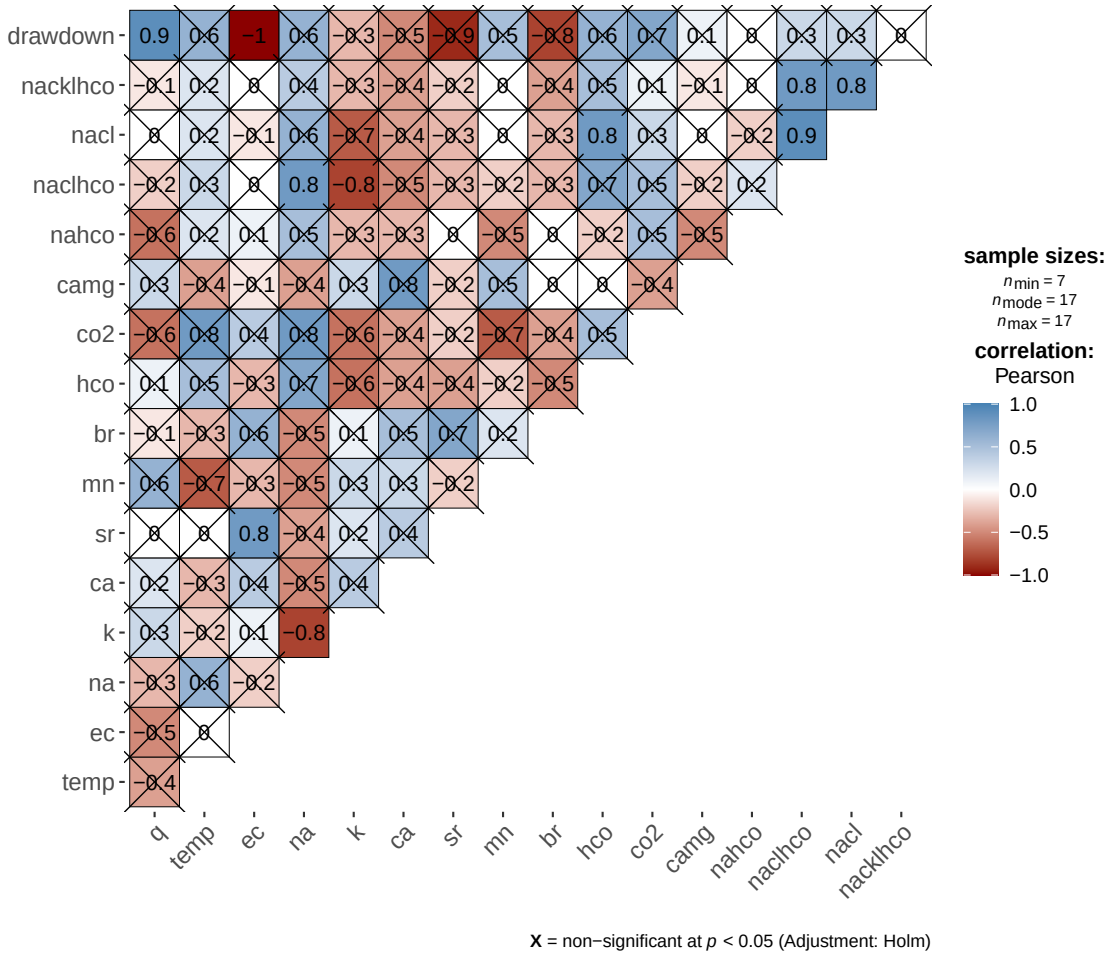

Figure 7.3 Correlogram showing the lack of statistically significant correlations, presumably due to insufficient data points. In addition to the hydrochemical and physical parameters, the following ratios were used: nacklhco: $(\mathrm{Na}^+ + \mathrm{K}^+ - \mathrm{Cl}^-)/\mathrm{HCO_3}^-$; nacl: $\mathrm{Na}^+/\mathrm{Cl}^-$; naclhco: $(\mathrm{Na}^+ - \mathrm{Cl}^-)/\mathrm{HCO_3}^-$; nahco: $\mathrm{Na}^+/\mathrm{HCO_3}^-$; camg: $\mathrm{Ca}^{2+}/\mathrm{Mg}^{2+}$.

The NAFB well Bad Abbach Kaisertherme offered two such data sets, and the idea of using VS was tested by analyzing correlations between the online and offline data points. Due to the limited yearly data available, the resulting correlations were either statistically insignificant (Fig. 7.3), dependent on just one or two data points, or nonexistent. In an effort to find correlations, certain ion ratios were examined in addition to the individual ions and physical parameters; however, they remained too limited (Fig. 7.3). The most prominent ions (e.g., Na^+, Cl^-, $HCO_3{}^-$) showed some correlations with each other, but a holistic derivation of ionic information based on correlations with the online data remained beyond the capabilities of simple correlation analysis.

Ironically, this lack of correlations between parameters needed to train VS to combat the lack of data was, in turn, caused by the lack of available data. Due to the limited data sets, most correlations missed statistical significance, causing a vicious cycle due to insufficient data. In addition, the lack of correlations might be explained by non-linear or temporally lagging relationships, which cannot be represented by linear regression. For example, the extent to which a specifically operationally intensive year (or the opposite) influences the hydrochemical composition medium- to long-term should be considered within the next

months to year(s). Given the slow regeneration rate of deep aquifers, induced hydrochemical changes might only become visible after quite a long time. The length of these reaction times depends on local and regional hydrogeological conditions and should be assessed on these spatial scales [40].

Correlation between parameters is not the only statistical aspect affected by data scarcity. The study further showed that the current database is insufficient for state-of-the-art algorithms like autoregressive integrated moving average (ARIMA) forecasting, which is afflicted by two shortcomings in this context. When training an ARIMA forecast on yearly data, the resulting confidence intervals do not cover current EC fluctuations observed in the online data. This shows that any future estimates based on annual data will only predict future data points based on the same stress state of the aquifer as the yearly training data and thereby ignore seasonal variations. Thus, the training dataset must cover a more extended time period and be complemented by additional data points throughout the year. In addition, ARIMA, while one of the most common prediction algorithms, is a univariate model that bases its predictions solely on the time series of data points available up to the start of the prediction period [87]. Additional factors that could influence the water's chemical composition, such as competing local wells or changes in flow paths, are thus not depicted in the prognosis. Also, temporal and local auto-correlation should be examined closely to understand their impact on a well's hydrochemical composition and changes therein.

Although VS could not be trained at this stage, the second publication did not conclude that their application is entirely unfeasible in the context of deep groundwater monitoring. It rather emphasizes the need for more hydrochemical data to enable effective training of VS in the future in order to use VS as a low-cost strategy to improve the deep groundwater data situation. An important contribution of this study to the field of deep groundwater research is a statistically backed recommendation concerning an improved groundwater sampling frequency. In an ideal world, complete hydrochemical analyses of deep groundwater wells would be available on a quarterly or monthly basis in order to depict seasonal fluctuations. Previous studies have suggested intervals of two weeks for the optimal characterization of shallow sand and gravel groundwater aquifers in Illinois, USA [7]. Another suggestion was made by [109], who, considering three quantitative components to compare sampling intervals (trend detection, determination of seasonal variability, and estimation of mean), derived an optimal sampling interval for hydrochemical and geophysical analyses of 1 month. These suggested intervals pose a financial and logistical dilemma to most, if not all, deep groundwater well operators. This thesis' second study determined that based on the Nyquist-Theorem, the minimum sampling frequency in the NAFB is >2 samples/year. This would cover the yearly seasonal behavior of the well Bad Abbach Kaisertherme, which displays a seasonal oscillation with one positive and one negative peak per year and should still lie within the capabilities of the well operators. Considering the stark difference in information content between annual and sub-daily data, as presented in detail in this second publication, the increased insights into the well's hydrochemical behavior should be worth the additional financial investment (assuming the cost of one analysis is around EUR 2,000, this would amount to EUR 4,000 in additional costs per year, which should be negligible compared to the loss of a well's certification as a medical spa).

Considering these results, even the most sophisticated algorithms of factor analysis are useless without enough data to train them. In its guideline on deep aquifers, the LfU underlines that a more stringent monitoring strategy for deep groundwater is necessary, specifying the need for an increased amount of

monitoring wells and the application of isotope analyses and tracer tests which would help to characterize age structure, inflow dynamics, and mass transfer [40]. While it does not give a concrete number regarding sampling frequency, it demands a well-specific approach to designing the monitoring network, which the developed workflow in the first publication and the assessments conducted in the second publication were able to contribute to. But how many samples should deep groundwater researchers aim for exactly before starting to train VS? According to [73], the minimum sample size is often suggested to be 3 - 20 times the number of variables, which in this case are the eight main ions that should be derived from the online data; thus, the minimum total number of samples ranges between 24 and 160. At a minimum sampling rate of 3 samples a year, this translates to between 8 and roughly 50 years of sampling; especially the upper end of this range is highly impractical, but it could be lowered with an increase in sampling frequency. These numbers underscore the importance of increasing sampling frequencies and investing in high-quality and robust probes, sensors, and analytical equipment, in addition to an improved system and process understanding. Ultimately, improving data frequency and quality is essential not only to train VS but also to enhance our overall understanding of flow-path systems, recharge ratios, and the effects of (net) discharge on the aquifer and other nearby wells.

7.2.3 Evaluating Microscopy for Assessing Pore Propagation: Strengths, Limitations, and Alternatives

Autoclave experiments on solid rock samples (as opposed to powders) often result in surface-level alterations that are difficult to assess at the pore scale [90]. This occurs because the dissolution affects the entire surface uniformly, so that by the end of the experiment, changes may appear as a general roughening rather than distinct pathways. As a result, precise examinations of preferential flow path formation become challenging. To overcome this, a new sample preparation approach was developed and integrated with a well-established autoclave setup. By coating a calcite sample cube with a water- and heat-resistant two-component lacquer, drying it, and then applying a second coat, the majority of the sample was shielded effectively from exposure to the undersaturated fluid inside the autoclave. Dissolution could only take place at two artificial disturbances drilled into the coated rock with a mini-drill: one point-shaped (“hole”) and one line-shaped (“cut”). Localizing the dissolution effects intensified the contrast between altered and unaltered surfaces, allowing for a clear before-and-after comparison using three different microscopy techniques.

Once the ThorLab stage and camera were installed, operating the optical microscope was straightforward and simple in its application. Special attention was given to avoiding proprietary software, which had no impact on image quality but made image stacking time-intensive, a process that could be streamlined in future applications. Image acquisition time was comparable to 3D micro-scanning but significantly longer than that of CLSM by a factor of 20 to 30. In terms of spatial resolution, optical microscopy performed well, coming close to CLSM ($0.34 \times 0.34\,\mu m^2$). However, due to its orthogonal camera position, it could not capture areas hidden beneath overhangs. Its main advantage lies in its affordability and versatility, making it one of the most widely used laboratory tools worldwide. In the context of this third publication, it served as an effective method for initial observations and qualitative analysis of surface changes, such as flow path widening, before applying more resource-intensive techniques like 3D micro-scanning and CLSM.

Using 3D micro-scanning in this study was particularly intriguing, as it was the first time this device had been applied to monitor changes in rock samples. It quickly demonstrated a key advantage over the other two methods: despite offering the lowest spatial resolution ($29 \times 29\,\mu m^2$), it was the only technique capable of capturing details beneath overhangs. This was made possible by the multi-axial rotation of the sample stage, although viewing-angle limitations, as discussed in the publication, imposed some constraints. Still, the scanner successfully examined the sample from multiple perspectives, reaching areas of complex morphology inaccessible to optical microscopy and CLSM. Image acquisition took approximately the same time as optical microscopy (30 – 40 minutes) and produced a 3D point cloud, which was then exported for further analysis using open-source software (e.g., CloudCompare). This multi-software adaptability further enhanced its utility.

CLSM delivered the highest xy-resolution ($0.1 \times 0.1\,\mu m^2$) and the fastest image acquisition (1 – 10 minutes per disturbance), and produced true-color images. Its ability to detect fine-scale changes in surface morphology became particularly valuable when combined with the broader-scale surface model provided by 3D micro-scanning. While interpolation was necessary for areas beneath overhangs, since, like optical microscopy, CLSM could not access these regions, the combination of both techniques enabled an almost complete morphological model of the entire disturbance. Like 3D micro-scanning, CLSM generated data in multiple formats, allowing for cross-verification with other techniques and improving the overall reliability of our findings.

Regardless of their unique advantages and limitations, all three methods observed that the artificial disturbances had widened after the autoclave treatment, which translates to the formation of preferential flow paths developing at the injection well and possibly facilitating an early onset of thermal breakthrough. Since this is clearly an undesired development, as it would cut down the longevity of a geothermal plant significantly, efforts based on various methodologies have been undertaken in order to better understand these dynamics. These extend beyond the methods assessed in this study, where the selection of methods was based on availability and accessibility. For example, pore geometry and surface roughness have been studied before using X-ray computed tomography (XCT) [79] or 3D NMRI [28].

NMRI focuses on the contrast between solid and fluid components. This creates internal magnetic field gradients that distort measurements, especially at high fields (B_O > 3T). These gradients affect T_2 relaxation times, making it difficult to accurately quantify fluid volumes. Unlike in medicine, where NMRI is used for qualitative imaging, core analysis requires precise fluid measurements, which high-field NMRI struggles to provide [71]. MCT, on the other hand, provides high spatial resolution and a non-destructive assessment of a rock plug's interior structure, attributes that have made MCT a superior tool for digital core analysis, pore-scale characterization, fluid flow analysis, and predictive modeling [108]. However, these advantages come at a price. The cost of acquisition of the MCT hardware can be assumed to start at USD 200,000 and even reach USD 2 million. Especially when a resolution of less than 1 µm is required, one should expect an initial financial investment of USD 1 million and over [20], which is practically incompatible with many smaller laboratories or municipal energy and water providers. Thus, the methods used in this study provide lower-cost alternatives, albeit with some trade-offs in resolution and depth penetration.

No single approach emerges as a clear winner among the three methods evaluated in this study. Each method has distinct advantages, e.g., high resolution (CLSM), low acquisition costs (optical microscopy),

user-friendliness, or non-destructive imaging of internal structures (3D micro-scanning), as well as limitations, including low spatial resolution (3D micro-scanning), inability to assess areas within or obstructed by opaque materials (CLSM and optical microscopy), or high acquisition costs (CLSM). Future studies should expand this comparison by incorporating predictive modeling to assess the value these methods bring to this application. While this study has successfully characterized structural changes and provided insights into the dynamics near injection wells, the next step is to determine which method yields the most reliable and effective data for integration into predictive hydrogeochemical models. This will be essential for optimizing geothermal plant operations in the most sustainable manner.

7.3 Practical Implications and Future Directions

Considering the definition of "renewability" (section 2.2), and the long (re-)generation times as well as the old age of deep thermal groundwater [81, 100, 40], deep geothermal waters should not be classified as a renewable resource. As such, it is critical to develop and employ sustainable exploitation regimes to make this resource last for many generations to come. This dissertation offers three specific approaches to reach this target, as it was written with the goal of contributing to and advancing sustainable deep groundwater management strategies, mitigating environmental risks, and improving water quality monitoring efforts. The first two publications of this dissertation lead to practical implications and recommendations for policy-makers regarding well operation practices and hydrochemical sampling strategies, highlighting the shortcomings of the current version of the EU's WFD [33] regarding its limited consideration of deep groundwater aquifers. And while *Deutscher Heilbäderverband* has established a sampling protocol using hydrochemical indicators, their proposed fluctuation threshold values are arbitrary and ignore a well's unique natural fluctuation behavior [22]. Individual well characteristics, however, were deemed especially important to consider by the LfU [40].

Through a combination of continuously fine-tuning the natural and action corridors with every additional hydrochemical sample, a statistically robust and reproducible quantification of a "good qualitative status", and a well-specific approach, the proposed workflow of this thesis' first study will improve the hydrochemical stability in a well by inhibiting the technically legal but hydrogeochemically malign over-exploitation of the deep groundwater aquifer within currently allowed thresholds. The proposed workflow was developed to be adopted and integrated by the LfU in a new directive regarding the exploitation of deep aquifers, resulting in an updated procedure of assessing the stress state of Bavarian deep groundwater wells (Fig. 7.4).

The DQS also determines the minimum deep groundwater sampling frequency of one sample a year. While yearly sampling might be a sufficient data basis for assessments like the one presented [24], it neglects *seasonal* hydrochemical fluctuations. Previous studies have suggested aquifer sampling frequencies that are reasonable in shallow aquifers that react quickly to meteorological and anthropogenic impacts and that are relatively easy to sample; however, this study showed that deep groundwater aquifers display seasonal, but not weekly or even daily fluctuations. Still, in order to depict these fluctuations, which by far exceed the fluctuations detected in the yearly samples, the sampling frequency must be increased to at least three samples taken every year. In addition, deep groundwater wells should be equipped with

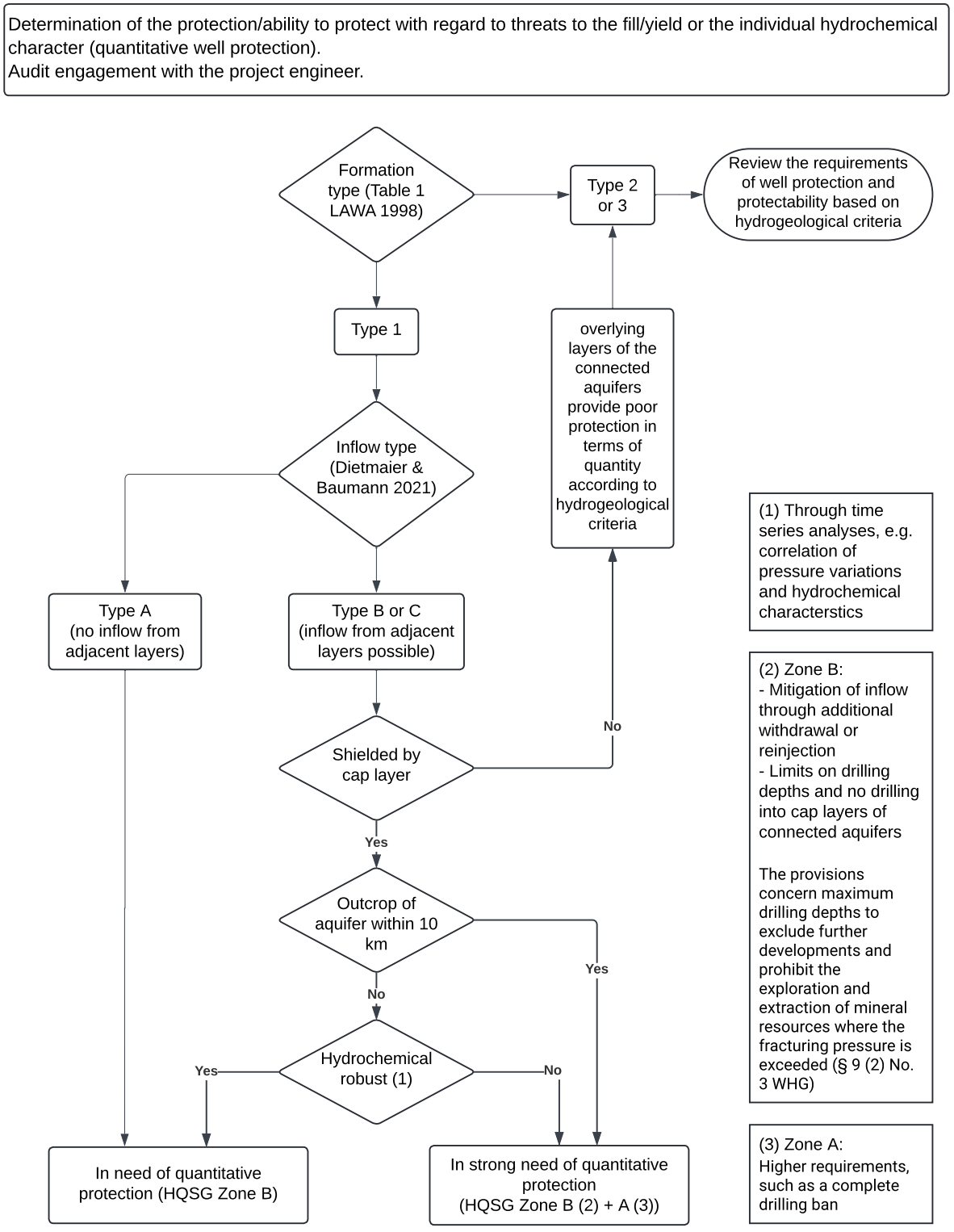

Figure 7.4 Adoption of the proposed workflow from the first publication on assessing the sustainable use of deep groundwater by the LfU. Adapted original design by LfU, Johannes Schneider [23].

online sensors monitoring parameters on a sub-daily basis. This assessment is based on a purely academic approach. One must consider that an actual increase in the sampling rate would result in a threefold increase in costs, which would have to be covered by the well operator. In order to sell this idea to well operators and to apply it successfully, the long-term advantages of an improved data basis need to be explained carefully to the involved decision-makers. Firstly, a higher sampling frequency would allow for much quicker detection of indicators of unsustainable well exploitation. This would help prevent cost-intensive emergency maintenance measures or even a deterioration of the well beyond the possibility of repair or de-certification (in the case of balneological wells). Simultaneously, this would result in stronger protection of the aquifer from an ecological and hydrogeological standpoint.

Further, an improved data basis could lead to the eventual implementation of VS as a low-cost, easy-to-maintain, and flexible monitoring system. Entezari et al. point out the large potential of applying artificial intelligence (AI) and machine learning in the field of managing, optimizing, and predicting the demand and status of energy systems [31], which could include the derivation of hydrochemical properties of deep well water based on online monitoring data at the wellhead. One might argue that VS have not yet been applied for this purpose solely due to the lack of available training data. However, the scientific community needs to break the cycle of having poor data in the future because of having poor data presently and start acquiring more high-quality data as soon as possible, which would then lead to a disproportionately more substantial improvement in data availability in the long run. Enhancing data collection methods and increasing data integrity constitute the groundwork for robust predictive models concerning real-time fluctuations in water quality. Informing well operators about the significance of this effort is critical in order to collaborate and encourage adherence to standardized data collection protocols. This will ultimately lead to a more comprehensive understanding of groundwater dynamics and better-informed decision-making in water resource management.

Improving our understanding of the local deep aquifer system goes beyond the production well and also includes characterizing structural changes in the aquifer rock matrix at the injection site caused by reinjecting undersaturated waters. Three imaging methods able to do just that were compared systematically. The widening and deepening of artificial disturbances in the rock samples, resulting from exposure to undersaturated fluid, suggest that dissolution processes can alter the aquifer matrix and drive the propagation of pore space around the reinjection well. The specific advantages and limitations of the three imaging techniques, as well as the importance of providing reliable data for predictive hydrogeochemical models, have been discussed in subsection 7.2.3.

Within the broader context of sustainable geothermal plant operation, it is important to recognize that the geothermal water cycle does not end at reinjection. As the reinjected fluid moves away from the well and through the hot aquifer matrix, its temperature gradually rises. Correspondingly, its pH increases, shifting the lime-carbonic-acid equilibrium once more. This ultimately leads to the precipitation of dissolved calcite. Unlike the earlier dissolution processes, this precipitation could narrow or even clog pore spaces, restricting fluid flow [41, 54, 92]. Over time, this can slow the system to a standstill or force water along previously non-existent pathways, altering the aquifer's most fundamental properties, such as flow velocity and chemical composition. In a homogeneous aquifer matrix setting, these processes happen along the edge of the cold water plume, which means that the area of rock matrix through which the reinjected

water flows is quite vast, usually leading to very slow flow velocities and small effects of precipitation. Still, in a worst-case scenario, e.g., in a geological setting with preferential flowpaths from the reinjection site to the production well, the affected geothermal doublet might have to be shut down, as was the case with the Mezőberény geothermal site in Hungary [64]. While hydrogeochemical models have been applied to avoid this, these models rely on vast data, which are often not available for proper training of the models, restricting their effectiveness in predicting and mitigating clogging risks [4, 52, 107, 64]. This, once again, hints at the utter importance of investing in the improvement of the current data basis concerning hydrochemical information on deep geothermal operations, as understanding these dynamics is crucial for managing geothermal plants truly sustainably.

8 Conclusion: Hydrochemical Indicators – A Compass for Deep Groundwater Reservoir Management

Deep geothermal groundwater is an invaluable resource, offering a stable supply of heat and, where the temperature is high enough, electric power generation. Unlike shallow groundwater aquifers, deep groundwater is naturally protected by overlying impermeable layers of rock, making deep aquifers resilient to short-term climate fluctuations and anthropogenic contamination. However, due to its extremely slow regeneration, its use comes with challenges regarding sustainability. Hydrothermal reservoirs are not truly renewable on human timescales, and their management requires a delicate balance between current production volumes and long-term sustainability. This dissertation contributes to the field of sustainable deep groundwater management by demonstrating how hydrochemistry can serve as a powerful tool for understanding reservoir dynamics and improving the sustainability of geothermal operations: a well's hydrochemical composition serves as a fingerprint, indicating the rock constellations with which the water interacted on its way to the production well, or the activation/deactivation and mixing ratios between adjacent aquifers. On the other end of the geothermal doublet, hydrochemistry governs water-rock interactions, which can lead to dissolution and, thereby, alterations in reinjection volumes. Thus, hydrochemistry constitutes a unique tool that allows a glance into a well's past, present, and future.

Using hydrochemical fingerprints was the basis for the development of a statistically robust method for assessing hydrochemical variations in deep geothermal wells. By applying two different clustering algorithms, this thesis introduced an adaptive approach that defines well-specific "natural" and "action" corridors based on hydrochemical parameters. Unlike conventional regulatory thresholds, which impose fixed percentage-based limits without accounting for site-specific geochemical conditions, this method continuously refines its respective corridors as new data become available. The workflow was successfully tested on datasets collected at eight wells in Lower Bavaria and Upper Austria, showing its ability to detect subtle trends that could serve as early indicators of reservoir inflow changes and, thereby, unsustainable well use; as a result, well operators are enabled to adapt their operation strategies in order to avoid inflicting significant physical or monetary damage to their wells and/or aquifers. These findings highlight how hydrochemical analysis can move beyond being a passive monitoring tool to becoming an active component of sustainable reservoir management.

Another key aspect of this research was the evaluation of hydrochemical monitoring strategies. Current regulations often rely on a single annual water sample to assess well conditions, a strategy that has been proven to be insufficient to adequately depict actual hydrochemical variations in this thesis. Annual data

clearly overlook notable seasonal variations that are probably linked to operational changes. This was shown through statistical comparisons of annual and sub-daily datasets, which revealed that substantial hydrochemical changes occur on much shorter timescales than is visible in yearly samples. As a result, this thesis strongly supports increasing the mandatory sampling frequency to at least three times per year to ensure that critical reservoir dynamics are captured more effectively and before far-reaching damage can be caused.

Beyond production wells, reinjection sites also play a crucial role in geothermal system sustainability, as dissolution processes could, at first, lead to increased reinjection volumes but run the risk of causing a thermal short-circuit. This dissertation used three different microscopy techniques to assess the visualization of dissolution-related structural changes at reinjection wells, focusing on pore-scale processes that affect permeability over time. The time-lapse experiments showed measurable widening, deepening, and roughening of artificial fractures, which have implications for long-term injectivity and operational efficiency. Each microscopy method had its limitations and advantages, such as trade-offs between spatial resolution, acquisition costs, and user-friendliness. The comparative approach helped clarify the strengths and weaknesses of different analytical techniques in a semi-quantitative fashion, facilitating future studies of geochemical interactions in geothermal reservoirs.

In summary, this dissertation advances the use of hydrochemical data as a proxy for tracking and projecting reservoir changes in order to advance the sustainability of geothermal management strategies. By integrating statistical analysis with experimental investigations, it provides a comprehensive assessment of deep geothermal system behavior at multiple scales. The findings emphasize the need for more detailed and frequent monitoring while demonstrating the potential of hydrochemical datasets to inform both regulatory frameworks, e.g., a national implementation of the WFD in Germany for deep aquifers and operational decision-making.

Moving forward, hydrochemistry deserves to play a more central role in thermo-hydro-chemo-mechanial (THCM) modeling to improve our understanding of geothermal reservoir evolution. While thermal and hydraulic aspects are well established and often prioritized, chemical interactions between the water and the rock of an aquifer are equally critical in shaping reservoir behavior, influencing scaling, dissolution, and, thereby, long-term sustainability. A truly integrated approach that fully incorporates geochemical data alongside reservoir engineering and numerical modeling will be key to ensuring the sustainable management of deep geothermal resources for future generations.

Bibliography

[1] Prognos AG, Öko Institut e.V., and Wuppertal Institut für Klima Umwelt Energie gGmbH. Towards a Climate-Neutral Germany by 2045. How Germany can reach its climate targets before 2050. Executive Summary conducted for Stiftung Klimaneutralität, Agora Energiewende and Agora Verkehrswende. Technical report, Agora Energiewende, 2021.

[2] Jean-Andre Agemar, Birgit Alten, Joachim Ganz, Klaus Kuder, Karsten Kühne, Stefan Schumacher, and Rainer Schulz. The geothermal information system for germany – geotis. *Zeitschrift der Deutschen Gesellschaft für Geowissenschaften*, 165(2):129–144, 2014. doi:10.1127/1860-1804/2014/0060.

[3] William M. Alley, E. Scott Bair, and Michael Wireman. "Deep" groundwater. *Groundwater*, 51(5):653–654, 2013. doi:10.1111/gwat.12098.

[4] Jasper Alsemgeest, Luis F. Auqué, and Maria J. Gimeno. Verification and comparison of two thermodynamic databases through conversion to phreeqc and multicomponent geothermometrical calculations. *Geothermics*, 91:102036, 2021. doi:10.1016/j.geothermics.2021.102036.

[5] Nicole Baran, Annette Elisabeth Rosenbom, Ronald Kozel, and Dan Lapworth. Pesticides and their metabolites in European groundwater: Comparing regulations and approaches to monitoring in France, Denmark, England and Switzerland. *Sci. Total Environ.*, 842(October 2021):156696, 2022. doi:10.1016/j.scitotenv.2022.156696.

[6] Maurizio Barbieri, Marino Domenico, Barberio Francesca, Andrea Billi, Tiziano Boschetti, Stefania Franchini, Francesca Gori, and Marco Pettita. Climate change and its effect on groundwater quality. *Environ. Geochem. Health*, 5, 2021. doi:10.1007/s10653-021-01140-5.

[7] Michael J. Barcelona, Harold A. Wehrmann, Michael R. Schock, Mark E. Sievers, and John R. Karny. *Sampling frequency for groundwater quality monitoring*. U.S. Environmental Protection Agency, Office of Research and Development, Environmental Monitoring Systems Laboratory, Las Vegas, 1989.

[8] Matthias Bauer, Willi Freeden, Hans Jacobi, and Thomas Neu. *Handbuch tiefe Geothermie*. Springer Spektrum. Berlin, 2014. doi:10.1007/978-3-642-54511-5.

[9] Thomas Baumann, Jörn Bartels, Mark Lafogler, and Frank Wenderoth. Assessment of heat mining and hydrogeochemical reactions with data from a former geothermal injection well in the Malm Aquifer, Bavarian Molasse Basin, Germany. *Geothermics*, 66:50–60, 2017. doi:10.1016/j.geothermics.2016.11.008.

[10] Bayerisches Landesamt für Umwelt. Messstellen, 2021. Accessed 2023-11-09. URL: https://www.lfu.bayern.de/wasser/grundwasserstand/messstellen/index.htm.

[11] Bayerisches Staatsministerium für Wirtschaft, Landesentwicklung und Energie. *Bayerischer Geothermieatlas*. Munich, 2024.

[12] Johannes Birner. *Hydrogeologisches Modell des Malmaquifers im Süddeutschen Molassebecken*. PhD thesis, 2013. URL: https://refubium.fu-berlin.de/handle/fub188/1492.

[13] Bundesministerium der Justiz und für Verbraucherschutz. Bundesberggesetz. 1980. Zuletzt geändert durch Art. 39 G v. 23.10.2024 I Nr. 323. Accessed 2025-04-01. URL: https://www.gesetze-im-internet.de/bbergg/.

[14] Bundesministerium der Justiz und für Verbraucherschutz. Mineral- und Tafelwasserverordnung. 1984. Zuletzt geändert durch Art. 2 V v. 20.6.2023 I Nr. 159. Accessed 2025-03-28. URL: https://www.gesetze-im-internet.de/min_tafelwv/.

[15] Bundesministerium der Justiz und für Verbraucherschutz. Gesetz für den Ausbau erneuerbarer Energien. *Bundesgesetzblatt*, 1(49), 2016. Zuletzt geändert durch Art. 1 G v. 21.2.2025 I Nr. 52. Accessed 2025-08-20. URL: https://www.gesetze-im-internet.de/eeg_2014/.

[16] Bundesministerium für Umwelt Naturschutz und nukleare Sicherheit. Bundes-Klimaschutzgesetz. pages 1–19, 2021. Zuletzt geändert durch Art. 1 G v. 15.7.2024 I Nr. 235. Accessed 2025-04-01. URL: https://www.gesetze-im-internet.de/ksg/BJNR251310019.html.

[17] Bundesverband Geothermie. Geothermie in Zahlen, 2023. Accessed 2023-10-27. URL: https://www.geothermie.de/aktuelles/geothermie-in-zahlen.

[18] Ben Callow, Ismael Falcon-Suarez, Hector Marin-Moreno, Jonathan M Bull, and Sharif Ahmed. Optimal x-ray micro-ct image based methods for porosity and permeability quantification in heterogeneous sandstones. *Geophysical Journal International*, 223(2):1210–1229, 06 2020. doi:10.1093/gji/ggaa321.

[19] Maria Clara Castro, Albert Jambon, Ghislain De Marsily, and Peter Schlosser. Noble gases as natural tracers of water circulation in the Paris Basin. 1. Measurements and discussion of their origin and mechanisms of vertical transport in the basin. *Water Resour. Res.*, 34(10):2443–2466, 1998. doi:10.1029/98WR01956.

[20] Rigaku Holdings Corp. What is micro-ct?, 2025. Accessed 2025-03-20. URL: https://rigaku.com/products/imaging-ndt/x-ray-ct/learning/micro-ct?utm_source=chatgpt.com#cost-of-a-micro-ct-scanner.

[21] H. Corson-Dosch, C. Nell, R. Volentine, A.A. Archer, E. Bechtel, J.L. Bruce, N. Felts, T. A. Gross, D. Lopez-Trujillo, C. E. Riggs, and E. K. Read. The water cycle. Technical report, United States Geological Survey, 2022. Accessed 2024-11-20. URL: https://www.usgs.gov/media/images/water-cycle-png.

[22] Deutscher Heilbäderverband and Deutscher Tourismusverband. 14. Auflage. Begriffsbestimmungen / Qualitätsstandards für Heilbäder und Kurorte, Luftkurorte, Erholungsorte - einschließlich der Prädikatisierungsvoraussetzungen - sowie für Heilbrunnen und Heilquellen. Technical report, Berlin, 2023.

[23] Annette Dietmaier and Thomas Baumann. Qualitative Zustandsbeurteilung des grenzüberschreitenden Tiefengrundwasserkörpers im niederbayerisch-oberösterreichischen Molassebecken - non-public final report. Technical report, Technical University of Munich, Munich, 2021.

[24] Annette Dietmaier and Thomas Baumann. Assessing sustainable development of deep aquifers. *Water Resour. Manag.*, 37(10):3857–3874, 2023. doi:10.1007/s11269-023-03529-6.

[25] Annette Dietmaier and Thomas Baumann. Forecasting changes of the flow regime at deep geothermal wells based on high resolution sensor data and low resolution chemical analyses. *Adv. Geosci.*, 58:189–197, 2023. doi:10.5194/adgeo-58-189-2023.

[26] Annette Dietmaier, Justin Mattheis, Daniel Weller, Ingrid Stober, Michael Drews, and Thomas Baumann. Visualization and semi-quantitative analysis of dissolution processes at artificial structures in carbonate rocks using optical, 3d micro-scanning and confocal laser scanning microscopy. *Geothermal Energy*, 13(1):32, 2025. doi:10.1186/s40517-025-00355-4.

[27] Peter Dijk, Brian Berkowitz, and Peter Bendel. Investigation of flow in water-saturated rock fractures using nuclear magnetic resonance imaging (nmri). *Water Resources Research*, 35(2):347–360, 1999. doi:10.1029/1998WR900044.

[28] Peter Erik Dijk and Brian Berkowitz. Measurement and analysis of dissolution patterns in rock fractures. *Water Resour. Res.*, 38(2), 2002. doi:10.1029/2001WR000246.

[29] Walter Dragoni and B. S. Sukhija. Climate change and groundwater: a short review. *Geological Society, London, Special Publications*, 288:1–12, 2008. doi:10.1144/SP288.2.

[30] Sam Earman and Michael D. Dettinger. Potential impacts of climate change on groundwater resources: a global review. *Journal of Water and Climate Change*, 2(4):213–229, 2011. doi:10.2166/wcc.2011.034.

[31] Ashkan Entezari, Alireza Aslani, Rahim Zahedi, and Younes Noorollahi. Artificial intelligence and machine learning in energy systems: A bibliographic perspective. *Energy Strateg. Rev.*, 45(April 2022):101017, 2023. doi:10.1016/j.esr.2022.101017.

[32] European Commission. European Green Deal: Delivering on our targets, 2021. Accessed 2025-08-20. URL: https://ec.europa.eu/commission/presscorner/api/files/attachment/869807/EGD_brochure_EN.pdf.

[33] European Parliament and Council. Directive 2000/60/ec of the european parliament and of the council establishing a framework for community action in the field of water policy, 10 2000. Accessed 2025-08-20. URL: https://eur-lex.europa.eu/legal-content/EN/TXT/?uri=CELEX:32000L0060.

[34] Federal Ministry for Economic Affairs and Climate Action. Integrated national energy and climate plan of Germany. (663):1–262, 2020. Accessed 2025-08-20. URL: https://energy.ec.europa.eu/system/files/2022-08/de_final_necp_main_en.pdf.

[35] Grant Ferguson, Mark O. Cuthbert, Kevin Befus, Tom Gleeson, and Jennifer C. McIntosh. Rethinking groundwater age. *Nat. Geosci.*, 13(9):592–594, 2020. doi:10.1038/s41561-020-0629-7.

[36] Grant Ferguson, Jennifer C. McIntosh, Scott Jasechko, Ji Hyun Kim, James S. Famiglietti, and Jeffrey J. McDonnell. Groundwater deeper than 500 m contributes less than 0.1% of global river discharge. *Commun. Earth Environ.*, 4(1):1–8, 2023. doi:10.1038/s43247-023-00697-6.

[37] Grant Ferguson, Jennifer C. McIntosh, Oliver Warr, Barbara Sherwood Lollar, Christopher J. Ballentine, James S. Famiglietti, Ji Hyun Kim, Joseph R. Michalski, John F. Mustard, Jesse Tarnas, and Jeffrey J. McDonnell. Crustal groundwater volumes greater than previously thought. *Geophys. Res. Lett.*, 48(16):1–9, 2021. doi:10.1029/2021GL093549.

[38] R. Allan Freeze and John A. Cherry. *Groundwater*. Prentice Hall, Englewood Cliffs, NJ, 1979.

[39] Bayerisches Landesamt für Umwelt. Balneologische Nutzung, 2025. Accessed 2025-08-20. URL: https://www.lfu.bayern.de/wasser/thermische_nutzung/thermalwassernutzung/balneologische_nutzung/index.htm.

[40] Bayerisches Landesamt für Umwelt. Tiefengrundwasser, 2025. URL: https://www.bestellen.bayern.de/application/applstarter?APPL=eshop&DIR=eshop&ACTIONxSETVAL(artdtl.htm,APGxNODENR:4015,AARTxNR:lfu_was_00337,AARTxNODENR:369419,USERxBODYURL:artdtl.htm,KATALOG:StMUG,AKATxNAME:StMUG,ALLE:x)=X.

[41] Haonan Gan, Zhiming Liu, Xiao Wang, Yu Zhang, Yuzhong Liao, Gui Zhao, Jichu Zhao, and Zhitao Liu. Effect of temperature and acidification on reinjection of geothermal water into sandstone geothermal reservoirs: laboratory study. *Water*, 14(19):2955, 2022. doi:10.3390/w14192955.

[42] Geotis. Overview of all geothermal installations within bavaria, 2025. Accessed 2025-03-17. URL: https://www.geotis.de/geotisapp/templates/locationall.php?bula=D.

[43] Johann Goldbrunner. Zur Hydrogeologie des Oberösterreichischen Molassebeckens. *Steirische Beiträge zur Hydrogeologie*, 36:83–102, 1984.

[44] Nico Goldscheider, Judit Mádl-Szonyi, Anita Eross, and Eva Schill. Review: Thermal water resources in carbonate rock aquifers. *Hydrogeol. J.*, 18(6):1303–1318, 2010. doi:10.1007/s10040-010-0611-3.

[45] Anita E. Gue, Bernhard Mayer, and Stephen E. Grasby. Origin and geochemistry of saline spring waters in the Athabasca oil sands region, Alberta, Canada. *Appl. Geochemistry*, 61:132–145, 2015. doi:10.1016/j.apgeochem.2015.05.015.

[46] Klaus H. Hebig, Nobuo Ito, Thomas Scheytt, and Atsuyuki Marui. Review: Deep groundwater research with focus on germany. *Hydrogeology Journal*, 20(2):227–243, 2012. doi:10.1007/s10040-011-0815-1.

[47] Michael Heidinger, Florian Eichinger, Roland Purtschert, Peter Mueller, Jake Zappala, Gunther Wirsing, Tobias Geyer, Thomas Fritzer, and Doris Groß. Altersbestimmung an thermalen Tiefenwässern im Oberjura des Molassebeckens mittels Krypton-Isotopen. *Grundwasser*, 24:287–294, 2019. doi:10.1007/s00767-019-00431-0.

[48] Florian Heine and Florian Einsiedl. Groundwater dating with dissolved organic radiocarbon: A promising approach in carbonate aquifers. *Appl. Geochemistry*, 125(November 2020):104827, 2021. doi:10.1016/j.apgeochem.2020.104827.

[49] William Henry. Experiments on the quantity of gases absorbed by water, at different temperatures, and under different pressures. Technical report, Royal Society, 1803. doi:10.1098/rstl.1803.0004.

[50] G. Holland, B. Sherwood Lollar, L. Li, G. Lacrampe-Couloume, G. F. Slater, and C. J. Ballentine. Deep fracture fluids isolated in the crust since the Precambrian era. *Nature*, 497(7449):357–360, 2013. doi:10.1038/nature12127.

[51] Sebastian Homuth, Annette E. Götz, and Ingo Sass. Reservoir characterization of the upper jurassic geothermal target formations (molasse basin, germany): Role of thermofacies as exploration tool. *Geothermal Energy Science*, 3(1):41–49, 2015. doi:10.5194/gtes-3-41-2015.

[52] Thorsten Hörbrand, Thomas Baumann, and Helge C. Moog. Validation of hydrogeochemical databases for problems in deep geothermal energy. *Geothermal Energy*, 6(1):20, 2018. doi:10.1186/s40517-018-0106-3.

[53] IPCC. Climate Change 2022: Impacts, Adaptation and Vulnerability. Technical report, Intergovernmental Panel on climate Change, Cambridge, UK and New York, NY, USA, 2022. doi:10.1017/9781009325844.Front.

[54] Omer Izgec, Birol Demiral, Henri Bertin, and Serhat Akin. Calcite precipitation in low temperature geothermal systems: an experimental approach. In *30th Workshop on Geothermal Reservoir Engineering, Stanford University, Stanford, California, TR-176*, 2005.

[55] Scott Jasechko, Debra Perrone, Kevin M. Befus, M. Bayani Cardenas, Grant Ferguson, Tom Gleeson, Elco Luijendijk, Jeffrey J. McDonnell, Richard G. Taylor, Yoshihide Wada, and James W. Kirchner. Global aquifers dominated by fossil groundwaters but wells vulnerable to modern contamination. *Nat. Geosci.*, 10(6):425–429, 2017. doi:10.1038/ngeo2943.

[56] Keegan Jellicoe, Jennifer C. McIntosh, and Grant Ferguson. Changes in deep groundwater flow patterns related to oil and gas activities. *Groundwater*, 60(1):47–63, 2022. doi:10.1111/gwat.13136.

[57] Mary Kang, James E. Ayars, and Robert B. Jackson. Deep groundwater quality in the southwestern United States. *Environ. Res. Lett.*, 14(3), 2019. doi:10.1088/1748-9326/aae93c.

[58] Mary Kang and Robert B. Jackson. Salinity of deep groundwater in California : Water quantity , quality , and protection. *PNAS*, 113(28):7768 – 7773, 2016. doi:10.1073/pnas.1600400113.

[59] Werner Kanz. Grundwasserfließwege und Hydrogeochemie in tiefen Graniten und Gneisen. *Geologische Rundschau*, 76(1):265–283, 1987. doi:10.1007/BF01820587.

[60] Leonard Kaufman and Peter J. Rousseeuw. *Finding groups in data: an introduction to cluster analysis*. John Wiley & Sons, Hoboken, New Jersey, 1990.

[61] Aristidis Likas, Nikos Vlassis, and Jakob J. Verbeek. The global k-means clustering algorithm. *Pattern Recognit.*, 36(2):451–461, 2003. doi:10.1016/S0031-3203(02)00060-2.

[62] Li Hung Lin, Pei Ling Wang, Douglas Rumble, Johanna Lippmann-Pipke, Erik Boice, Lisa M. Pratt, Barbara Sherwood Lollar, Eoin L. Brodie, Terry C. Hazen, Gary L. Andersen, Todd Z. DeSantis, Duane P. Moser, Dave Kershaw, and T. C. Onstott. Long-term sustainability of a high-energy, low-diweniff crystal-biome. *Science (80-.).*, 314:479–482, 2006. doi:10.1126/science.1127376.

[63] Jurgen Mahlknecht, Diego A. Padilla Reyes, Edrick Ramos, Luisa Ma Reyes, and Mario Moises Álvarez. The presence of SARS-CoV-2 RNA in different freshwater environments in urban settings determined by RT-qPCR: Implications for water safety. *Sci. Total Environ.*, 784:147183, 2021. doi:10.1016/j.scitotenv.2021.147183.

[64] Ábel Markó, Maren Brehme, Daniele Pedretti, Günter Zimmermann, and Ernst Huenges. Controls of low injectivity caused by interaction of reservoir and clogging processes in a sedimentary geothermal aquifer (mezőberény, hungary). *Geothermal Energy*, 12(1):40, 2024. doi:10.1186/s40517-024-00317-2.

[65] Dominik Martin, Niklas Kühl, and Gerhard Satzger. Virtual Sensors. *Bus. Inf. Syst. Eng.*, 63(3):315–323, 2021. doi:10.1007/s12599-021-00689-w.

[66] Nicolas C.M. Marty, Virginie Hamm, Christelle Castillo, Dominique Thiéry, and Christophe Kervévan. Modelling water-rock interactions due to long-term cooled-brine reinjection in the Dogger carbonate aquifer (Paris basin) based on in-situ geothermal well data. *Geothermics*, 88(November 2019):101899, 2020. doi:10.1016/j.geothermics.2020.101899.

[67] Christina Mayrhofer. *Hydrochemische Untersuchungen im Malmaquifer im bayerischen Molassebecken*. PhD thesis, Technical University of Munich, 2013.

[68] Christina Mayrhofer, Reinhard Niessner, and Thomas Baumann. Hydrochemistry and hydrogen sulfide generating processes in the Malm aquifer, Bavarian Molasse Basin, Germany. *Hydrogeol. J.*, 22(1):151–162, 2014. doi:10.1007/s10040-013-1064-2.

[69] Jennifer C. McIntosh and Grant Ferguson. Deep meteoric water circulation in earth's crust. *Geophys. Res. Lett.*, 48(5):1–10, 2021. doi:10.1029/2020GL090461.

[70] Ayaz Mehmani, Shaina Kelly, Carlos Torres-Verdín, and Matthew Balhoff. Capillary Trapping Following Imbibition in Porous Media: Microfluidic Quantification of the Impact of Pore-Scale Surface Roughness. *Water Resour. Res.*, 55(11):9905–9925, 2019. doi:10.1029/2019WR025170.

[71] Jonathan Mitchell, T. C. Chandrasekera, Daniel J. Holland, Lynn F. Gladden, and E. J. Fordham. Magnetic resonance imaging in laboratory petrophysical core analysis. *Physics Reports*, 526(3):165–225, 2013. doi:10.1016/j.physrep.2013.01.003.

[72] Climate Change Mitigation. Ipcc special report on renewable energy sources and climate change mitigation. *Renewable Energy*, 20(11), 2011.

[73] Daniel J. Mundfrom, Dale G. Shaw, and Tian Lu Ke. Minimum sample size recommendations for conducting factor analyses. *International Journal of Testing*, 5(2):159–168, 2005. doi:10.1207/s15327574ijt0502_4.

[74] Niedrigwasser-Informationsdienst Bayern and Bayerisches Landesamt für Umwelt. Oberes Grundwasser-Stockwerk Bayern. Grundwasserstände vom 25.10.2023, 2023. URL: https://www.nid.bayern.de/grundwasser/tabellen.

[75] Karsten Osenbrück, Stefan Fiedler, Kay Knöller, Stephan M. Weise, Jürgen Sültenfuß, Harald Oster, and Gerhard Strauch. Timescales and development of groundwater pollution by nitrate in drinking water wells of the Jahna-Aue, Saxonia, Germany. *Water Resour. Res.*, 42(12):1–20, 2006. doi:10.1029/2006WR004977.

[76] O. A. Pfiffner. *Geologie der Alpen*. UTB. Stuttgart, 2010.

[77] R. Prestel. Hydrogeothermische Energiebilanz und Grundwasserhaushalt des Malmkarstes im süddeutschen Molassebecken - Teilbericht Hydrochemie zum Forschungsvorhaben 03E-6240 A/B (im Auftrag des Bundesministerium für Forschung und Technologie). Technical report, Bayer. LfU; LGRB, München, Freiburg, 1988.

[78] R. Prestel, P. Stier, M. Jobmann, R. Schulz, G. Strayle, J. Wendebourg, J. Werner, L. Wolf, M. Eichinger, J. Salvamoser, S. Weise, and P. Fritz. Hydrogeothermische Energiebilanz und Grundwasserhaushalt des Malmkarstes im süddeutschen Molassebecken. Technical report, Bayer. LfW und LGRB, München, Freiburg, 1991.

[79] A. Randi, J. Sterpenich, C. Morlot, J. Pironon, C. Kervévan, M. H. Beddelem, and C. Fléhoc. CO_2-DISSOLVED: A novel concept coupling geological storage of dissolved CO_2 and geothermal heat recovery - Part 3: Design of the MIRAGES-2 experimental device dedicated to the study of the geochemical water-rock interactions triggered by CO_2 laden brine. *Energy Procedia*, 63:4536–4547, 2014. doi:10.1016/j.egypro.2014.11.487.

[80] Gabriela Rosiles-González, Victor Hugo Carrillo-Jovel, Liliana Alzate-Gaviria, Walter Q. Betancourt, Charles P. Gerba, Oscar A. Moreno-Valenzuela, Raúl Tapia-Tussell, and Cecilia Hernández-Zepeda. Environmental Surveillance of SARS-CoV-2 RNA in Wastewater and Groundwater in Quintana Roo, Mexico. *Food Environ. Virol.*, 13(4):457–469, 2021. doi:10.1007/s12560-021-09492-y.

[81] Ladislaus Rybach. Geothermal energy: Sustainability and the environment. *Geothermics*, 32(4-6):463–470, 2003. doi:10.1016/S0375-6505(03)00057-9.

[82] Frank Sacher, Frank Thomas Lange, Heinz Jürgen Brauch, and Iris Blankenhorn. Pharmaceuticals in groundwaters: Analytical methods and results of a monitoring program in Baden-Württemberg, Germany. *J. Chromatogr. A*, 938(1-2):199–210, 2001. doi:10.1016/S0021-9673(01)01266-3.

[83] Roman B. Schmidt, Kurt Bucher, Kirsten Drüppel, and Ingrid Stober. Experimental interaction of hydrothermal Na-Cl solution with fracture surfaces of geothermal reservoir sandstone of the Upper Rhine Graben. *Appl. Geochemistry*, 81:36–52, 2017. doi:10.1016/j.apgeochem.2017.03.010.

[84] Roman B. Schmidt, Kurt Bucher, and Ingrid Stober. Experiments on granite alteration under geothermal reservoir conditions and the initiation of fracture evolution. *Eur. J. Mineral.*, 30(5):899–916, 2018. doi:10.1127/ejm/2018/0030-2771.

[85] R. Schulz and M. Jobmann. Hydrogeothermische Energiebilanz und Grundwasserhaushalt des Malmkarstes im süddeutschen Molassebecken - Teilgebiet: Hydrogeothermik. Abschlussbericht Archiv-Nr. 105 040, Geowissenschaftliche Gemeinschaftsaufgaben (GGA), Hannover, 1989.

[86] Michael Seidel, Lars Jurzik, Ingrid Brettar, Manfred G. Höfle, and Christian Griebler. Microbial and viral pathogens in freshwater: current research aspects studied in Germany. *Environ. Earth Sci.*, 75(20), 2016. doi:10.1007/s12665-016-6189-x.

[87] Sima Siami-Namini, Neda Tavakoli, and Akbar Siami Namin. A Comparison of ARIMA and LSTM in Forecasting Time Series. *Proc. - 17th IEEE Int. Conf. Mach. Learn. Appl. ICMLA 2018*, pages 1394–1401, 2018. doi:10.1109/ICMLA.2018.00227.

[88] Olga Singurindy and Brian Berkowitz. The role of fractures on coupled dissolution and precipitation patterns in carbonate rocks. *Adv. Water Resour.*, 28(5):507–521, 2005. doi:10.1016/j.advwatres.2005.01.002.

[89] S. Stadler, J. Sültenfuß, H. M. Holländer, A. Bohn, C. Jahnke, and A. Suckow. Isotopic and geochemical indicators for groundwater flow and multi-component mixing near disturbed salt anticlines. *Chemical Geology*, 294:226–242, 2012. doi:10.1016/j.chemgeo.2011.12.006.

[90] Yuhao Sun, Michael Aman, and D. Nicolas Espinoza. Assessment of mechanical rock alteration caused by CO_2-water mixtures using indentation and scratch experiments. *Int. J. Greenh. Gas Control*, 45:9–17, 2016. URL: http://dx.doi.org/10.1016/j.ijggc.2015.11.021, doi:10.1016/j.ijggc.2015.11.021.

[91] Agnes Tegen, Paul Davidsson, Radu Casian Mihailescu, and Jan A. Persson. Collaborative sensing with interactive learning using dynamic intelligent virtual sensors. *Sensors (Switzerland)*, 19(3), 2019. doi:10.3390/s19030477.

[92] Pierre Ungemach. Reinjection of cooled geothermal brines into sandstone reservoirs. *Geothermics*, 32(4):743–761, 2003. doi:10.1016/S0375-6505(03)00074-9.

[93] United Nations. Water and Climate Change, 2022. URL: https://www.unwater.org/water-facts/water-and-climate-change.

[94] United Nations. Sustainability, 2023. Accessed: 2023-10-31. URL: https://www.un.org/en/academic-impact/sustainability.

[95] United Nations. What is renewable energy?, 2023. Accessed: 2025-08-20. URL: https://www.un.org/en/climatechange/what-is-renewable-energy.

[96] United Nations. Department of Economic and Social Affairs. Sustainable development. The 17 goals, 2015. Accessed: 2025-08-20. URL: https://sdgs.un.org/goals.

[97] Oliver Warr, Thomas Giunta, Tullis C. Onstott, Thomas L. Kieft, Rachel L. Harris, Devan M. Nisson, and Barbara Sherwood Lollar. The role of low-temperature 18O exchange in the isotopic evolution of deep subsurface fluids. *Chem. Geol.*, 561(December 2020):120027, 2021. doi:10.1016/j.chemgeo.2020.120027.

[98] S. M. Weise, M. Wolf, P. Fritz, W. Rauert, W. Stichler, R. Prestel, B. Bertleff, and M. Stute. Isotopenhydrologische Untersuchungen im Süddeutschen Molassebecken. In Bayerisches Landesamt für Wasserwirtschaft and Geologisches Landesamt Baden-Württemberg, editors, *Hydrogeothermische Energiebilanz und Grundwasserhaushalt des Malmkarstes im Süddeutschen Molassebecken (Schlussbericht - Forschungsvorhaben 03 E 6240 A/B)*, page 104. München, Freiburg, 1991.

[99] Hang Wen, Li Li, Dustin Crandall, and Alexandra Hakala. Where lower calcite abundance creates more alteration: Enhanced rock matrix diffusivity induced by preferential dissolution. *energy&fuels*, 30, 2016. doi:10.1021/acs.energyfuels.5b02932.

[100] F. Wenderoth, T. Fritzer, M. Gropius, B. Huber, and A. Schubert. Numerische 3D-Modellierung eines geohydrothermalen Dublettenbetriebs im Malmkarst. *Geotherm. Energ.*, 48:12, 2005.

[101] Frank Wenderoth. Dreidimensionale Modellierung geohydrothermaler Prozesse zur Beurteilung von Aquiferen hinsichtlich ihrer wirtschaftlichen Nutzbarkeit. Technical report, 1988.

[102] Charles J. Werth, Changyong Zhang, Mark L. Brusseau, Mart Oostrom, and Thomas Baumann. A review of non-invasive imaging methods and applications in contaminant hydrogeology research, 4 2010. doi:10.1016/j.jconhyd.2010.01.001.

[103] Theis Winter and Florian Einsiedl. Combining $^{14}C_{DOC}$ and ^{81}Kr with hydrochemical data to identify recharge processes in the South German Molasse Basin. *J. Hydrol.*, 612(PA):128020, 2022. doi:10.1016/j.jhydrol.2022.128020.

[104] F. Wisotzky, N. Cremer, and S. Lenk. *Angewandte Grundwasserchemie, Hydrogeologie und hydrogeochemische Modellierung*. Springer Spektrum. Berlin, Berlin, 2 edition, 2018. doi:10.1007/978-3-662-55558-3.

[105] Hartmut Wittenberg. Effects of season and man-made changes on baseflow and flow recession: Case studies. *Hydrol. Process.*, 17(11):2113–2123, 2003. doi:10.1002/hyp.1324.

[106] Stephen R.H. Worthington and D.C. Ford. Self-organized permeability in carbonate aquifers. *Groundwater*, 47(3):326–336, 2009. doi:10.1111/j.1745-6584.2009.00551.x.

[107] Lilly Zacherl and Thomas Baumann. Quantification of the effect of gas–water–equilibria on carbonate precipitation. *Geothermal Energy*, 11(1):11, 2023.

[108] Penghui Zhang, Yong Il Lee, and Jinliang Zhang. A review of high-resolution X-ray computed tomography applied to petroleum geology and a case study. *Micron*, 124(June):102702, 2019. doi:10.1016/j.micron.2019.102702.

[109] Yangxiao Zhou. Sampling frequency for monitoring the actual state of groundwater systems. *J. Hydrol.*, 180(1-4):301–318, 1996. doi:10.1016/0022-1694(95)02892-7.